

4.01 Earthquake Seismology: An Introduction and Overview

GC Beroza, Stanford University, Stanford, CA, USA

H Kanamori, California Institute of Technology, Pasadena, CA, USA

© 2015 Elsevier B.V. All rights reserved.

4.01.1	Introduction	2
4.01.2	Seismicity	3
4.01.2.1	Earthquake Size	3
4.01.2.2	Earthquakes in the Context of Plate Tectonics	5
4.01.2.2.1	Transcurrent plate boundaries	6
4.01.2.2.2	Divergent plate boundaries	7
4.01.2.2.3	Convergent plate boundaries	7
4.01.2.2.4	Intraplate earthquakes	11
4.01.2.2.5	Hot spot volcanism	13
4.01.2.3	The Largest and Deadliest Earthquakes	13
4.01.2.4	Historic and Prehistoric Earthquakes	15
4.01.2.5	Earthquake Size Distribution	15
4.01.2.6	Earthquake Location	16
4.01.3	The Earthquake Source	17
4.01.3.1	Point-Source Parameters	17
4.01.3.2	Sense of Faulting from First Motions	18
4.01.3.3	Moment Tensor Representation	19
4.01.3.4	Seismic Energy	19
4.01.3.5	Extended-Source Models of Earthquakes	20
4.01.3.5.1	Kinematic source models	20
4.01.3.5.2	Dynamic source models	20
4.01.3.6	Volcano Seismology	22
4.01.4	Slip Behavior	24
4.01.4.1	Brittle Failure	24
4.01.4.2	Creep	25
4.01.4.3	Aseismic Transients and Tremor	27
4.01.5	Physics of the Earthquake Source	30
4.01.5.1	Friction	30
4.01.5.2	Energy Budget	31
4.01.5.3	Microscopic Processes	31
4.01.5.3.1	Hydrologic processes	32
4.01.5.3.2	Melting and flash heating	32
4.01.5.3.3	Thermal pressurization	33
4.01.5.3.4	Silica gel formation	33
4.01.5.4	Fault-Zone Structure	34
4.01.5.5	Borehole Observations, Fault-Zone Drilling, and Seismicity in Mines	34
4.01.5.6	Earthquakes as a Complex System	35
4.01.6	State of Stress, Nucleation, and Triggering	35
4.01.6.1	State of Stress	35
4.01.6.2	Earthquake Nucleation and Short-Term Earthquake Prediction	37
4.01.6.3	Earthquake Forecasting	38
4.01.6.4	Static Stress Triggering	39
4.01.6.5	Dynamic Triggering	40
4.01.6.6	Temporal Distribution of Earthquakes	40
4.01.7	Associated Problems	40
4.01.7.1	Strong Motion Prediction	40
4.01.7.2	Tsunamis	43
4.01.7.3	Test Ban Treaty Verification	43
4.01.7.4	Solid Earth–Atmospheric Coupling	43
4.01.8	Earthquake Risk Mitigation	44
4.01.9	Conclusions	44
References		46

4.01.1 Introduction

In general usage, the term ‘earthquake’ describes a sudden shaking of the ground. Earth scientists, however, typically use the word ‘earthquake’ differently – to describe the *source* of seismic waves, which is nearly always sudden shear slip on a fault within the Earth. In this chapter, we follow the scientific usage of the term and focus our review on how earthquakes are studied using the motion of the ground remote from the earthquake source itself, that is, by interpreting the same shaking that most people consider to be ‘the earthquake.’ The field defined by the use of seismic waves to understand earthquakes is known as *earthquake seismology* ([Figure 1](#)).

The nature of the earthquakes makes them intrinsically difficult to study. Different aspects of the earthquake process span a tremendous range in length scales – all the way from the size of individual mineral grains to the size of the largest plates. They span a tremendous range in timescales as well. The smallest microearthquakes rupture faults for only a small fraction of a second, and the duration of even the very largest earthquakes can be measured in 100 s of seconds. Compare this with the length of strain accumulation in the earthquake cycle, which can be measured in decades, centuries, and even millennia in regions of slow strain rate. The evolution of fault systems spans longer times still, since that can require the action of thousands of earthquakes. At different physical dimensions or temporal scales, different physical mechanisms may become important or perhaps negligible. Earthquakes occur in geologically, and hence physically, complicated environments. The behavior of earthquakes has been held up as a type example of a complex natural system. The sudden transformation of faults from being locked, or perhaps slipping quasistatically, to slipping



Figure 1 Earthquakes are due to slip on faults within the Earth. In large earthquakes, fault slip can reach the Earth’s surface. Photo shows surface rupture of the 1906 San Francisco earthquake offset this fence horizontally by ~8.5 ft. (Plate 1-B, US Geological Survey Bulletin 324 – from <http://libraryphoto.cr.usgs.gov/>, San Francisco Earthquake, plate 41.)

unstably at large slip speeds, as is nearly universally observed for earthquakes, also makes them a challenging physical system to understand.

Despite these challenges, seismologists have made tremendous progress in understanding many aspects of earthquakes – elucidating their mechanisms based on the radiated seismic wave field, determining where they occur and the deep structure of faults with great precision, documenting the frequency and the regularity (or irregularity) with which they occur (and recur) over the long term, gaining insight into the ways in which they interact with one another, and so on. Yet, the obvious goal of short-term prediction of earthquakes, that is, specifying the time, location, and size of future significant earthquakes on a timescale shorter than decades, remains elusive. Earthquakes are different in this sense from nearly all other deadly natural hazards such as hurricanes, floods, tornadoes, and even volcanic eruptions, which to varying degrees are predictable over a timescale of hours to days. The worst earthquakes rank at the very top of known disasters. The deadliest known earthquake killed over half a million people in a matter of minutes, a level of sudden destruction that no other catastrophe in recorded history – either natural or human-made – has attained.

Our inability to predict earthquakes is one reason they cause such apprehension. This lack of warning is compounded by the fact that they strike so abruptly. No one can see an earthquake coming and it is only a matter of seconds from the initial perception of the first-arriving waves of a large earthquake before dangerous strong ground motion begins. Moreover, large, damaging earthquakes occur infrequently (fortunately) at any given point on the Earth relative to a human life span. This means that most people who experience a major earthquake are doing so for the first time, so the experience is unfamiliar. Finally, there is something fundamentally unsettling about the movement of the ‘solid’ Earth.

The unpredictability, sudden onset, and their unfamiliarity make earthquakes a uniquely terrifying phenomenon. As testament to this, other extreme and catastrophic events in the affairs of humankind – if they are devastating enough – are described with the simile ‘like an earthquake.’ The point of origin of an extreme event of any kind is often described as ‘the epicenter,’ a term borrowed from seismology.

The unpredictability of earthquakes also renders them difficult to study. Since we do not know where, and particularly when, large earthquakes will strike, collecting data on earthquakes has to be approached passively. Seismologists deploy instruments to measure seismic waves where we expect earthquakes to occur and then wait for nature to carry out the experiment. The wait can last decades, or more, for a large earthquake. Inevitably, with finite budgets and finite patience, this leads to seismic monitoring instruments being widely, and hence too thinly, dispersed in an attempt to gather data from at least *some* earthquakes wherever and whenever they might occur.

Finally, the combination of unpredictability, sudden onset, long intervals between events, and unfamiliarity means that the risk created by earthquake hazards is extremely difficult for both policymakers and the general public to manage. Because earthquakes are not predicted and occur infrequently relative to other hazards, it is understandably tempting for

governments and individuals to focus on the many immediate and predictable problems that impact society more frequently. The unpredictability and sudden onset of earthquakes, however, mean that once an earthquake begins, it is too late to do much more than duck, cover, and hold on.

4.01.2 Seismicity

4.01.2.1 Earthquake Size

Perhaps, the most familiar earthquake source parameter is magnitude. Earthquake magnitude and the characteristics of earthquake behavior that it is used to define, such as Gutenberg–Richter statistics (discussed further in [Section 4.01.2.5](#)), are purely empirical observations in the sense that they rely only on measurements of seismic waves as recorded on seismographs and do not require much in the way of assumptions about earthquake source physics. It is impossible to completely represent a complex physical process like an earthquake with a single number that measures its size. Nevertheless, several definitions of earthquake size have proven extremely useful for reaching a better understanding of earthquakes.

Earthquake size is traditionally measured by one of various magnitude scales. M_L , the local magnitude scale, was devised by Richter in the early 1930s ([Richter, 1935](#)). He was cataloging data from the Southern California seismic network, and although locations, depths, and origin times for many earthquakes were available, there was no measurement of earthquake size. So he invented one, using the relation

$$M_L = \log(A) - \log(A_0)$$

where A is the measured amplitude of the seismic trace on a standardized Wood–Anderson seismograph ([Figure 2](#)) at a distance of 100 km and A_0 is the amplitude of a reference earthquake with $M_L=0.0$. The particular definition of the zero level is that an earthquake of magnitude 0 has an amplitude of 0.000001 m at a distance of 100 km. Thus, an earthquake of magnitude 3.0 has an amplitude of 1 mm at the same distance and a magnitude 7.0 earthquake would have an amplitude of 10 m. Wood–Anderson instruments record on photographic paper and saturate at an amplitude of about 20 cm.

Until recently, quoted magnitudes for local earthquakes were often correctly described as the Richter magnitude. The old

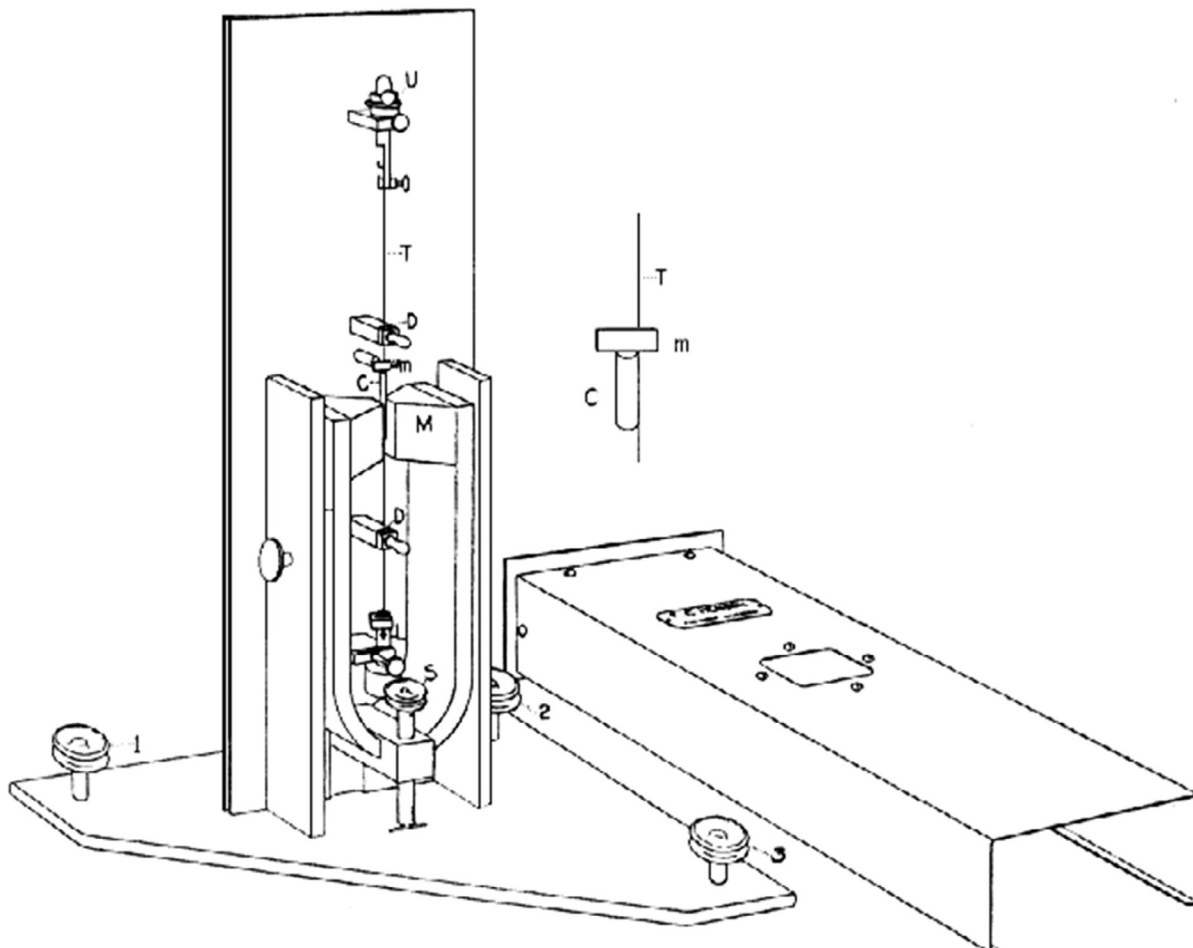


Figure 2 Diagram of a Wood–Anderson torsion seismometer, which is used to define M_L . Ground motion causes rotation of an inertial mass, C , which is attached to a thin wire under high tension, T . Seismograms are recorded on photographic paper using a beam of light reflected off a mirror, M , that is mounted on the inertial mass. Reproduced from <http://www.data.scec.org/Module/s3inset3.html>.

Wood–Anderson instruments, though state of the art when the magnitude scale was developed, are not now used. Instead, if one wants to calculate the local magnitude, data from modern instruments must be degraded to mimic recordings from the old instruments (Figure 3). Although the magnitude scale has proven extremely useful for routine cataloging of earthquake behavior, there are several shortcomings of M_L , among them:

- (1) If the station is not 100 km from the earthquake, one must correct for propagation effects – this is difficult because at different distances, different wave types have the largest amplitude.
- (2) Excitation of waves can vary strongly with depth and this must be corrected for to compare the size of earthquakes at different depths.
- (3) Earthquakes have complex radiation patterns so that the azimuthal direction of the seismograph from the earthquake strongly affects the amplitude of the recorded waves.
- (4) The Wood–Anderson instruments respond primarily to ground motion at periods less than about 1 s. Once the size of an earthquake approaches magnitude 7.0, 1 s waves start to saturate in amplitude due to interference effects arising from the finite size and duration of the fault. This occurs even if the seismograph is operated at low gain and the waves are all on scale. Beyond $M_L \sim 7$, the local magnitude is no longer a reliable measure of earthquake size.

To some extent, difficulties (1)–(3) can be corrected for empirically and by averaging over many stations. Nevertheless, M_L is frequently uncertain by as much as 0.25 magnitude units, and it does not extend to earthquakes

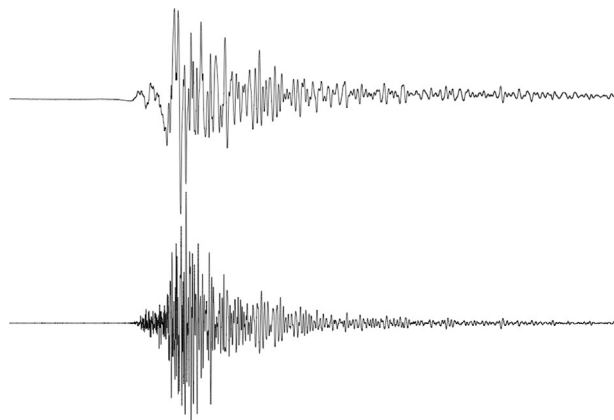


Figure 3 Upper seismogram shows data for the 28 September 2004 Parkfield, California, earthquake from a modern broadband instrument at station JRSC (Jasper Ridge, Stanford, California), and lower seismogram shows the same ground motion as it would have been recorded on a Wood–Anderson instrument (lower). Time increases from left to right and a total of 600 s is shown. Vertical axis shows north–south component of displacement. Maximum peak-to-peak displacement of the broadband record is ~ 0.4 cm. At frequencies < 1 Hz, the Wood–Anderson instrument is flat to acceleration, which means that the displacement response decays rapidly. The lower seismogram is multiplied by a factor of 20 for comparison. Standard magnification for these instruments was 2800, which would have slightly exceeded the dynamic range of the photographic recording system for this earthquake.

recorded at distances in excess of 300 km. Hence, it is not suitable for global earthquake monitoring. To remedy this, and to address difficulty (4), seismologists invented a variety of different magnitude scales. Usually, it is one of these other magnitude scales that is used to characterize the size of an earthquake.

m_b , the body wave magnitude scale, is defined using the initial P-waves from earthquakes that occur very far away so that it can be used to compare earthquakes all over the world. It has been adjusted to agree approximately with the Richter magnitude at short distances. Since it uses short-period waves, it also saturates above magnitude 7.0. The application of the body wave magnitude scale has varied with time – particularly in whether or not the maximum amplitude of the entire P-wave train, rather than just the first few cycles, is measured. Prior to 1964, it was determined using the formula

$$m_b = \log(A/T) + Q$$

where A is the amplitude, T is the period, and Q is a factor that corrects for distance and depth. Unlike the local magnitude scale, the amplitude measurement for the body wave magnitude represents the ground motion amplitude after correcting for instrument response, rather than the amplitude as recorded on the instrument. With the advent of the Worldwide Standardized Seismographic Network (WWSSN), m_b was defined using the high-frequency channel of those instruments, for which the response is strongly peaked at a period of 1 s.

M_s , the surface wave magnitude scale, is a measure of the amplitude of surface waves (Rayleigh waves) at a period of 20 s as measured very far from the event. This magnitude is often quoted by the press as the Richter magnitude. The internationally adopted definition (Vanek et al., 1962) of the surface wave magnitude scale is

$$M_s = \log(A/T)_{\max} + 1.66 \log \Delta + 3.3$$

where A is the peak amplitude of vertical ground motion (as for the body wave magnitude, it is corrected for instrument response) and Δ is the angular distance from the earthquake to the seismograph. This definition of the surface wave magnitude closely resembles the original definition of Gutenberg and Richter (1936), which used a fixed period of 20 s. M_s is usually a better estimate of earthquake size, especially for larger earthquakes, than either m_b or M_L . It only saturates for ‘great’ earthquakes when M_s is much over eight. For intermediate and deep earthquakes, however, it does a poor job of representing earthquake size because such events do not strongly excite surface waves.

The magnitude scales described earlier do not tie magnitude to a physical parameter. An obvious physical parameter of interest that is strongly linked to the strength of an earthquake is the total amount of energy radiated in the form of seismic waves. This is often referred to as the radiated seismic energy, or the seismic energy for short. Gutenberg and Richter (1942, 1956) attempted to relate the seismic energy to the surface wave magnitude. For the seismic energy, E_s , expressed in Joules, they found

$$\log E_s = 1.5M_s + 4.8$$

This relationship assumes proportionality between the energy radiated as Rayleigh waves at ~ 20 s period and the

entire radiated field. As with the surface wave magnitude scale, this is a reasonable assumption until M_s approaches eight. For larger earthquake, the effects of fault finiteness start to become important for 20 s Rayleigh waves and the surface wave magnitude is no longer representative of the total radiated energy. Nevertheless, this relationship shows that the radiated energy increases very rapidly with magnitude. A unit increase in magnitude corresponds to a factor of 32 ($10^{1.5}$) increase in the seismic energy.

M_0 , the seismic moment, is another physical parameter related to the size of an earthquake and has become the parameter that seismologists most often use to describe the size of an earthquake. The seismic moment is a measure of the size of the equivalent force system needed to generate the waves that the earthquake faulting generated. M_0 was first calculated by [Aki \(1966\)](#) in his study of the Niigata, Japan, earthquake. It is a more robust estimate of the size because it is done, in theory, at infinite period and radiation pattern effects due to the orientation of faulting are explicitly accounted for when it is calculated. Another advantage it has is that it can be applied to aseismic transients, which by definition do not radiate detectable seismic waves. Seismic moment does not saturate and is directly proportional to the amount of slip across a fault times the fault area. If the faulted area is A , the shear modulus is μ , and the average slip over the faulted area is s , then the seismic moment, M_0 , is

$$M_0 = \mu A s$$

The MKS unit for seismic moment is Newton meters. Earlier work in seismology typically used dyne cm, the cgs unit, to express seismic moment.

M_w , the moment magnitude scale, is a magnitude scale based directly on the measurement of the seismic moment so it does not saturate. M_w was constructed to agree with the M_L and M_s scales before they saturate but retains the same relationship to seismic moment thereafter ([Hanks and Kanamori, 1979](#)). Assuming the seismic moment is expressed in Nm, the moment magnitude relation can be written

$$\log M_0 = 1.5M_w + 9.05$$

and hence, the moment magnitude scale is determined from the seismic moment by the relation

$$M_w = 2/3 \log M_0 - 6.03$$

A unit increase in M_w does *not* mean a factor of 10 increase in earthquake size. Rather, the increase in size of the earthquake, as measured by M_0 , is about factor of 32 ($10^{1.5}$) for each magnitude unit.

As is apparent from all of the definitions mentioned previously, magnitude scales do not vary from 1 to 10, but are open-ended. In practice, even M_w is limited on the high end both by the strength of the rocks that earthquakes occur in and by the size of the fault. On the low end, M_w is limited by the size of the smallest faults and/or fault patch that can slip unstably. Earthquakes that are recorded by sensitive borehole instruments or *in situ* in deep mines routinely have negative magnitudes. There are many other magnitude scales, most of which are tailored to suit either the practicalities or different goals of earthquake, volcano, and nuclear explosion monitoring. These

include magnitude scales derived from measurements as diverse as the duration of the coda of scattered waves following an earthquake, the amplitude of guided waves in the continental crust, and the amplitude of the tsunami that an earthquake generates.

Instrumental seismology began in the last decade of the nineteenth century; however, many earthquakes of interest happened before then. For such earthquakes, seismologists must resort to more subjective and indirect estimates of earthquake magnitude. The most common approach to determining the magnitude of preinstrumental earthquakes is through the interpretation of seismic intensity observations.

Intensity is different from magnitude in that it is not a measure of the intrinsic size of an earthquake; rather, it is a local measure of the strength of shaking as perceived by people or as it affects buildings or natural features. There are many different intensity scales, but the most widely used is probably the modified Mercalli intensity (MMI) scale ([Richter, 1958](#)). Traditionally, intensities are denoted with Roman numerals, and the MMI scale ranges from I to XII. [Table 1](#) contains the MMI scale as abridged by [Bolt \(1993\)](#).

Earthquake magnitude can be determined from the intensity distribution in several ways. Some methods use the area encompassed by intensities of a certain level ([Toppozada, 1975](#)), whereas others use individual intensity observations directly ([Bakun and Wentworth, 1997](#)). [Toppozada et al. \(1981\)](#) used intensity distributions to estimate the magnitudes of California earthquakes from the preinstrumental period. Because the stronger intensities are direct measures of damage in earthquakes, there have been attempts to relate intensities to measures of ground motion, like peak ground acceleration (PGA), that are thought to correlate strongly with damage ([Gutenberg and Richter, 1956](#)). More recently, instrumental recordings of ground motion have been used to estimate instrumental intensities. [Wald et al. \(1999\)](#) found the following relation between PGA and the MMI level, I_{mm} :

$$I_{mm} = 3.66 \log (\text{PGA}) - 1.66 \quad (\sigma = 1.08)$$

Intensity data have also been used as a proxy to study strong ground motion from significant earthquakes where such data are lacking, such as for the 1906 San Francisco, California, earthquake ([Boatwright and Bundock, 2005](#)). The intensity map of the 1886 Charleston, South Carolina, earthquake is shown in [Figure 4](#).

4.01.2.2 Earthquakes in the Context of Plate Tectonics

Scientists have long recognized that some portions of the Earth are characterized by frequent earthquake activity, while others have essentially no earthquake activity whatsoever. [Figure 5](#) shows the first global map of earthquake activity ([Mallet and Mallett, 1858](#)), which shows a remarkably accurate view of global seismicity, particularly since it predicated the invention of the seismograph by decades.

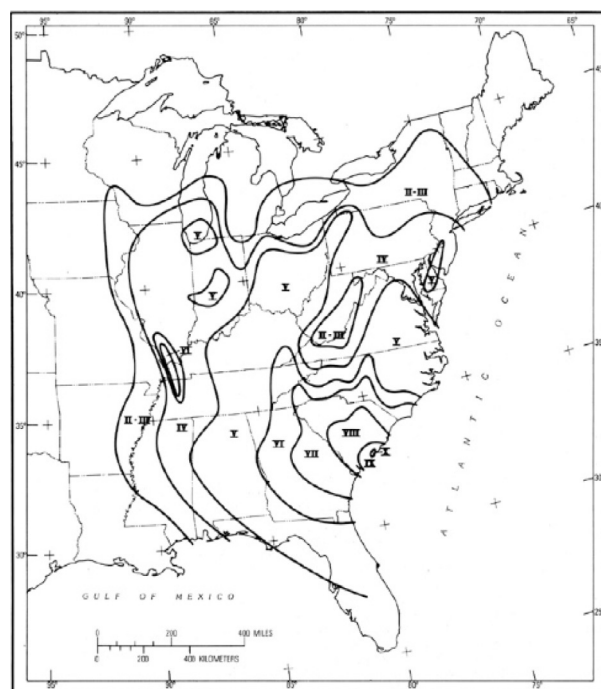
In 1954, Beno Gutenberg and Charles Richter published the second edition of *Seismicity of the Earth*. To this day, their book provides a remarkably complete description of the locations, depth, and size of earthquakes, as well as the distribution and types of volcanoes, worldwide ([Figure 6](#)). What the book lacks

Table 1 The modified Mercalli intensity scale

I	Not felt except by a very few under especially favorable circumstances
II	Felt only by a few persons at rest, especially on upper floors of buildings. Delicately suspended objects may swing
III	Felt quite noticeably indoors, especially on upper floors of buildings, but many people do not recognize it as an earthquake. Standing automobiles may rock slightly. Vibration like passing of truck
IV	During the day, felt indoors by many, outdoors by few. At night, some awakened. Dishes, windows, doors disturbed; walls make creaking sound. Sensation like heavy truck striking building. Standing automobiles rocked noticeably
V	Felt by nearly everyone, many awakened. Some dishes, windows, and so on broken; cracked plaster in a few places; unstable objects overturned. Disturbances of trees, poles, and other tall objects sometimes noticed. Pendulum clocks may stop
VI	Felt by all, many frightened and run outdoors. Some heavy furniture moved; a few instances of fallen plaster and damaged chimneys. Damage slight
VII	Everybody runs outdoors. Damage negligible in buildings of good design and construction, slight to moderate in well-built ordinary structures, considerable in poorly built or badly designed structures, some chimneys broken. Noticed by persons driving cars
VIII	Damage slight in specially designed structures, considerable in ordinary substantial buildings with partial collapse, great in poorly built structures. Panel walls thrown out of frame structures. Fall of chimneys, factory stack, columns, monuments, and walls. Heavy furniture overturned. Sand and mud ejected in small amounts. Changes in well water. Persons driving cars disturbed
IX	Damage considerable in specially designed structures; well-designed frame structures thrown out of plumb; great in substantial buildings, with partial collapse. Buildings shifted off foundations. Ground cracked conspicuously. Underground pipes broken
X	Some well-built wooden structures destroyed, most masonry and frame structures destroyed with foundations, ground badly cracked. Rails bent. Landslides considerable from riverbanks and steep slopes. Shifted sand and mud. Water splashed, slopped over banks
XI	Few (masonry), if any, structures remain standing. Bridges destroyed. Broad fissures in ground. Underground pipelines completely out of service. Earth slumps and land slips in soft ground. Rails bent greatly
XII	Damage total. Waves seen on ground surface. Lines of sight and level distorted. Objects thrown into the air

is a unified model to tie all those observations together, explaining the where and the why of the Earth's earthquake and volcanic activity. The theory of plate tectonics, which was established within a decade following publication of that second edition, provides that context. *Seismicity of the Earth* underscores both just how much was known about the systematics of earthquake and volcanic activity before the theory of plate tectonics was formulated and what a wide range of phenomena plate tectonics explains.

Earthquakes delineate plate boundaries, the vast majority of earthquakes occur at plate boundaries (Figures 7 and 8), and the type of boundary – transcurrent, divergent, and convergent – exerts a profound effect on the nature of earthquake activity



Isoseismal Map of Sept. 1, 1886 South Carolina Earthquake Magnitude 7.3

Figure 4 Isoseismal map for the 1886 Charleston, South Carolina, earthquake. The lines enclosing areas of equal intensity are referred to as 'isoseismal' lines. Reproduced from <http://earthquake.usgs.gov/learning/teachers/isoseismalMaps.pdf>.

on it. Thus, it is natural to organize a discussion of earthquakes and volcanoes by plate boundary type. In this section, we are only able to offer a cursory review of the systematics of earthquakes and volcanoes.

4.01.2.2.1 Transcurrent plate boundaries

Most transcurrent plate boundary earthquakes, in which plates slide past one another horizontally on strike-slip faults, occur on oceanic transform faults deep under the ocean surface. Such oceanic transform fault earthquakes do not pose much hazard to humankind. That and their remoteness from seismic monitoring instruments render them difficult to study; however, some transform plate boundaries traverse continental crust where they do pose a significant hazard and are more easily monitored. Transform fault earthquakes, whether in the oceans or on continents, are limited in their size by the depth extent of the seismogenic crust, which is at most a few tens of kilometers, and the fact that transform faults tend to cut through the Earth's crust at angles very close to vertical.

Despite this limitation on size, continental transform fault earthquakes that occur in places such as Turkey, New Zealand, and California can be devastating and include some of the most infamous earthquakes in history. When they occur in continental crust, the shallow extent of the seismogenic zone means that waves are generated everywhere very close to the Earth's surface and hence have little opportunity to spread out or attenuate, and thus reduce in amplitude, before impacting the built environment. Although strike-slip deformation

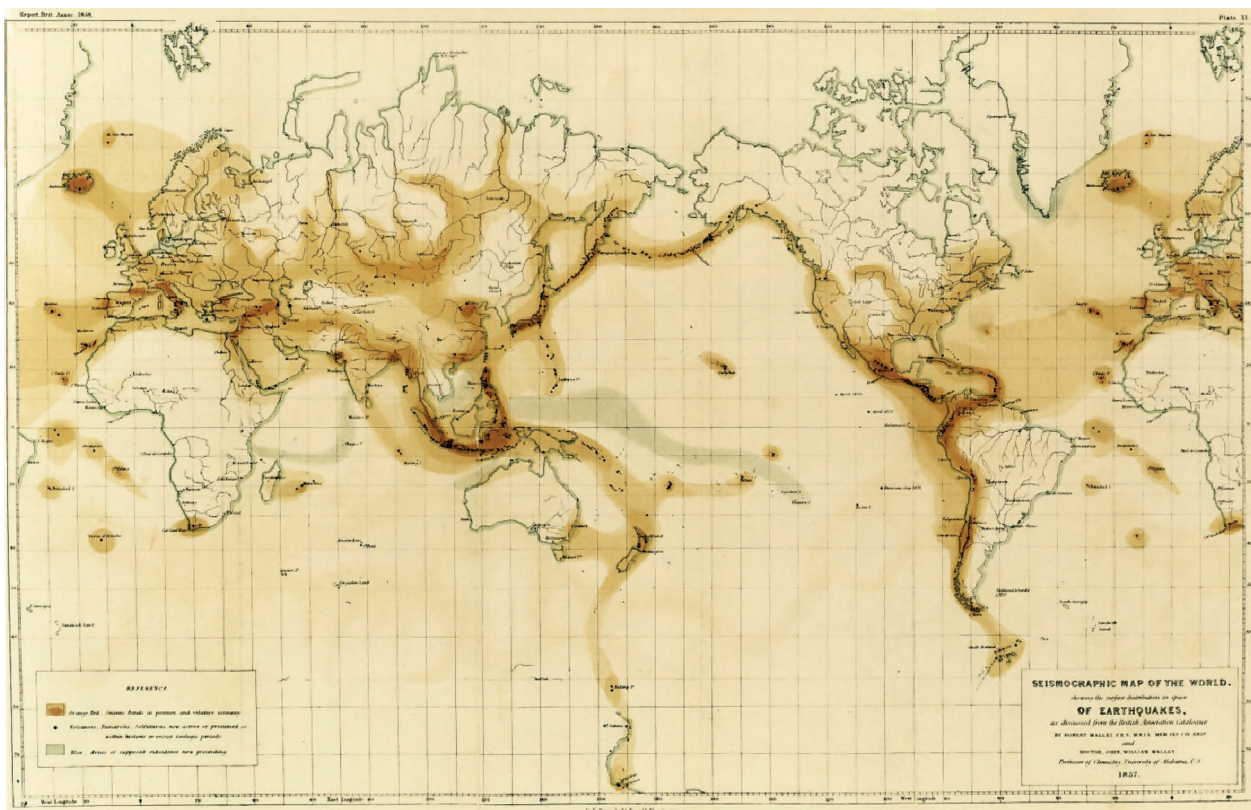


Figure 5 Global distribution of earthquakes as represented by Mallett and Mallett (1858). The principal zones of seismicity are well represented, with the exception of the mid-ocean ridge system, for which the earthquakes were too small and too remote from land to detect. This map preceded instrumental seismology and was based entirely on felt reports of earthquakes.

predominates at transform plate boundaries, such plate boundaries are not perfectly parallel to the direction of relative plate motion. For this reason, there are often significant reverse and normal faulting earthquakes at such boundaries too, particularly for continental transform boundaries, which typically involve much more broadly distributed fault systems than oceanic transforms.

4.01.2.2.2 Divergent plate boundaries

Earthquakes at plate boundaries where plates diverge from one another on normal faults have the least societal impact of any type of plate boundary earthquakes. Most such plate boundaries occur as mid-ocean ridges situated several kilometers beneath the ocean surface. Exceptions to this include Iceland and the Galápagos Islands, where the effects of mid-ocean ridges and hot spots are superimposed, and East Africa, where the divergent plate boundary is not yet mature enough to have separated sufficiently for an ocean to form. Divergent plate boundaries are characterized by effusive basaltic volcanism through which new crust is formed.

A great deal of the deformation at these plate boundaries appears to take place aseismically. The largest normal faulting earthquakes that occur on extensional plate boundaries are small relative to the largest earthquakes at other plate boundaries owing to the fact that the high temperatures in newly formed crust limit the depth extent of the seismogenic crust. Normal faulting predominates at extensional plate boundaries,

but extensional rifts are often irregular, and it is not uncommon for strike-slip earthquakes to occur in such settings across local transform faults within a rift. In some cases, these earthquakes are significant.

Mid-ocean ridge volcanism for the most part occurs under several kilometers of ocean. Hence, until the 1950s, the extent and systematics of the mid-ocean ridge system were unknown. Nevertheless, as the source of new oceanic crust, it is a key element of plate tectonics, and the creation of oceanic crust at mid-ocean ridges is the key behavior that distinguishes the theory of plate tectonics from the theory of continental drift. The mid-ocean ridge volcanoes form the longest mountain chain on Earth – some 40 000 km in total extent. The hydrothermal plumbing of these magmatic systems is complex, depends on the spreading rate, and gives rise to a range of unusual hydrothermal deep-sea vents. Although eruptions on mid-ocean ridge systems have been inferred from signals detected on hydrophone arrays, they have not yet been directly observed.

4.01.2.2.3 Convergent plate boundaries

By almost any measure, earthquakes at convergent plate boundaries dominate the seismicity of the Earth. At such plate boundaries, all factors work towards the generation of frequent large earthquakes. Relatively cool crust is subducted into the Earth, resulting in reduced temperatures at depth, which increases the depth extent of the seismogenic zone.

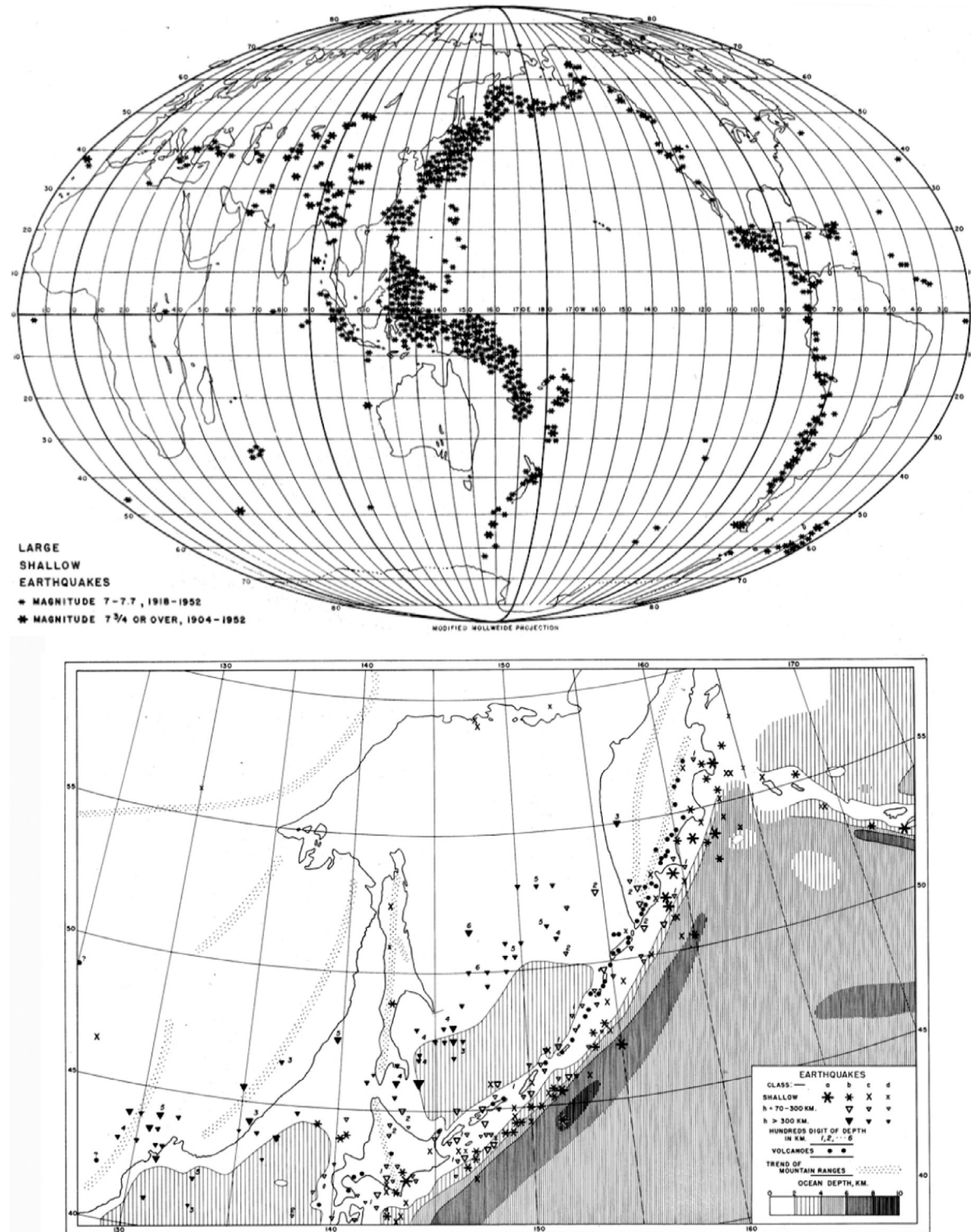


Figure 6 (a) Seismicity map showing worldwide distribution of shallow earthquakes. (b) Close-up of subduction zone seismicity including Honshu, the Kuril Islands, and Kamchatka. The principal features including trench offshore, increasing depth of earthquakes to the northwest, and volcanoes were subsequently explained by the theory of plate tectonics. Reproduced from Gutenberg B and Richter CF (1954) Seismicity of the Earth and Associated Phenomenon, 2nd edn., Princeton: Princeton University Press.

Moreover, unlike other plate boundaries, the plate interface of some subduction zones traverses the seismogenic zone at a very shallow angle – in places $< 10^\circ$ from horizontal – meaning that the seismogenic width of the plate boundary in places like

Sumatra, Alaska, and Chile can be 100 s of kilometers across. As a result, the great majority of large earthquakes, and nearly all earthquakes larger than magnitude 8, occur at convergent plate boundaries with reverse faulting mechanisms. The very largest

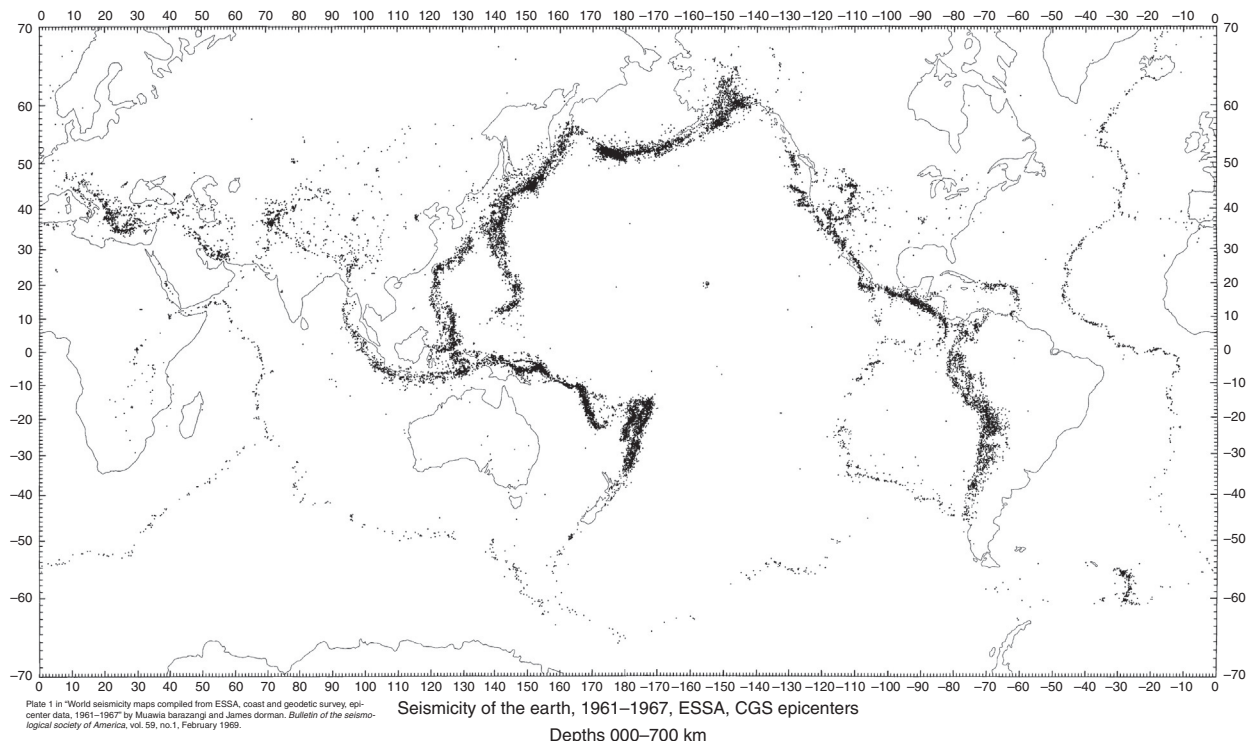


Figure 7 Global seismicity as shown by [Barazangi and Dorman \(1969\)](#) from 1961 to 1967, which comprises 29 553 earthquakes of magnitude > 4.0. The narrowbands of seismicity running through the Earth's oceans are readily apparent in this figure.

recorded earthquakes are all of this type, including the M_w 9.5 1960 Chile earthquake, the M_w 9.3 Alaska earthquake of 1964, the M_w 9.2 Sumatra earthquake of 2004, the M_w 9.0 Kamchatka earthquake of 1952, and the M_w 9.0 Tohoku-Oki earthquake of 2011. These five earthquakes dominate the total seismic activity of the Earth over the past 100 years. Of these largest recorded earthquakes, the Sumatra earthquake caused the most widespread and large-scale devastation, and that was due to the tsunami it generated. The tsunami, rather than strong shaking, caused nearly all of the damage and loss of life in the Tohoku-Oki earthquake as well. There are several factors that mitigate the damaging effects of these earthquakes somewhat. One is the depth of faulting, which is several 10 s of kilometers. Another is that the strongest shaking in an earthquake is usually in the direction of rupture, which for typical subduction geometries means that the strongest shaking can be expected to occur updip and offshore.

There are emerging evidences that the area of strongest high-frequency wave propagation in these extremely large subduction zone earthquakes is the downdip end and that when rupture approaches the surface under the deep ocean, it may slip massively but without generating strong high-frequency seismic waves ([Lay et al., 2012](#)). There are several mechanisms that may contribute to this behavior including the interaction of a shallow-dipping fault with the free surface ([Kozdon and Dunham, 2013](#)), possibly enhanced by relatively compliant hanging wall material ([Ma and Beroza, 2008](#)), strongly velocity-weakening fault material ([Shibasaki et al., 2011](#)), and pore fluid pressurization ([Mitsui et al., 2012](#)).

A particular kind of earthquake occurs in a region known as the 'outer rise.' The outer rise is an area of relatively high

topography, seaward of the trench, caused by flexural stresses from the downward bending of the subducting plate. Outer-rise earthquakes are thought to occur in response to these localized stresses in the subducting plate ([Chapple and Forsyth, 1979](#)). Despite the fact that convergent plate boundaries accommodate compressional deformation, both reverse and extensional normal faulting earthquakes are known to occur in the outer rise. These outer-rise earthquakes can be quite large. The damage due to shaking from them is usually less severe than for earthquakes on the subduction interface because they are more distant from land; however, outer-rise earthquakes can give rise to large and devastating tsunamis, such as in the case of the 1933 M_w 8.4 Sanriku event.

In some subduction zones, such as Japan, there is considerable deformation of the overriding plate as well. In the case of Japan, the upper-plate deformation is largely strike slip and is widely distributed. In cases where the plate convergence direction is highly oblique to the subduction zone, the slip is usually partitioned into trench-normal reverse slip on the subduction megathrust and trench-parallel strike slip in the overriding plate ([Fitch, 1972](#); [Yu et al., 1993](#)). Several explanations have been offered for this partitioning. [Savage \(1983\)](#) suggested that the downdip edge of the coupled zone would lead to localized horizontal shear arising from the strike-slip component of the relative plate motion at that locale. [Beck \(1983\)](#) suggested that shear strain in the overriding plate was controlled by a weak zone corresponding to the volcanic arc. Another explanation is that slip partitioning would occur on distributed fault systems if each fault will have a smaller total area than one large fault. Thus, the total resisting force, which is the product of the frictional strength and the fault area, will

Preliminary Determination of Epicenters

358,214 Events, 1963 - 1998

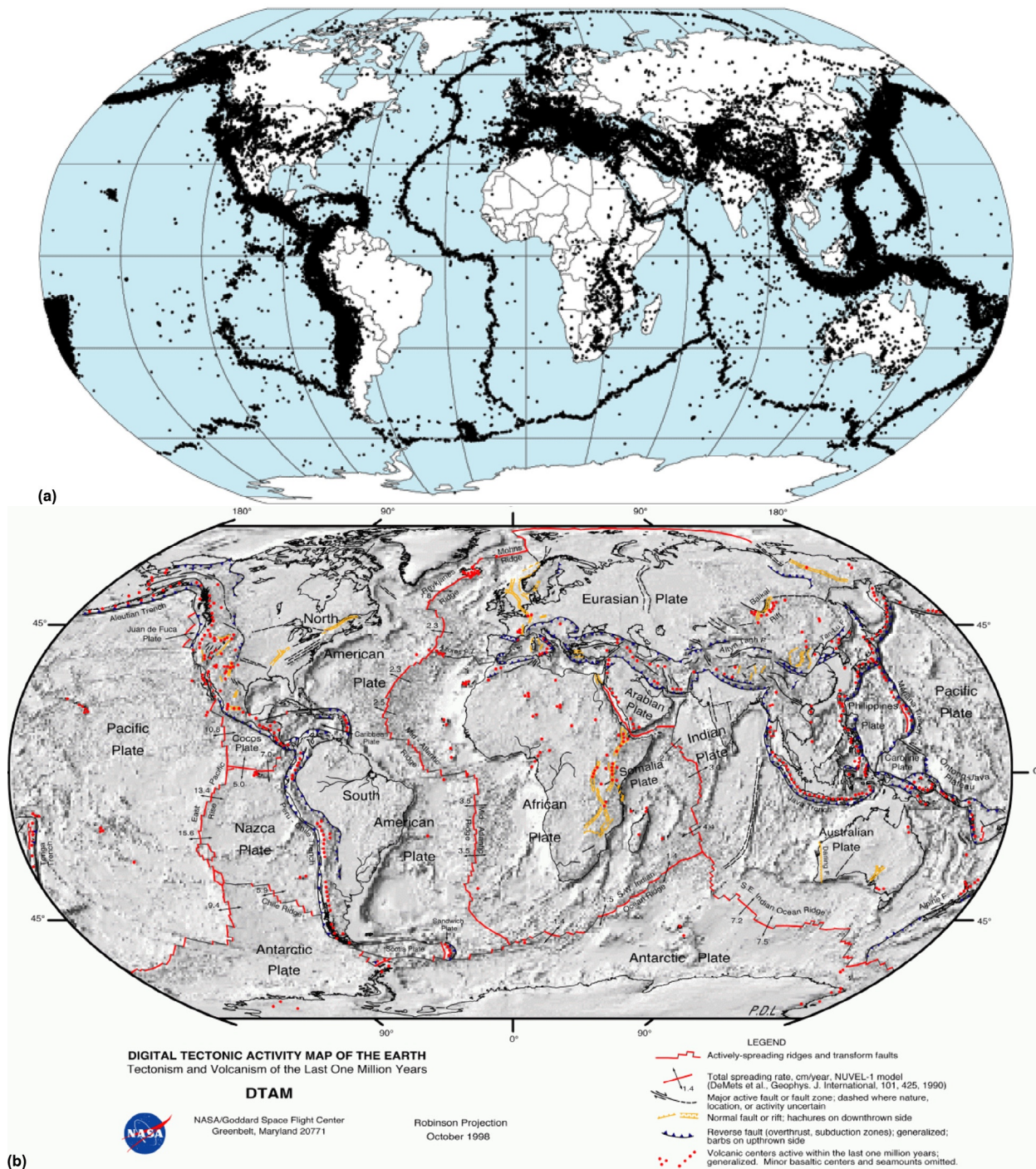


Figure 8 (a) Seismicity of the Earth for a 25-year time interval. Each black dot represents an earthquake and shows how earthquake activity limns global tectonic plate boundaries (reproduced from <http://denali.gsfc.nasa.gov/dtam/seismic/>). (b) Topography/bathymetry and the major tectonic plate boundaries of the Earth for a 25-year time interval. Note the close correspondence between plate boundaries and earthquake activity in **Figure 1(a)** (reproduced from NASA via Wikipedia Commons).

be lower, and hence, less force will be required to cause fault slip (McCaffrey, 1992). In subduction zones with oblique convergence, the strike-slip component of motion can be accommodated with less total frictional resistance if it occurs on a vertical strike-slip fault. Of course, this comes at the expense of having slip in more earthquakes. The trade-off between the two factors has been explored by Michael (1990), who determined simple geometries for which partitioning was energetically favorable.

Intermediate and deep-focus earthquakes, usually defined as earthquakes at depths of 70–300 km and 300–680 km, respectively, occur exclusively at convergent plate boundaries within subducting lithosphere. Figure 9 shows the global depth distribution of intermediate and deep-focus earthquakes. In some cases, the subduction zone that gave rise to the lithosphere at depth may no longer be active at the surface, such as for the Spanish deep-focus earthquake of 1954 (Chung and Kanamori, 1976). The mechanism of intermediate and deep-focus earthquakes is a topic of continuing debate as Earth materials at such great pressures and temperatures are expected to deform plastically; however, several mechanisms have been put forward to explain their occurrence.

Deep earthquakes are most numerous in places such as Tonga, where cold material is rapidly subducted to great depth. The Tonga-Kermadec region accounts for nearly 2/3 of the seismicity of >300 km depth. The largest known deep-focus earthquake is the M_w 8.3 Bolivia event of 1994 (Wu et al., 1995). A thorough investigation of deep earthquakes can be found in Chapter 4.13. Figure 10 shows the depth distribution of earthquakes in the Tonga subduction zone.

The spatial distribution of intermediate-depth earthquakes is less well understood than that of deeper earthquakes, though plate bending and subduction zone coupling appear to play important roles (Astiz et al., 1988). The largest known

intermediate-depth earthquake is the magnitude 8.1 Ryukyu Islands event of 1911. There is a great deal of variation in the behavior of intermediate-depth earthquakes. Intermediate-depth earthquakes reach magnitudes of at least M_w 7.8 (Astiz et al., 1988). For both intermediate and deep-focus earthquakes, we lack the kinematic plate tectonic boundary conditions that enable us to constrain the long-term probabilities of interplate earthquakes; hence, long-term forecasting of such earthquakes is by necessity based solely on statistical empiricism.

Some convergent plate boundaries involve continental crust on both plates. This occurs most notably along the Alpide belt, which includes the collision of Africa, Arabia, and India with southern Eurasia. Although in places, such as the eastern Mediterranean, this involves the subduction of small relict ocean basins, for the most part, continental collision zones entail the collision of relatively buoyant and weak continental crust that is not easily subducted. Deformation in these regions can extend many 100 s of kilometers from the main collision zone. In East Asia, the buoyancy of continental crust leads to the rise of the Himalayas and the Tibetan Plateau, as well as large strike-slip fault systems that allow buoyant crust to effectively flow away from the convergence zone. These zones give rise to some of the largest known strike-slip earthquakes, such as the great M_w 8.3 1905 Mongolia earthquake (Okal, 1992), and include major strike-slip fault zones, such as the North Anatolian Fault in Turkey.

As with earthquakes, much of the systematics of subduction zone volcanism was recognized before the advent of plate tectonics. Island arc volcanoes occur over subducting or recently subducted slabs. The melt that drives island arc volcanism is created when phase changes in the subducting slab give off water and other volatiles. When these come in contact with the surrounding mantle, the melting point is lowered, which in turn creates a buoyant melt that ascends and results in explosive volcanism. For detailed explanation of volcanic processes, see Chapter 4.14.

4.01.2.2.4 Intraplate earthquakes

Intraplate earthquakes occur far from plate boundaries and thus are not explained by the theory of plate tectonics. We distinguish here between earthquakes that occur within broad zones of plate boundary deformation, such as those in the Basin and Range province of western North America, and truly intraplate earthquakes, such as those in the New Madrid seismic zone of central North America. Earthquakes that fall into a sort of gray area between plate boundary earthquakes and true intraplate earthquakes include earthquakes in central and southern India and earthquakes in the East African Rift system. Locales of true intraplate earthquakes include Central Australia, Europe's Rhine Graben, Central Brazil, and large parts of oceanic crust under the Indian and Pacific Oceans. The M_w 8.6 11 April 2012 earthquake off the coast of Sumatra was a borderline intraplate event. It occurred under the Indian Ocean, offshore from the 2004 Sumatra earthquake, but the region in which it occurred had previously been identified as a potentially incipient plate boundary between the Australian and Capricorn plates (Royer and Gordon, 1997).

Why do intraplate earthquakes occur? About half of all intraplate earthquakes are observed to occur in failed

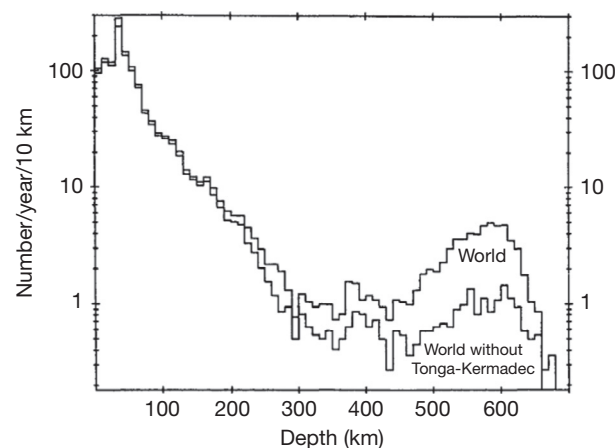


Figure 9 Depth distribution of earthquakes for the period 1/1964–2/1986 with mb five and larger. There is a steady decrease of seismicity up to ~300 km depth followed by a marked increase in seismicity below 500 km, with a maximum at ~600 km depth. The distribution is similar whether or not the prolific source of deep earthquakes in the Tonga–Kermadec region is included. Reproduced from Frohlich C (1989) The nature of deep focus earthquakes. *Annual Review of Earth and Planetary Science* 17: 227–254.

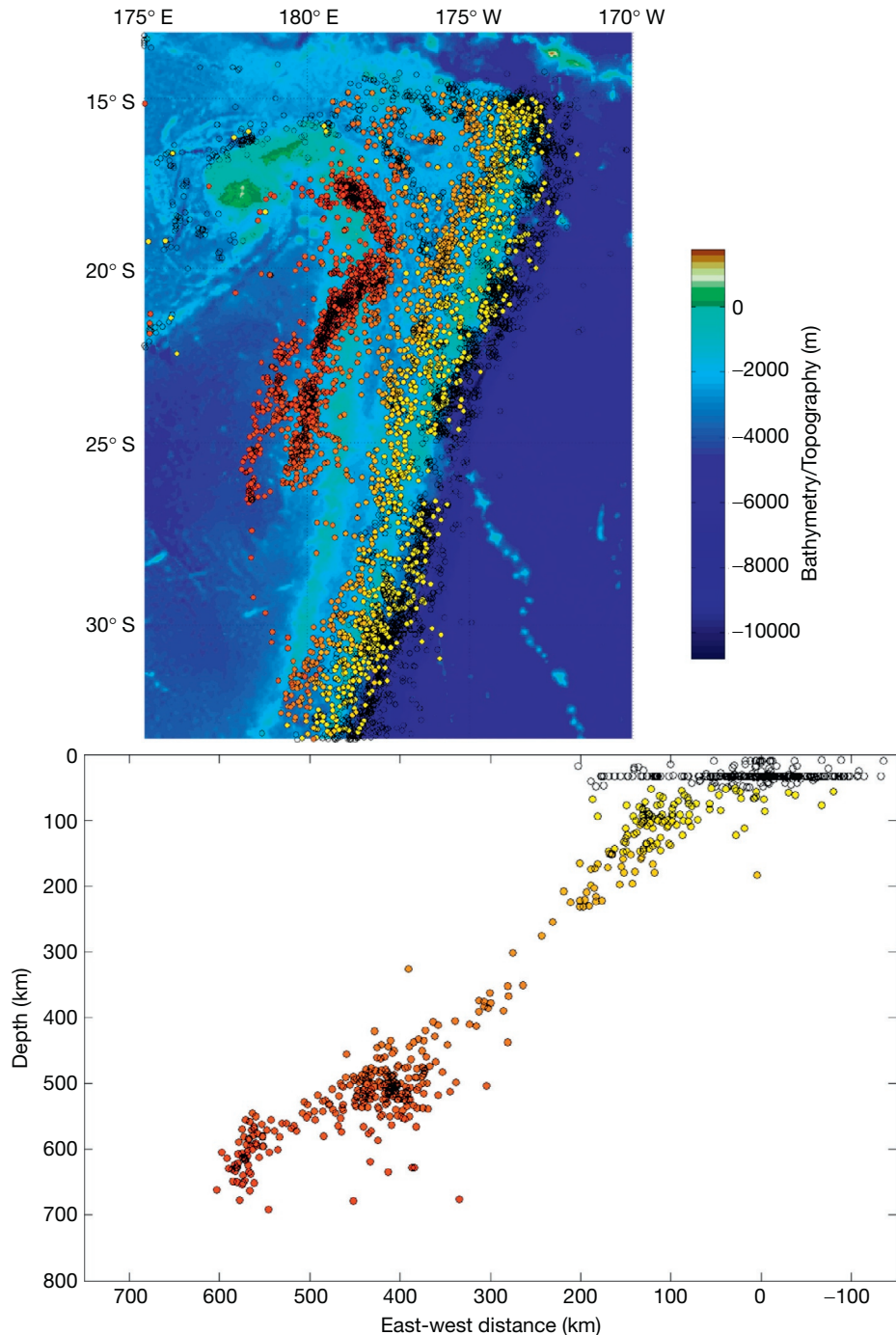


Figure 10 Top panel shows $M > 5$ seismicity (from CISN catalog for 1964–2006) in the Tonga region color-coded by depth of hypocenter. Tonga Trench is dark blue lineation in bathymetry. Open symbols represent earthquakes <50 km depth, yellow 50–100 km depth, and increasing red tone denotes increasing depth up to nearly 700 km. Horizontal lineation at 15 km is default depth used when depth is indeterminate. Lower panel shows E–W cross section at (24–27°S latitude). Rapid subduction of old lithosphere results in the world's most prolific source of intermediate and deep-focus earthquakes.

continental rifts ([Johnston and Kanter, 1990](#)). These are likely to be weaker than the unlifted continental crust around them, so it is reasonable to conclude that such intraplate earthquakes exploit this relative weakness. This does not appear to provide a universal explanation, however, as intraplate earthquakes in places such as Australia and oceanic plates do not occur on

such structures. Intraplate earthquakes respond to the ambient stress field, which supports the possibility that they are occurring due to relative lack of strength, rather than excess of stress. Other explanations for the driving mechanism behind intraplate earthquakes include stresses induced by the emplacement or sinking of plutons ([Kane, 1977](#)), postglacial rebound

(Arvidsson, 1996), and stress concentration due to the presence of a weak zone in otherwise strong crust (Campbell, 1978; Sbar and Sykes, 1973).

Regardless of their mechanism, it is clear that intraplate earthquakes do not account for a very large fraction of lithospheric deformation. If they did, then global plate motion models would fail closure tests. Strain rates due to intraplate deformation have an upper bound of 4×10^{-10} year $^{-1}$ (Gordon, 1998). Johnston and Kanter (1990) found that the cumulative seismic moment of intraplate earthquakes was about 0.5% of that of the Earth's total. Despite this small percentage, intraplate earthquakes do pose a significant seismic hazard and are occasionally quite large, such as in the 1886 Charleston earthquake, with an estimated moment magnitude of 7.6, or the New Madrid earthquake sequence of 1811–12, which by some estimates included three earthquakes of moment magnitude approximately equal to 8. More recent estimates of the magnitude of the large earthquakes in the New Madrid sequence are closer to 7.0 (Hough and Page, 2011).

4.01.2.2.5 Hot spot volcanism

As with intraplate earthquakes, there are important types of volcanoes for which plate tectonics does not have a ready explanation. These are known as hot spot volcanoes – areas of profuse volcanism that persist for 10 s of millions of years. Examples of hot spot volcanoes include some of the most famous and well-studied volcanic systems on Earth, such as Hawaii, Kerguelen, and Iceland. Yellowstone is a classic example of a continental hot spot volcano. Hot spot volcanism in the Earth's oceans tends to be characterized by effusive basaltic eruptions, whereas the interaction of basaltic magma with continental crust can lead to large-scale explosive rhyolitic volcanism. The ultimate magmatic source of hot spot volcanism remains a matter of some debate (Montelli et al., 2004), with some evidence pointing to a source in the lowermost mantle, while other evidence favors a shallower origin.

4.01.2.3 The Largest and Deadliest Earthquakes

The 12 largest instrumentally recorded earthquakes (updated from Kanamori, 1977) are listed in Table 2. All but one of them are plate boundary earthquakes in subduction zones. The largest instrumentally recorded earthquake was the 1960 Chile earthquake, which had a moment magnitude of 9.5 (instrumentation adequate for calculating reliable magnitudes has only been available since about 1900). The 1964 Good Friday earthquake in Alaska had a surface wave magnitude of 8.4 and a moment magnitude of 9.2. Put another way, the Alaska earthquake was 20 times larger than would be estimated from the surface wave magnitude. The 1989 Loma Prieta earthquake had a moment magnitude of 6.9. For comparison, the 1960 Chile earthquake involved nearly 7000 times the seismic moment of the Loma Prieta earthquake. The 1964 Alaska earthquake had nearly 3000 times the potency of Loma Prieta. The 1906 San Francisco earthquake had a moment magnitude of ~ 7.9 (this is more uncertain than the other estimates due to the sparse instrumentation at the time); hence, the seismic moment for that earthquake was about 30 times higher than for the Loma Prieta earthquake. There is no evidence for events

Table 2 The 12 largest earthquakes

Year	Location	M _w
1960	Chile	9.5
1964	Alaska	9.2
2004	Sumatra	9.2
2011	Japan	9.0
1952	Kamchatka	9.0
2010	Chile	8.8
1906	Ecuador	8.8
1965	Aleutians	8.7
2005	Indonesia	8.6
2012	Off-Sumatra	8.6
1957	Aleutians	8.6
1950	Assam	8.6

larger than the 1960 earthquake in the geologic record, and the extreme length, width, and slip of the 1960 Chile earthquake are impressive; however, given that the instrumental era in seismology spans only slightly more than 100 years, yet larger earthquakes have to be considered possible.

Half of the 12 largest recorded earthquakes have occurred in the past 10 years, which suggests a nonrandom clustering of great events. Several tests of significance, however, reveal that this flurry of activity does not represent a significant deviation from Poisson (random in time) behavior (Michael, 2011; Shearer and Stark, 2012).

Magnitude scales quantify the physical size and geologic impact of earthquakes, but the impact of earthquakes on human affairs depends strongly on where, when, and how they occur. Table 2 lists the ten deadliest earthquakes. In the case of the 2004 Sumatra earthquake, nearly all of the fatalities were caused by the tsunami that the earthquake generated. In the case of the 1923 Kanto earthquake, the firestorm that followed played a major role (Figure 11). In the 1556 Shaanxi and 1920 Gansu earthquakes, the widespread collapse of caves used as dwellings and carved into poorly consolidate loess magnified the losses tremendously. Five of the 12 deadliest earthquakes in history occurred in China, which is attributable to a long history of dense population in an earthquake-prone region (Table 3).

It is difficult to assess how reliable these numbers are. Certainly, for earthquakes that occurred 100 s of years ago, the reliability can be questioned. Even in the modern age, the devastation and confusion following such massive catastrophes, and the need to focus on recovery rather than counting fatalities in their immediate aftermath, mean that the true death tolls for these events will never be known accurately. For example, given the widespread and extreme devastation caused by the 2004 Indian Ocean earthquake and tsunami, the number of people lost in that catastrophe will never be known. Moreover, in some cases, political sensitivities may have influenced the reporting of casualties, contributing to the uncertainty. Unofficial estimates of the death toll of the 1976 Tangshan earthquake (Figure 12) range as high as 655 000. Following the 1999 Izmit, Turkey, earthquake (not listed), authorities stopped counting when the death toll reached $\sim 18\,000$. Using several lines of evidence, Marza (2004) suggested a lower bound of the death toll in this earthquake



Figure 11 Print depicting the firestorm that followed the 1923 Kanto, Japan, earthquake. The earthquake and firestorm that followed devastated the Tokyo–Yokohama metropolitan area and are estimated to have killed 143 000 people. Reproduced from <http://www.rekihaku.ac.jp/e-rekihaku/109/pic19.jpg>.

Table 3 The 12 deadliest earthquakes

Year	Location	Fatalities
1556	Shaanxi, China	830 000
2004	Sumatra, Indonesia	283 106
1976	Tangshan, China	255 000
1138	Aleppo, Syria	230 000
2010	Port-au-Prince, Haiti	228 000
856	Damghan, Iran	200 000
1927	Tsinghai, China	200 000
1920	Gansu, China	200 000
893	Ardabil, Iran	150 000
1923	Kanto, Japan	143 000
1948	Turkmenistan, USSR	110 000
2008	Wenchuan, China	87 000

as 45 000. There is considerable uncertainty about the loss of life in the 2010 Haiti earthquake as well. Whatever their precise toll, one thing is clear: earthquakes can be devastating. At their worst, they rank among the most extreme, sudden catastrophes humankind has to cope with.

Due to the rapid growth of the Earth's population, the concentration of that growth on the earthquake-prone areas of the Pacific Rim, and the urbanization accompanying that growth, vulnerability to earthquakes is growing. This is true despite steady and considerable progress in earthquake-



Figure 12 Photo showing nearly complete devastation in the Lunan District of the city of Tangshan from the 1976 Tangshan, China, earthquake (Huixian et al., 2002). Tangshan was a major industrial center with a population of one million before the earthquake, which occurred directly under the city at 3:42 a.m. About 93% of residential buildings and 78% of commercial buildings in the city were destroyed (Yong et al., 1988). The officially reported death toll is 255 000, but estimates are as high as 655 000.

resistant engineering. [Bilham \(1995\)](#) suggested that an earthquake within the next 30 years with over a million fatalities is not out of the question.

Loss of life represents the most important vulnerability to earthquakes, but it is not the only one. Economic losses in earthquakes can be grave as well. For example, by some estimates ([Risk Management Solutions Inc, 1995](#)), a repeat of the 1923 Kanto, Japan, earthquake would likely result in direct economic losses of over 2 trillion dollars (44–70% of Japan's GDP) – a financial event that would be without historical precedent and that would have far-reaching global consequences.

4.01.2.4 Historic and Prehistoric Earthquakes

For the purposes of discussion, we define 'historic' to denote an earthquake for which there are written accounts, but that occurred before the dawn of instrumental seismology in the last decade of the nineteenth century, so that there is no instrumental record of ground motion. We use the term 'prehistoric' to denote an earthquake that occurred so long ago that there is no written record of it.

Some earthquakes have had a significant impact on the course of history. Crushed skeletons in ruins of the ancient world provide compelling evidence that destructive earthquakes occurred in the cities of Troy, Megiddo, and Jericho. They may be the inspiration for the Old Testament story about the fall of the walls of Jericho. Megiddo (Armageddon) is thought to have been the inspiration for the biblical story of the apocalypse. The 1755 Lisbon earthquake made a deep impression on philosophers in eighteenth-century Europe. The earthquake occurred on a Catholic holiday, destroyed many churches and much of the city through a combination of strong shaking, fire, and tsunami. The Lisbon earthquake

([Figure 13](#)) coincides in time with, and may have helped bring about, the decline of Portugal as a major world power. Some have argued that the destruction and chaos brought about by the devastating 1923 Kanto earthquake led to fervent Japanese nationalism that helped fuel World War II. The expropriation of international relief funds for recovery from the 1972 Managua, Nicaragua, earthquake is thought to have helped bring about the communist takeover of that country shortly afterward. The devastation wrought by the 1976 Tangshan earthquake was followed within months by the death of Mao Tse-tung and the end of the Cultural Revolution. For a more detailed discussion on ancient earthquakes and the role of earthquakes in history, see [Chapter 4.22](#).

Prehistoric earthquakes are in some cases studied using archeology. It is far more common, however, to study them using geology. This field of earthquake science has come to be known as paleoseismology. The field of paleoseismology allows geologists to address questions, such as whether or not a fault is active and what the nature of earthquake recurrence is, that are difficult or even impossible to address by other means. For a detailed discussion of paleoseismology, see [Chapter 4.21](#).

4.01.2.5 Earthquake Size Distribution

Small earthquakes are much more common than large earthquakes. This statement is usually quantified in seismology using the frequency–magnitude relation – that is, an equation that describes the relative frequency of large versus small earthquakes. The frequency–magnitude relation is widely observed to follow Gutenberg–Richter statistics, named for the same seismologists who developed the magnitude scale. If $N(M)$ is the number of earthquakes of magnitude M or larger, then frequency–magnitude relation can be expressed as



Figure 13 Copper engraving depicting the 1755 Lisbon, Portugal, earthquake of 1 November 1755 with fire ravaging the city and a tsunami destroying ships and the waterfront.

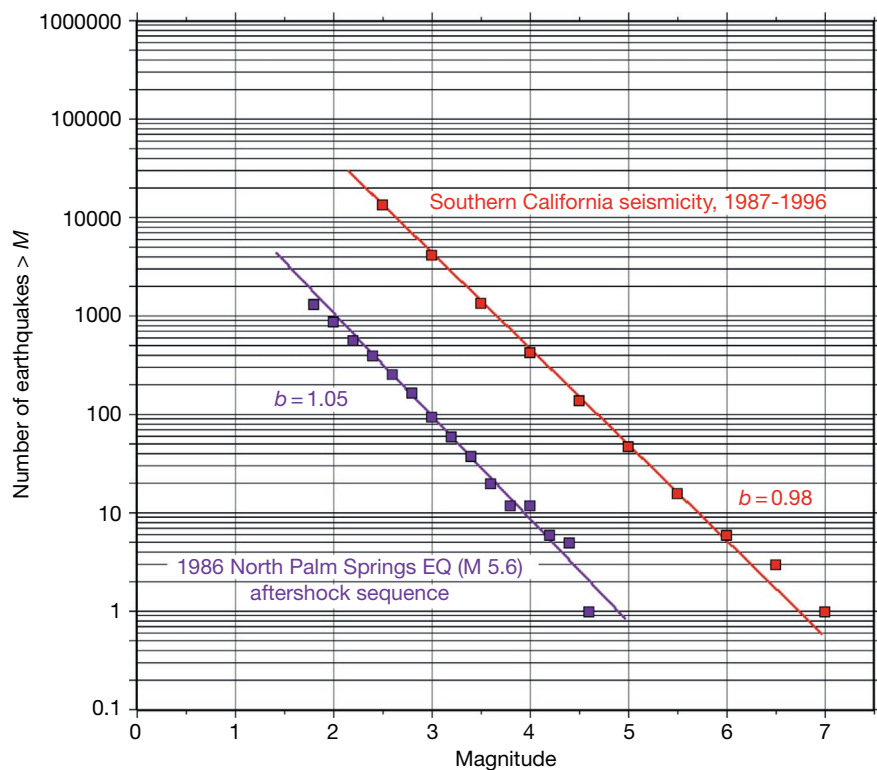


Figure 14 Fit of the cumulative form of the Gutenberg–Richter distribution for two earthquake populations: the 1986 North Palm Springs aftershock sequence (mainshock removed) and a decade of seismicity in all of Southern California. In both cases, the b -value is ~ 1 . Reproduced from <http://www.data.scec.org/Module/Pics/s2inset1.gif>.

$$\log N(M) = a - bM$$

(Gutenberg and Richter, 1956). Two examples of earthquake populations that follow such a frequency–magnitude relation are shown in Figure 14. This linearity in semilog space describes a power law, with the a -value (intercept) corresponding to the number of magnitude 0 or larger earthquakes in the population considered and the b -value (slope) describing the relative number of large versus small earthquakes. While, the a -value is dependent on the population size and hence has no obvious physical significance, the b -value describes the relative frequency of large and small events regardless of the population size. A b -value of 1 means that for each unit magnitude increase, there is a factor of 10 reduction in the number of earthquakes.

For many earthquake populations, including the global seismicity dataset, a b -value of ~ 1 describes the relative numbers of large versus small earthquakes. For individual faults, however, the frequency–magnitude relation may fail to describe earthquake populations adequately (Wesnousky, 1994), and to the extent that they do, there is evidence that the b -value for an individual fault may decrease systematically with the maturity of a fault system (Stirling et al., 1996). For volcanic systems, b -values are typically much higher than for tectonic faults, sometimes reaching values as large as three (McNutt, 2005), indicating that the seismicity associated with active magmatic systems can be extraordinarily rich in very small earthquakes.

By combining the definition of the moment magnitude with the frequency–magnitude relation, it is straightforward

to demonstrate that the largest earthquakes on a fault system dominate the slip budget. Combining the frequency–magnitude relation with the definition of the moment magnitude yields the following proportionality between the cumulative seismic moments as a function of earthquake magnitude, M :

$$\sum M_0(M_W) \sim 10^{(1.5-b)M_W}$$

From this, it is apparent that if the b -value is < 1.5 , the largest earthquakes will dominate the seismic moment budget. For the globally representative value of $b=1$, the seismic moment contribution increases by a factor of $10^{0.5}$, or ~ 3.2 , with each increase in magnitude. The relationship between magnitude and seismic energy has the same dependence (Gutenberg and Richter, 1942). Thus, as was recognized by Richter in his original paper on earthquake magnitude, nearly all the energy is released by the largest earthquakes. A direct consequence of this is that little earthquakes do not relieve appreciable strain energy in large fault systems and cannot act as a ‘safety valve’ for large earthquakes.

4.01.2.6 Earthquake Location

An earthquake’s hypocenter is defined as the temporal and spatial coordinates where seismic waves are first generated. Earthquake location has long been routine, but there continues to be important progress in developing more precise earthquake locations. The fundamental observations used to estimate earthquake locations are seismic wave arrival times. Over

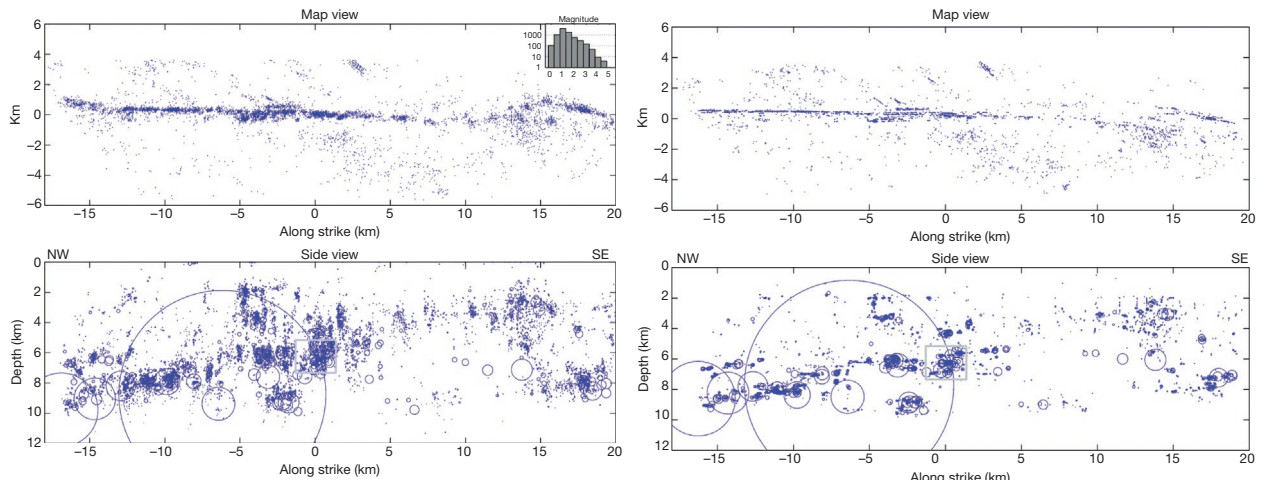


Figure 15 Seismicity on the Calaveras Fault before (left) and after (right) double-difference earthquake relocation using cross correlation-based arrival time measurements (Schaff et al., 2002). Both map and side views are shown for the two cases, which show nearly 8000 earthquakes. Earthquakes are shown as circular sources assuming constant stress drop. The improved locations are evident in the narrow width of fault structures at depth and in the large number of repeating earthquakes found on this fault. Such improved locations allow testing of diverse hypotheses regarding earthquake fault mechanics.

the last decade, precise earthquake location methods (e.g., Waldhauser and Ellsworth, 2000) coupled with the use of waveform cross correlation on large waveform databases to reduce measurement error (e.g., Schaff et al., 2004) have revolutionized our ability to resolve the fine structure of fault zones (Figures 15 and 16).

By using waveform cross correlation on large numbers of similar waveforms, seismologists have been able to reduce the uncertainty in arrival time measurements. For similar earthquakes, it is straightforward to reduce the measurement error of arrival times to several milliseconds for regional seismic networks. Since the measurement error maps directly into location uncertainty, the result is greatly improved earthquake locations. Arrival time measurement using cross correlation is not a new idea in seismology (Poupinet and Ellsworth, 1984), but only recently with the widespread availability of massive waveform datasets and computers capable of analyzing them has this approach reached its full potential.

The second advance that has led to improved locations is the expansion of the use of joint hypocentral location methods, particularly ones that are designed to minimize the effects of Earth structure on the solutions. These methods focus on precision (i.e., relative earthquake locations) rather than accuracy (absolute earthquake locations). These methods solve for the position of a large population of earthquakes simultaneously and when used with differential arrival time measurements allow seismologists to reduce the effects of unmodeled velocity structure on arrival times. Through such techniques, which are analogous to adaptive optics in astronomy, it is possible to reduce earthquake location errors dramatically. For the example shown in Figure 15, Schaff et al. (2002) documented a reduction in hypocentral uncertainty by an order of magnitude in their relocations. As with large-scale waveform cross correlation, enhanced computational capability has been an essential element in large joint hypocentral determinations.

An intriguing finding based on highly precise earthquake locations is the discovery of slip-parallel ‘streaks’ of seismicity

(Rubin et al., 1999; Figure 16). These streaks have been observed in diverse environments, including the southeast rift zone of Kilauea volcano, Hawaii, as well as the San Andreas, Calaveras, and Hayward Faults in California. Waldhauser et al. (2004) examined several such streaks along the Parkfield segment of the San Andreas Fault and concluded that, in one case, they may mark the boundary between locked and slipping parts of the fault, while in another case, they are more easily explained as a result of a discontinuity in geologic structure.

4.01.3 The Earthquake Source

Most of the measures of earthquake size and the determination of earthquake locations that we have discussed in the previous section, with the exception of the seismic moment, do not require a quantitative theory of the earthquake source. In this section, we outline some of the applications of earthquake source theory to seismology. Chapter 4.02 provides a much more detailed and complete treatment.

4.01.3.1 Point-Source Parameters

Quantitative studies of the earthquake source usually treat the Earth as an elastic continuum, with the exception of the fault itself, which is assumed to be a discontinuity having infinitesimal width. These are both approximations that are not uniformly valid and must be kept in mind when interpreting source characteristics. The source of nearly all earthquakes is shear slip on faults. To first order, faults represent planar discontinuities within the Earth and the shear slip occurring on them is parallel to that fault surface. Equation [45] of Chapter 4.02 expresses the displacement seismogram at a point, x , as a function of time, t , as an integral over the fault surface and time of the fault slip history, $\Delta u_j(x_0, \tau)$:

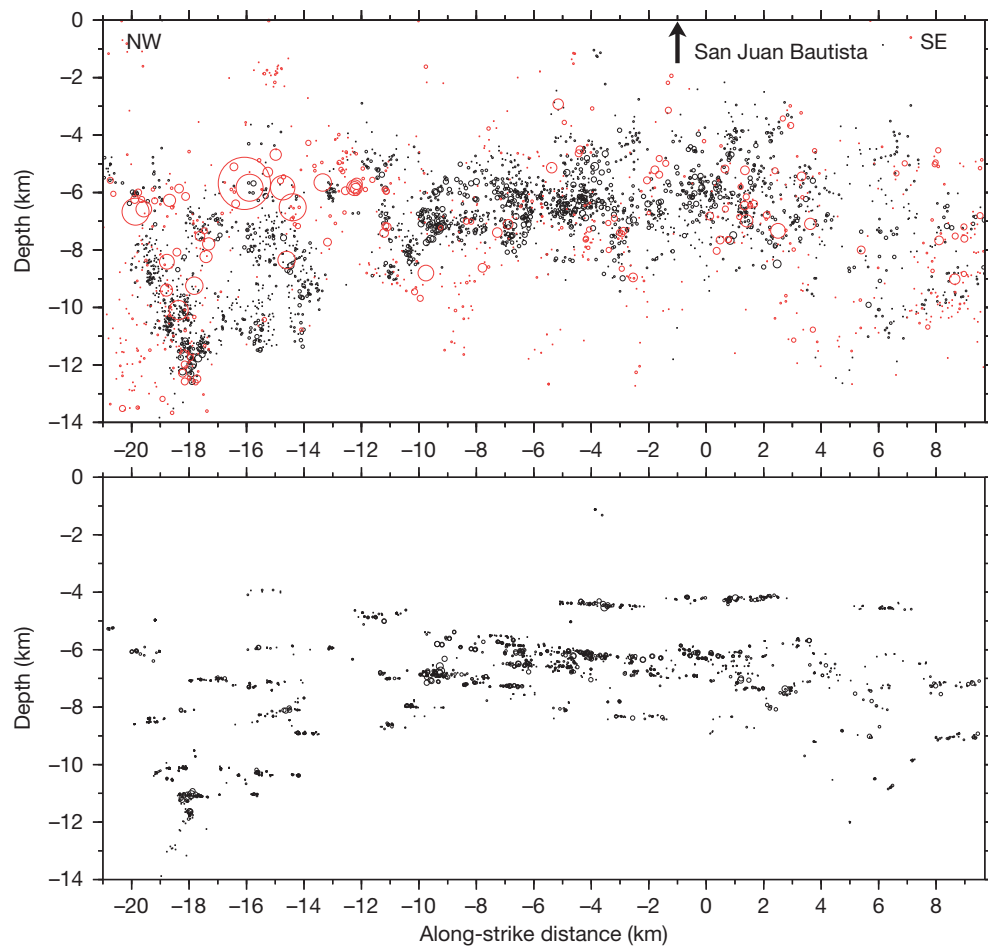


Figure 16 Network locations of microearthquakes on a vertical cross section along the San Andreas Fault near San Juan Bautista (Rubin et al., 1999) are shown on the upper panel. Red circles in upper panel represent larger events that were not relocated because waveforms were clipped. Circles denote estimated slip area for larger events. Lower panel shows same events after relocation. The horizontal seismicity streaks, which were previously obscured by location errors, emerge in the relocated catalog.

$$u_i(x, t) = \int_0^t \int_{S_{x_0}} \mu(x_0) \Delta u_j(x_0, \tau) G_{ij,k}(x, t | x_0, \tau) n_k(x_0) d^2 x_0 d\tau$$

The other terms in the integral – the shear modulus, μ ; Green's function gradient, $G_{ij,k}$; and the fault-plane normal vector, n_k – together represent the traction across the fault surface due to an impulsive point source acting at the receiver.

If the wavelengths considered are much larger than the rupture dimension, and if we record seismic waves sufficiently far away from the source, then we can make the point-source approximation. In this case, variations in Green's function, G , with position on the fault, x_0 , are negligible and the integration mentioned earlier becomes trivial. Other approximations include a high-frequency approximation, wherein only the far-field ($1/r$) terms in Green's function make important contributions to the seismogram. This approximation is valid once the receiver is several wavelengths from the source ($\omega r/\beta \gg 1$) and allows the integral mentioned earlier to be simplified since only terms that can be calculated using ray theory need be retained. An intermediate assumption, analogous to the Fraunhofer approximation in optics, is that Green's function varies over the fault plane, but only in phase. This leads to a simplification of the integral mentioned previously into one in which

the G is outside the integral and results in an expression for the far-field pulse shape, which represents the dependence of the far-field wave amplitude with time. The development of the theory and approximations outlined earlier are covered in greater detail in [Chapter 4.02](#).

4.01.3.2 Sense of Faulting from First Motions

The polarity of the first-arriving P-waves can be used to determine a focal mechanism, which is a representation that plots the polarity of waves as a function of takeoff angle from the source. For a shear-slip source, the P-waves will have four lobes, two of which have compressional first-arriving P-waves and two of which have dilatational first-arriving P-waves ([Figure 17](#)). At 45° , from these lobes are two planes for which the P-wave amplitude is nodal. One of these planes is the true fault plane of the earthquake, while the other is known as the 'auxiliary' plane. From the polarity of the P-waves, it is impossible to distinguish these two planes from one another. Indeed, in the point-source approximation, the entire seismogram, not just the first motion polarity, is identical for slip on either one of these planes. This leads to a fundamental fault-

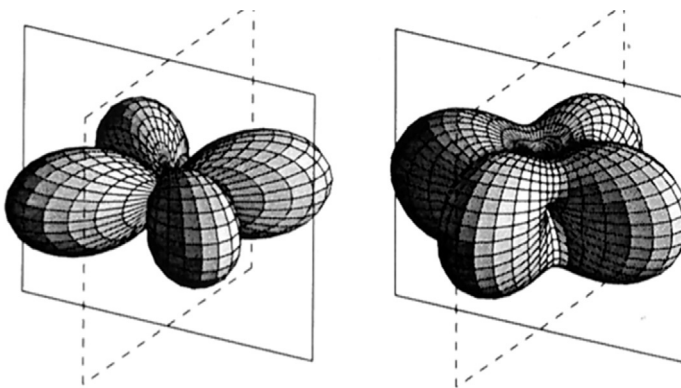


Figure 17 Radiation patterns for a strike-slip fault showing the amplitude of P-waves on the left and the amplitude of S-waves on the right. The four-lobed P-wave radiation pattern has two compressional and two dilatational lobes. The fault plane and auxiliary plane, for which P-wave amplitude is nodal, separate the four lobes. The lobes of the radiation pattern are separated by quadrants in the usual depiction of the focal mechanism. Reproduced from Julian BR, Miller AD, and Foulger GR (1998) Non-double-couple earthquakes 1. Theory. *Reviews of Geophysics* 36: 525–549.

plane/nodal-plane ambiguity. Without independent information, such as geologic information on the fault orientation, alignment of earthquake hypocenters, or finite-source effects in the waveforms (i.e., a breakdown of the point-source assumption), it is impossible to tell the two planes apart. The sense of faulting as determined using the P-wave radiation pattern using earthquake focal mechanism solutions provided a key test of the theory of plate tectonics in which the sense of motion on oceanic transform faults was found to be consistent with the plate tectonic prediction (Sykes, 1967).

4.01.3.3 Moment Tensor Representation

A more general representation of a point source of seismic waves is provided by the seismic moment tensor. The moment tensor can be used to represent the seismic source as a pair of force couples – the so-called double-couple solution, which is the point-source equivalent force distribution for a dislocation source. The determination of seismic moment tensors for earthquakes is now routine such that there exist catalogs of moment tensor solutions at both the regional scale and the global scale. Perhaps, the best known of these is the Harvard Centroid Moment Tensor (CMT) catalog (Dziewonski et al., 1981) and its successor the Global CMT Project, which contains moment tensor solutions for over 20 000 earthquakes worldwide (Figure 18). Similar catalogs of earthquake mechanisms, whether based on first motion focal mechanisms or waveform-based moment tensor inversions, are available for thousands of locally recorded earthquakes where local seismic networks provide the data to make such work possible.

The strength of the moment tensor representation is that it can be used to describe sources other than shear slip on faults. Sources with isotropic (volumetric), or deviatoric, but not planar shear slip, have been studied using seismic waves, most often in volcanic environments. Single-force solutions have also been applied to describe the sources of seismic waves for large landslides, such as the one that initiated the 1980 eruption of Mt. St. Helens (Kanamori and Given, 1982). For more details on moment tensors and their application to the study of earthquakes, see

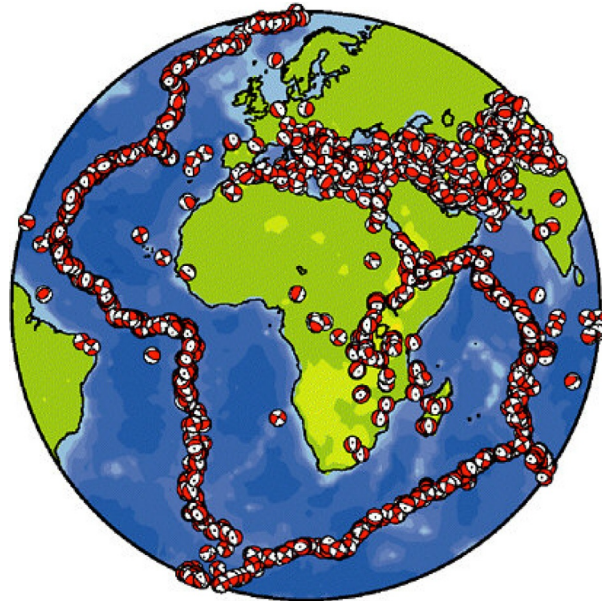


Figure 18 First motion focal mechanism representation of CMT solutions from the Harvard catalog for earthquakes around the continent of Africa for the 25-year period (1976–2000). Reproduced from National Research Council of the National Academies (2003) Living on an Active Earth, perspectives on earthquake science. Committee on the Science of Earthquakes Board on Earth Sciences and Resources Division on Earth and Life Studies. Washington, D.C.: The National Academies Press.

Chapters 4.02 and 4.18. For applications to volcano seismology, see Chapter 4.15.

4.01.3.4 Seismic Energy

A point-source parameter that is important, but for which estimates are far from routine, is the radiated seismic energy. The radiated energy is typically calculated by measuring the energy flux at a point, or points, where the wave field of an earthquake is recorded, and from that inferring the total energy flux in all directions from the earthquake source. The radiated energy is broadband, with most of the energy being radiated at frequencies higher than a frequency known as the ‘corner’ frequency (Singh and Ordaz, 1994).

Seismic sources can be characterized by an overall length scale. Waves of sufficiently low frequency will have corresponding wavelengths that are much larger than that source dimension. Waves of sufficiently high frequency, on the other hand, will have corresponding wavelengths that are much smaller than that of source dimension. In this latter case, the amplitude of seismic waves will suffer from interference effects and hence have smaller amplitudes in the far field. The crossover frequency, at which wavelengths are comparable to the seismic source dimension, is known as the corner frequency. The corner frequency can be used to infer the characteristic size of the seismic source.

Strictly speaking, because the corner frequency defines the frequency at which finite-source effects start to become important, the seismic energy is not truly a point-source parameter. As a scalar measure of earthquake strength, however, it is natural to consider it as such. Obtaining the necessary bandwidth with sufficient signal-to-noise ratio, and correcting for propagation effects over that wide bandwidth, is what makes the radiated energy so difficult to calculate reliably ([Ide and Beroza, 2001](#)). The study of seismic energy, both its measurement and its implications for the physics of earthquakes, is the subject of an entire AGU monograph ([Abercrombie et al., 2006](#)).

4.01.3.5 Extended-Source Models of Earthquakes

The success seismologists have had in cataloging basic point-source earthquake parameters, particularly location, origin time, moment tensor, and seismic moment contrasts with attempts to estimate higher-order source parameters. This is natural in that these extended-source measurements involve either spatial or temporal dimensions, that is, slip duration, directivity, stress drop, and moment-rate function, that can be difficult to resolve. Methods to recover these parameters remain an area of active research.

Studies of the earthquake source are sometimes divided into ‘kinematic’ and ‘dynamic’ studies. The adjective ‘kinematic’ is used in seismology to describe models of an earthquake that estimate source parameters without explicit consideration of the failure mechanism on the causative fault. This is not necessarily a negative property. With our incomplete knowledge of fault mechanics, it is likely that dynamic models, which seek to incorporate what we think we know about earthquake physics, may be incorrectly biased by those assumptions. The hope is that observations of earthquake kinematics will inform dynamic models of fault behavior and that dynamic models will motivate kinematic modeling that tests dynamic hypotheses. We start our discussion of kinematic source models with point-source models.

4.01.3.5.1 Kinematic source models

The moment tensor representation that is used to describe earthquakes in the point-source approximation can be extended to finite sources using an expansion in higher-order moments ([Backus and Mulcahy, 1976](#)). [McGuire et al. \(2002\)](#) applied this formalism to recover the degree-two moments of large earthquakes recorded at teleseismic distances. They found that in 80% of the earthquakes studied, rupture was unilateral (rupture initiated at one end of the rupture zone) rather than bilateral (rupture initiated near the center of the rupture zone).

For the most part, seismologists have not applied the formalism of higher-order moments to the study of the earthquake source. This may be due to a desire to image the source directly as the spatial and temporal evolution of slip on a fault.

A great deal of work has gone into imaging earthquake rupture directly as slip on a fault (or faults) using seismic waves. For some earthquakes, important additional constraints have been provided by geodetic measurements or field measurements of surface rupture. [Chapter 4.09](#) details approaches taken for imaging earthquake rupture.

As shown by [Ide et al. \(2005\)](#), the nonuniqueness of the fault slip inverse problem is extensive. When there are insufficient near-source data, such as for the 1999 Izmit, Turkey, earthquake, slip models developed by different investigators bear little resemblance to one another. In contrast, well-recorded earthquakes like the 1999 Chi-Chi, Taiwan, earthquake will yield much more robust results. For all but extremely large events ([Ishii et al., 2005](#)), extended-source images are difficult to recover without near-source data. As a result, most of the information available on source finiteness derives from well-instrumented areas like Japan and California.

A large earthquake may rupture multiple-fault segments. Modeling of strong ground motion recordings of large earthquakes suggests that fault rupture typically propagates at about 80% of the shear-wave velocity, although there is evidence that the rupture velocity can locally exceed the shear-wave velocity ([Bouchon and Vallée, 2003](#); [Bouchon et al., 2001](#); [Dunham and Archuleta, 2004](#)). The slip velocity across the fault is much more difficult to constrain but is thought to be on the order of meters per second in a large event ([Heaton, 1990](#)). In addition to constraints on the evolution of slip in earthquakes, it is clear from all studies that have sufficient resolution that slip is strongly variable with position on the fault ([Mai and Beroza, 2002](#)). [Figure 19](#) shows examples of variable slip models for five different earthquakes.

Following the 2004 Sumatra earthquake, [Ishii et al. \(2005\)](#) pioneered a new approach to source imaging. Their back-projection approach uses coherent signals recorded across an array to stack coherent energy over a relatively narrow frequency band. It has distinct advantages over slip inversion because it more readily allows for multiple-segment or temporally complex rupture such as observed in the 2012 off-Sumatra earthquake ([Meng et al., 2012](#)); however, it does not image a physical quantity (fault slip) as traditional kinematic source inversions do. More on back-projection and kinematic source inversion can be found in [Chapter 4.09](#).

4.01.3.5.2 Dynamic source models

Dynamic source models differ from kinematic models in that they explicitly consider the stress associated with fault slip and attempt to model stress, slip, and the evolution of rupture using a failure criterion. In some cases, the evolution of the rupture is prescribed, and the relevant physical parameters are calculated. Quasidynamic rupture models ([Quin, 1990](#)) fall within this category. In others, the fault is allowed to evolve based on the initial conditions and a failure criterion for the fault surface. A dynamic model such as this is referred to as a ‘spontaneous’ model because once initiated, the rupture propagates spontaneously as long as the energy balance allows it to be self-sustaining ([Kostrov and Das, 1988](#)). A third class of

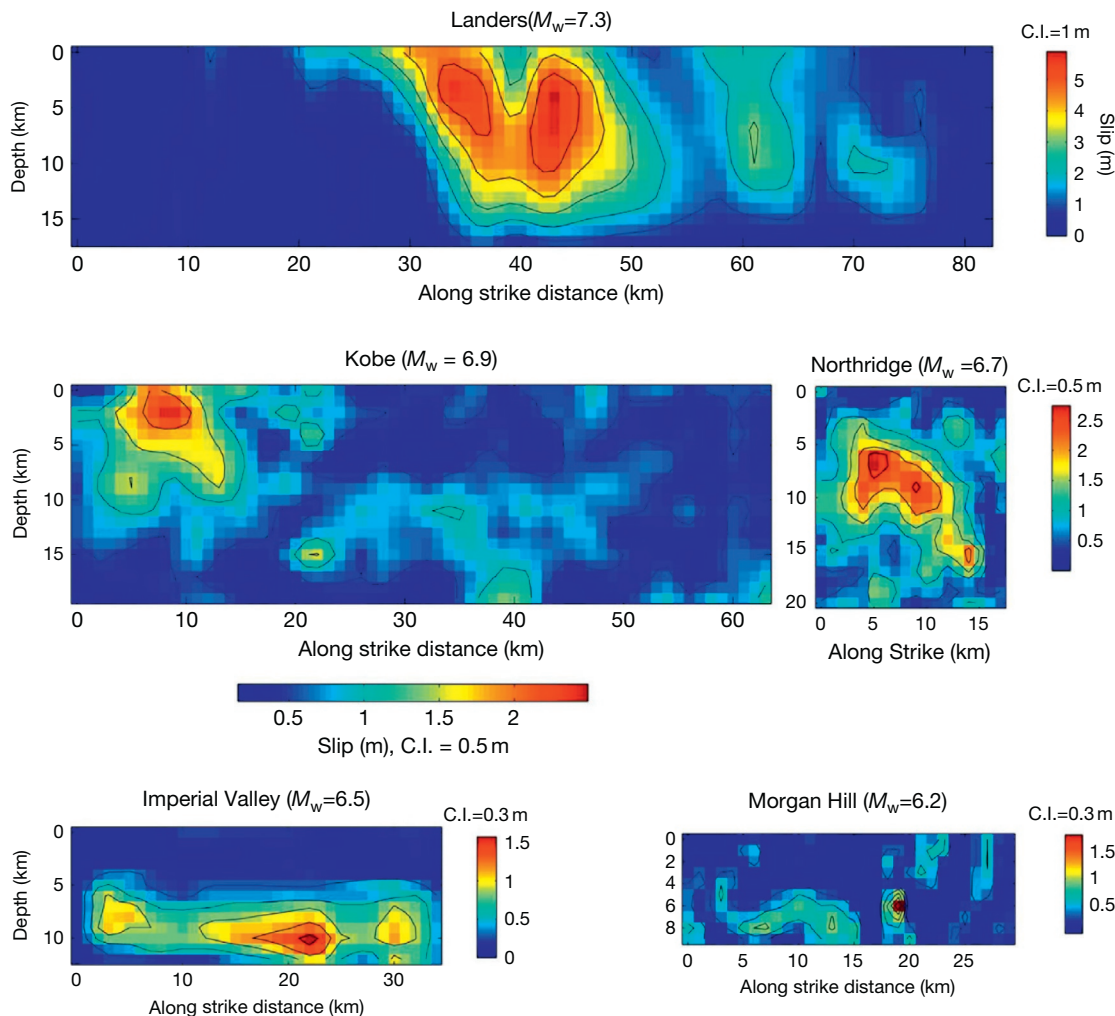


Figure 19 Side view of slip models for five different earthquakes, including the 1992 Landers, California; the 1995 Kobe, Japan; the 1994 Northridge, California; the 1979 Imperial Valley, California; and the 1984 Morgan Hill, California, earthquakes. In each case, slip is strongly variable over the fault surface. Reproduced from Mai PM and Beroza GC (2002) A spatial random-field model to characterize complexity in earthquake slip. *Journal of Geophysical Research* 107(B11): 2308, <http://dx.doi.org/10.1029/2001JB000588>.

dynamic rupture models does not assume the fault plane a priori but instead allows it to evolve based on a failure criterion for the medium. This is potentially quite important because as rupture speed increases, out-of-plane stresses come to dominate stresses in the direction of rupture and hence favor non-planar faulting.

Dynamic faulting models are typically based on fracture mechanics – an approach that was originally developed for tensile opening-mode cracks. In ideal elastic-brittle crack models, the crack tip separates unslipped from slipping fault surface. Stress in the unslipped region immediately ahead of the crack tip is infinite, but it is an integrable singularity such that the amount of energy expended at the crack tip is finite. Such a singularity is unrealizable in the real Earth, so models have been developed that require a breakdown zone ahead of the crack tip in which shear traction remains finite as the crack tip approaches. For a detailed treatment of the application of fracture mechanics to modeling earthquake dynamics, see Rice (1980) and Chapter 4.03.

Dynamic rupture modeling is challenging for several reasons. The need to keep track of stress during rupture means that the entire past history of faulting within the cone of causality is required to calculate the stress on each point on the fault. The need to simultaneously track the large scale of the entire fault rupture and the small-scale heterogeneity near the crack tip presents computational challenges. If grid size is not sufficiently small, then dynamic rupture models can develop an unphysical grid-size dependence. In the presence of material contrast across the fault or of strong velocity weakening, there is the additional complication of numerical instabilities to deal with. Finally, to model multiple earthquake cycles, steady strain accumulation with timescales of centuries and sudden release with timescales of seconds must both be resolved.

A complete discussion of dynamic source modeling is well beyond the scope of this chapter. Recent work in this area has addressed the possibility that material contrast across a fault zone might lead to a direction of preferred rupture (Andrews and Ben-Zion, 1997), whether strong velocity weakening

occurs during seismic faulting (Perrin et al., 1995), the origin of heterogeneity over many earthquake cycles (Lapusta et al., 2000), and attempts to generate dynamic rupture models that emulate the salient properties of kinematic rupture models as in Figure 20 (Peyrat et al., 2001).

There are several recent trends in dynamic rupture modeling. One is the inclusion of 3-D fault geometry to more accurately portray the likely effects of such heterogeneity on dynamics (Kozdon et al., 2013). Another is the inclusion of off-fault plastic deformation in the presence of large stress concentrations (Dunham et al., 2011), which may be particularly important near the Earth's surface where the confining stress is low (Ma and Andrews, 2010).

4.01.3.6 Volcano Seismology

As with earthquakes, seismology provides a key source of information on how volcanoes work. Unlike earthquakes, eruptions on well-instrumented volcanic systems are routinely predicted and seismological monitoring plays a key role in this capability. Volcanic systems are often highly seismic with literally millions of earthquakes. Volcanoes exhibit a rich range of behaviors that lead to diverse seismic signals.

Figure 21 shows a suite of long-period earthquakes at several volcanoes.

One signal of particular note is volcanic tremor. Volcanic tremor has a range of behaviors, but it often occurs as ground

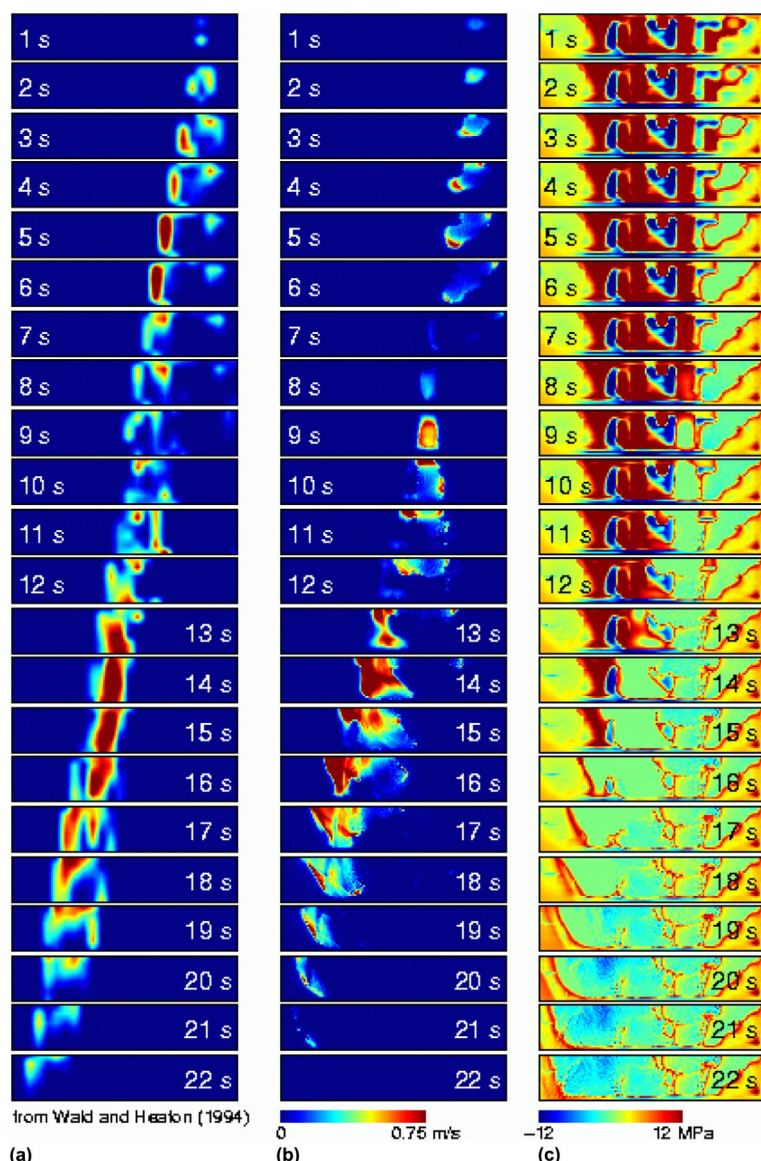


Figure 20 Comparison of kinematic and dynamic rupture models for the 1992 Landers, California, earthquake. Left column shows snapshots of kinematic model from [Wald and Heaton \(1994\)](#), middle column shows snapshots of dynamic rupture models of [Peyrat et al. \(2001\)](#), and right panel shows stress change accompanying dynamic model. Both models fit the long-period strong ground motion data, but predictions of strong ground motion at higher frequencies would vary markedly between the two models. Reproduced from [Peyrat S, Olsen KB, and Madariaga R \(2001\) Dynamic modeling of the 1992 Landers earthquake. *Journal of Geophysical Research* 106: 26467–26482.](#)

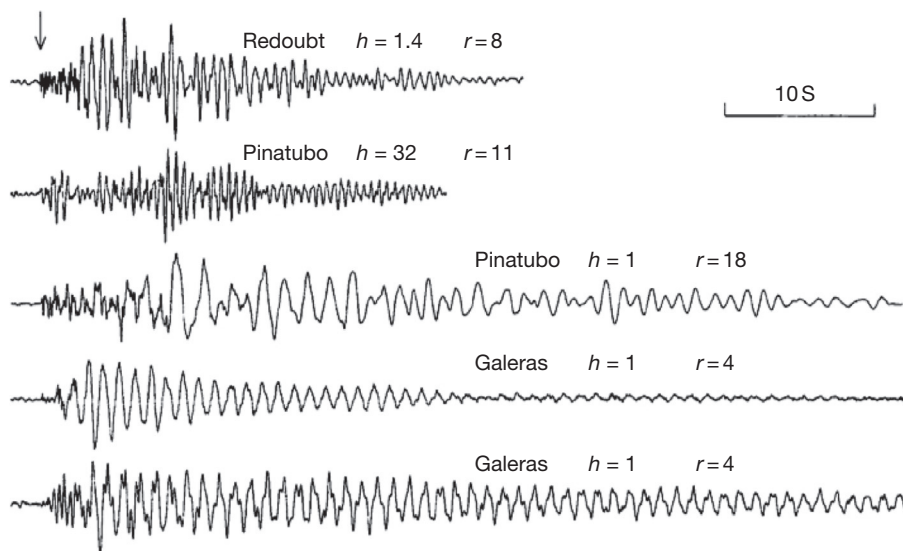


Figure 21 Long-period (LP) earthquakes recorded at Redoubt, Pinatubo, and Galeras volcanoes at source–receiver distance, r , and source depth, h . These events are thought to reflect pressure fluctuations at depth within a volcano’s magmatic system and are useful as a possible precursor to eruption. The lowermost LP earthquake has such a long coda that it verges on harmonic tremor. Reproduced from Chouet B (1996) Long-period volcano seismicity: Its source and use in eruption forecasting. *Nature* 380: 309–316.

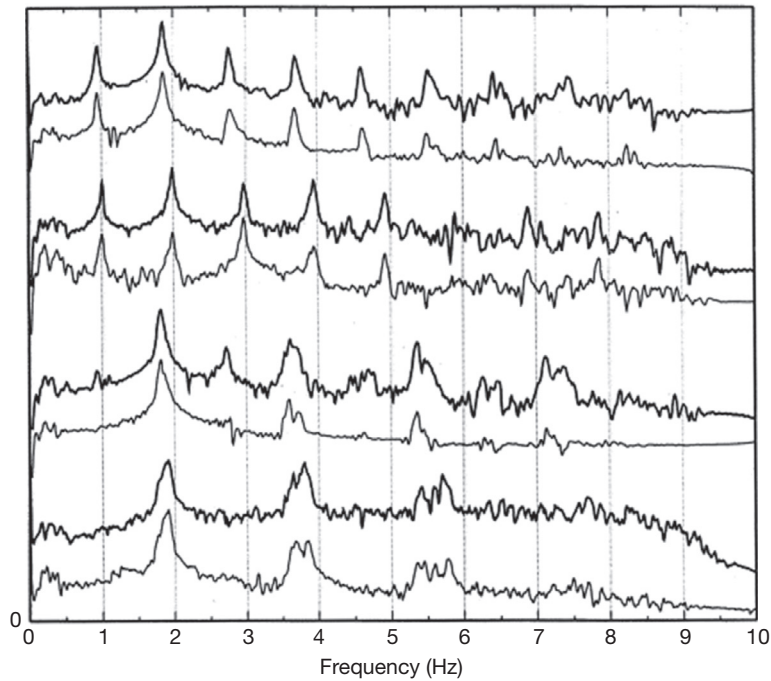


Figure 22 Spectra of velocity seismograms from two seismic stations during four different 30 s time windows during tremor episodes at Arenal volcano, Costa Rica (Hagerty et al., 2000). The peaks at ~ 1 , 3, 5, and 7 Hz are sometimes present and sometimes absent, which is a signature of period doubling.

motion primarily at a discrete set of frequencies. There are several theories for the generation of tremor. A notable example is that due to Julian (1994) who suggested that tremor is generated by a nonlinear interaction coupling between fluid flow and the surrounding elastic material. Among the predictions of this tremor model is that, with increasing flow, tremor

that is initially harmonic will undergo a cascade of period doubling as the tremor becomes chaotic. Since that paper was published, period doubling has been observed on several volcanoes including Arenal in Costa Rica (Figure 22).

Chapter 4.14 covers volcanic processes and Chapter 4.15 covers volcano seismology in detail.

4.01.4 Slip Behavior

The nature of slip on earthquake faults varies widely. It can occur suddenly, as in earthquakes. It can also occur quasi-statically, as in fault creep, in which faults slip so slowly that no detectable seismic waves are generated. Documenting the nature of slip behavior, and understanding the reasons for its variation, is a key goal of earthquake seismology.

4.01.4.1 Brittle Failure

The source of nearly all earthquakes is sudden shear slip across a fault. This sudden slip is sometimes referred to as 'brittle' failure. The domain over which brittle failure occurs is dependent on factors such as mineralogy, pressure, and temperature. Because each of these factors varies strongly with depth, synoptic models of earthquake fault behavior usually characterize the nature of slip as a function of depth.

At very shallow depths – such as the upper few kilometers of continental crust in California – geologic materials are weak and unable to store much elastic strain energy. This renders them unable to support sudden slip in earthquakes and is reflected in the depths of the shallowest microearthquakes. On the San Andreas Fault in California, for example, the depths of the shallowest microearthquakes are several kilometers. The San Andreas Fault Observatory at Depth (SAFOD) project targets some of the shallowest seismicity on the creeping section of the fault by piercing the fault at a depth of ~3.2 km. Above this, it is likely that faults slip relatively stably, unless dynamically driven during large earthquake ruptures that originate at greater depths. At somewhat greater depths, rocks have the potential to store elastic strain energy, and the friction on faults is such that they can slip unstably. This depth range is called the seismogenic zone. In California, the

seismogenic zone extends to a depth of ~15 km. In oceanic crust, where the mineralogy is characterized by higher melting points, the lower boundary of the seismogenic zone is deeper.

The depth of the lowermost earthquakes, where the mode of deformation changes from brittle to ductile, is sometimes termed the brittle ductile transition or, less commonly, the seismic–aseismic transition. The depth of this transition is controlled by mineralogy, temperature, and pressure. High strain rates, such as those occurring during an earthquake, can result in unstable faulting at greater depths than earthquakes nucleate. High strain rate during aftershock sequences can have a similar effect (Schaff et al., 2002). Figure 23 shows a schematic interpretation of the depth dependence of geologic processes and their seismological consequences.

Intermediate and deep-focus earthquakes pose an interesting case. The variation with depth of deep earthquakes and the cutoff of the very deepest earthquakes appear to be related to phase changes in the mantle. Because phase changes result in more compact crystal structure, seismologists have long sought a volumetric (isotropic) component to the mechanism of deep-focus earthquakes. They have found, however, that earthquakes at all depths are dominated by deviatoric failure, with deep earthquakes having at most small volumetric components. The fact that deep earthquakes have far fewer aftershocks further distinguishes them from shallow seismicity (Frohlich, 1989). In any case, it is difficult to understand how deep earthquakes can undergo brittle failure at temperatures and pressures where rocks are expected to deform plastically. Possible mechanisms behind deep earthquakes – among them thermal runaway, phase transitions, and transformational faulting – are discussed in Chapter 4.13. Regardless of the mechanism, the clear dependence of deep earthquake behavior on the thermal parameter (Figure 24) illustrates the important role played by relatively cold subducted lithosphere at great depth.

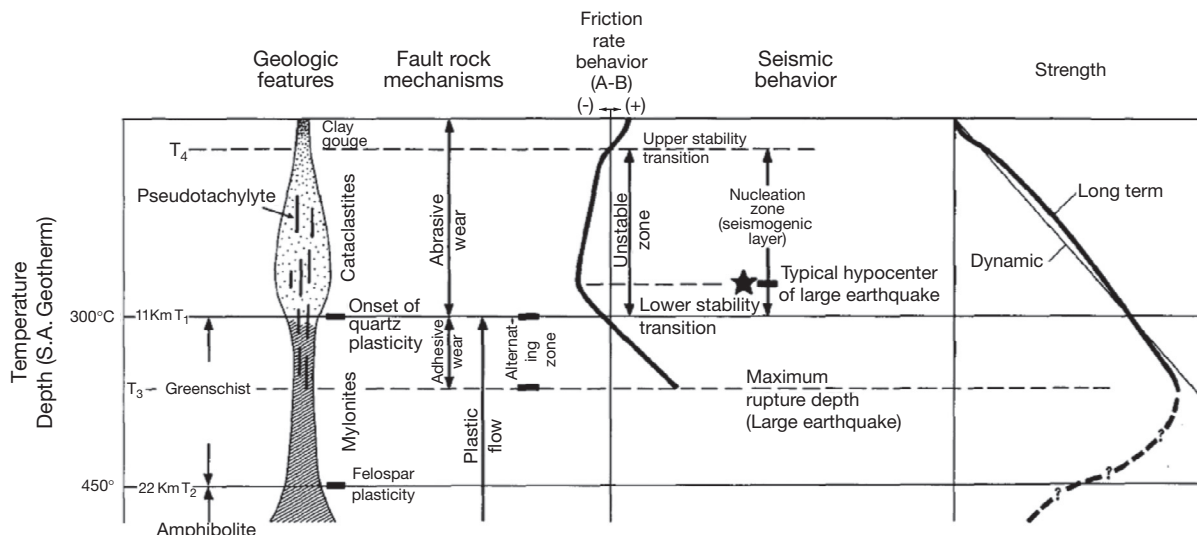


Figure 23 Schematic diagram showing aspects of shear zones and faulting in the Earth. Increasing temperature with depth is shown on the left axis. Geologic manifestation of deformation is shown next to that together with the underlying deformation mechanism. In the middle is frictional behavior, which closely follows the seismogenic zone. Reproduced from Scholz CH (1989) Mechanics of faulting. *Annual Review of Earth and Planetary Sciences* 17: 309–334.

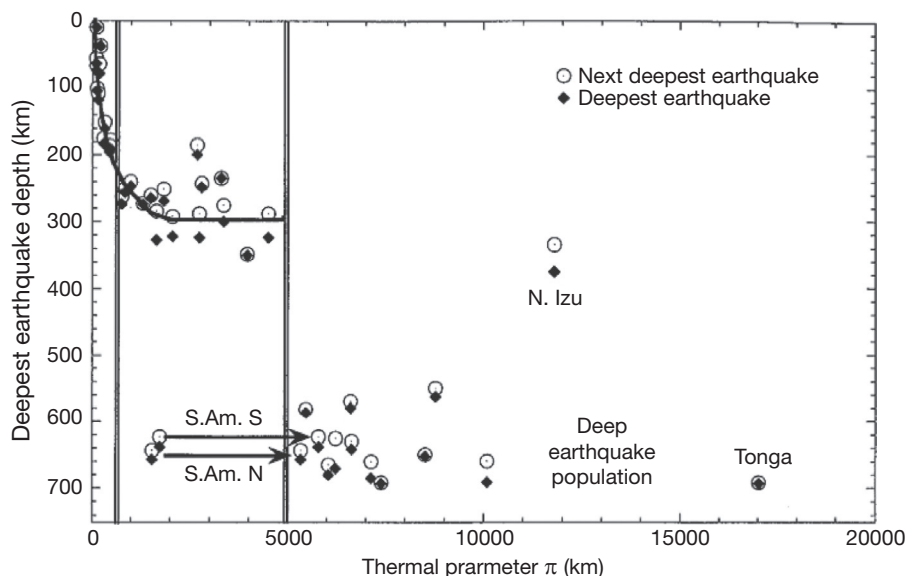


Figure 24 Depth of the deepest earthquake versus the thermal parameter, which is defined by Molnar et al. (1979) as the product of plate age and vertical descent rate, for different subduction zones. A threshold thermal parameter of 5000 appears to separate two domains of behavior. Reproduced from Kirby S, Engdahl ER, and Denlinger R (1996a) Intermediate-depth intraslab earthquakes and arc volcanism as physical expressions of crustal and uppermost mantle metamorphism in subducting slabs. In: Bebout GE, et al. (eds.), *Subduction: Top to Bottom*. Geophysical Monograph 96: 195–214.2043, <http://dx.doi.org/10.1029/2001JB000522>, American Geophysical Union; Kirby SH, Stein S, Okal EA, and Rubie DC (1996b) Metastable mantle phase transformations and deep earthquakes in subducting oceanic lithosphere. *Reviews of Geophysics* 34: 261–306.

4.01.4.2 Creep

If slip on a fault occurs slowly enough, then it is possible that no detectable seismic waves will be generated. Such slip is referred to as ‘aseismic.’ It has long been known that slip occurs aseismically on some faults, such as the San Andreas Fault in central California (Nason and Tocher, 1970). Such slip has come to be called ‘creep’ and the section of the San Andreas Fault where most of the fault motion occurs aseismically has come to be known as ‘the creeping section.’ Figure 25 shows GPS velocity vectors adjacent to the creeping section of the San Andreas Fault in central California, and Figure 26 shows that creep on this section of the fault at the surface closely matches that inferred over the depth of the seismogenic zone. Once global plate motion models provided predictions about long-term slip rates across plate boundaries, a comparison of earthquake history with seismic slip rates indicated that many plate boundaries have far too little seismic slip (Brune, 1968). Similarly, geodetically measured deformation following significant earthquakes is always observed to be much greater than can be accounted for by slip in aftershocks. The natural inference in both instances is that much of the total fault slip must occur aseismically. An important question about this aseismic slip is whether it is continuous or episodic.

Observations of creep on the San Andreas Fault indicate that creep occurs episodically in a range of sizes that is not unlike the Gutenberg–Richter distribution that applies to ordinary earthquakes (Wesson, 1988). Aseismic transients at depth are sometimes referred to by the oxymoron ‘silent earthquakes.’ Because they do not radiate seismic waves as ordinary earthquakes do, these events are very difficult to detect; however, they can be detected geodetically using GPS, radar

interferometry, creepmeters, tiltmeters, or strainmeters. As these measuring systems become more widespread, the detection of aseismic transients is becoming more common (Figure 27). GPS measurements of crustal deformation over subduction zones have led to the discovery of silent earthquakes as large as $M_w \sim 7.5$ (Kostoglodov et al., 2003).

Intermediate between silent earthquakes and ordinary earthquakes are a class of events referred to as ‘slow’ earthquakes. Slow earthquakes are identified by having low-frequency seismic waves that are much larger than would be predicted based on their strength as measured by seismic waves at high frequencies. They are thought to be slip events in which the rupture velocity and/or slip velocity is significantly lower than ordinary earthquakes. Oceanic transform faults are one environment in which slow earthquakes are common (Okal and Stewart, 1982). They also occur in subduction zones, with some giving rise to devastating tsunamis (Kanamori, 1972). A new class of slow events (Figure 28) has recently been discovered in the accretionary prism of the Nankai Trough of Japan (Ito and Obara, 2006). Recently discovered slow events show interesting scaling properties (Figure 29).

An earthquake initiates at a point known as the hypocenter. Thereafter, as an earthquake grows, there is a boundary between the part of the fault that is slipping, or has already slipped, and the part of the fault that is as yet unruptured. This boundary is known as the rupture front and the speed at which the rupture front propagates is known as the rupture velocity. The effect of rupture velocity on seismograms was first recognized for the 1952 Kern County, California, earthquake (Gutenberg, 1955) from the asymmetry of the surface wave radiation. Seismological estimates of the average rupture velocity for crustal earthquakes are typically in the range of ~70–90% of the S-wave velocity, or

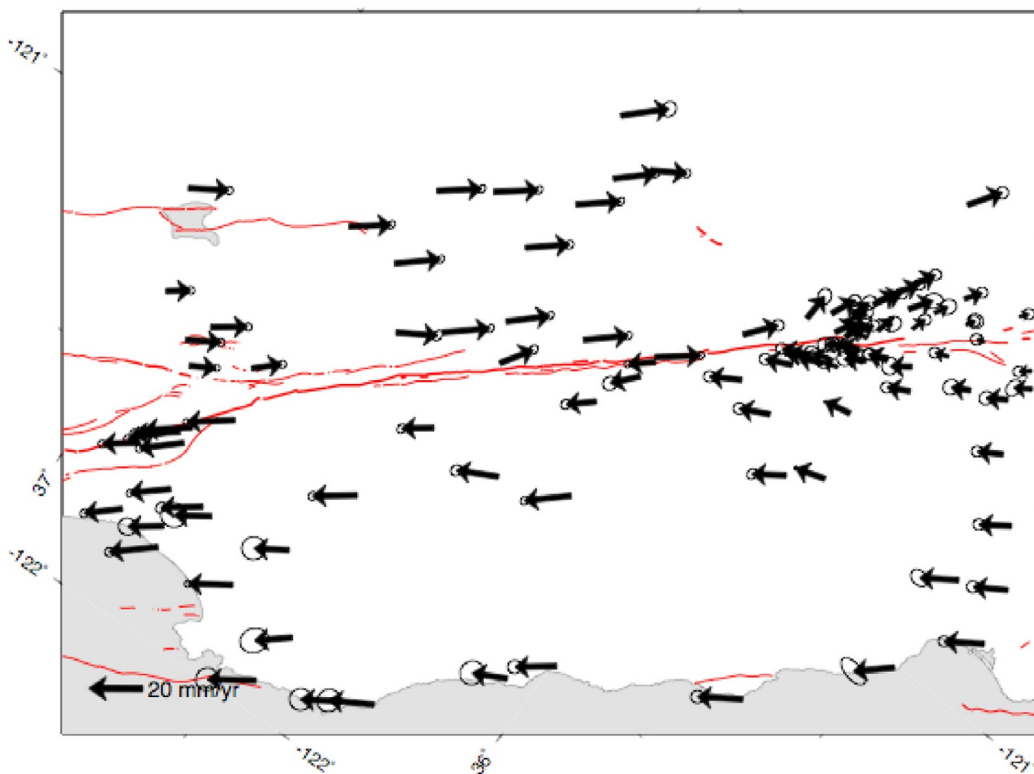


Figure 25 From R. Bürgmann (personal communication) showing faults in red. The San Andreas system of faults crosses the center of the figure. The section between the branching of the fault near San Juan Bautista, on the left of the figure, and Parkfield, the area of dense observations on the right, is known as the creeping section of the San Andreas Fault. GPS velocity vectors shown with arrows and 95% confidence ellipses show nearly block motion of the two sides of the fault (i.e., there is very little velocity gradient with distance away from the fault). Farther to the northwest and to the southeast, the velocity gradient indicates that the fault is locked between large earthquakes.

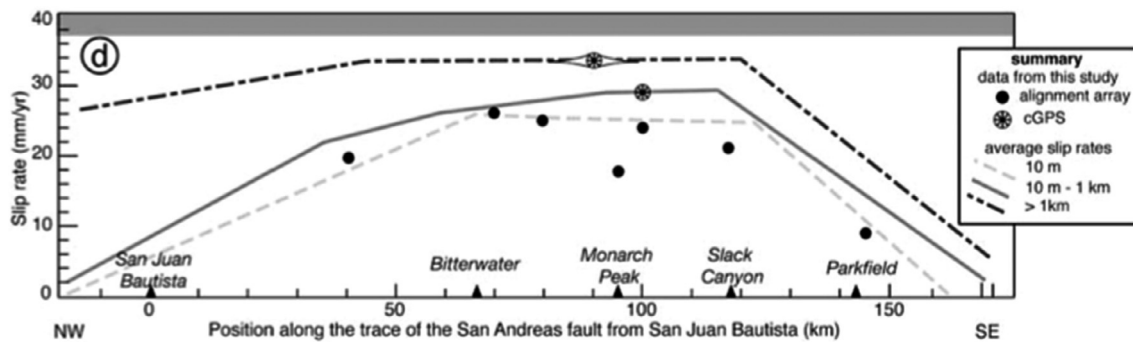


Figure 26 From Titus et al. (2006) showing slip rate parallel to the strike of the San Andreas Fault as a function of distance along the fault from NW (left) to SE (right) as inferred from geodetic measurements. Pale dashed line shows rates determined from measurements within 10 m of the fault and can be considered the surface creep rate. Gray line shows measurements taken within 1 km of the fault and can be considered to represent the slip rate in the upper few kilometers. Dark dashed line shows larger-scale measurements, which include GPS measurements. These estimated slip rates reflect slip to greater depths. The similarity of the curves indicates that creep occurs throughout the depth of the seismogenic zone and the comparison with the model of Argus and Gordon (2001) for the motion of the Pacific plate relative to the Sierra Nevada-Great Valley block indicates that much of that relative motion is taken up by creep at this latitude. The creep rate decays to zero at both the northwest end and the southeast end of the creeping section.

on the order of $2.5\text{--}3.0 \text{ km s}^{-1}$. There is no evidence that rupture velocity varies with magnitude, with even microearthquakes having rupture velocities in the same range (Frankel et al., 1986). Rupture velocities that are a large fraction of the shear-wave velocity lead to pronounced directivity in strong ground

motion, particularly for shear waves, and lead to strong fault-normal pulses of ground motion in the near field of major faults (Somerville et al., 1997).

From the point of view of earthquake dynamics, it is not clear why earthquakes rupture at these velocities. The simplest models

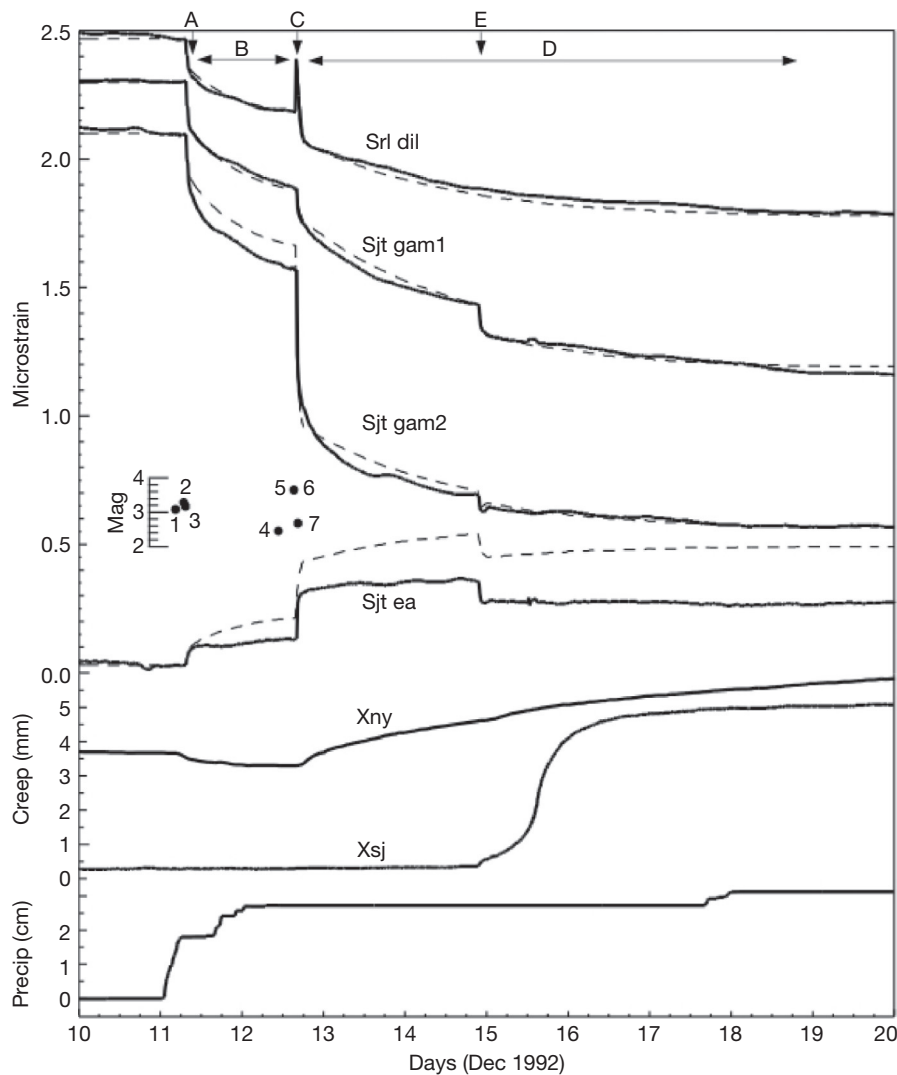


Figure 27 An aseismic transient recorded on the San Andreas Fault near San Juan Bautista. Strain data for stations SRL and SJT, with effects of tides and atmospheric pressure fluctuations removed, are shown as solid lines. Creepmeters (XNY and XSJ) are also shown. Labels A–E denote aseismic transients. Model of strain due to aseismic slip on the San Andreas is shown with dashed lines. Small earthquakes occurred at the same time, but are orders of magnitude too small to explain the observed signals. Reproduced from Linde AT, Gladwin MT, Johnston JS, and Gwyther RL (1996) A slow earthquake sequence on the San Andreas fault. *Nature* 383: 65–69.

based on ideal elastic-brittle fracture theory hold that shear failure ought to accelerate quickly to a limiting velocity that depends on the rupture mode: either the shear-wave velocity for antiplane rupture or the Rayleigh wave velocity (about 92% of the shear-wave velocity) for in-plane rupture (Freund, 1990). Fracture mechanics models also predict that out-of-plane stresses will grow as the limiting velocity is approached, which should promote rupture bifurcation and a lower rupture velocity.

Although sub-Rayleigh rupture velocity is found for most earthquakes, there is increasing evidence that supershear rupture, that is, rupture velocities that exceed the shear-wave velocity, may be an important property of large strike-slip earthquakes. Supershear rupture velocities are expected in slip-weakening rupture models (Andrews, 1976) and have been observed in laboratory fracture experiments (Rosakis et al., 1999). Rupture velocity has apparently exceeded the

S-wave velocity for at least several recent large earthquakes with the 1999 Izmit, Turkey (Bouchon et al., 2001); the 2001 Kunlunshan, Tibet (Bouchon and Vallée, 2003); and the 2002 Denali, Alaska (Dunham and Archuleta, 2004) earthquakes all showing characteristics of supershear rupture. If supershear rupture propagation should prove common, it will have important implications for earthquake hazards because the strong ground motion from supershear rupture is qualitatively different from the subshear case (Aagaard and Heaton, 2004). For a full discussion of theoretical, laboratory, and observational aspects of shear rupture velocity, see Chapter 4.08.

4.01.4.3 Aseismic Transients and Tremor

Perhaps, the most exciting recent discovery in the field of earthquake seismology is that of large silent earthquakes and

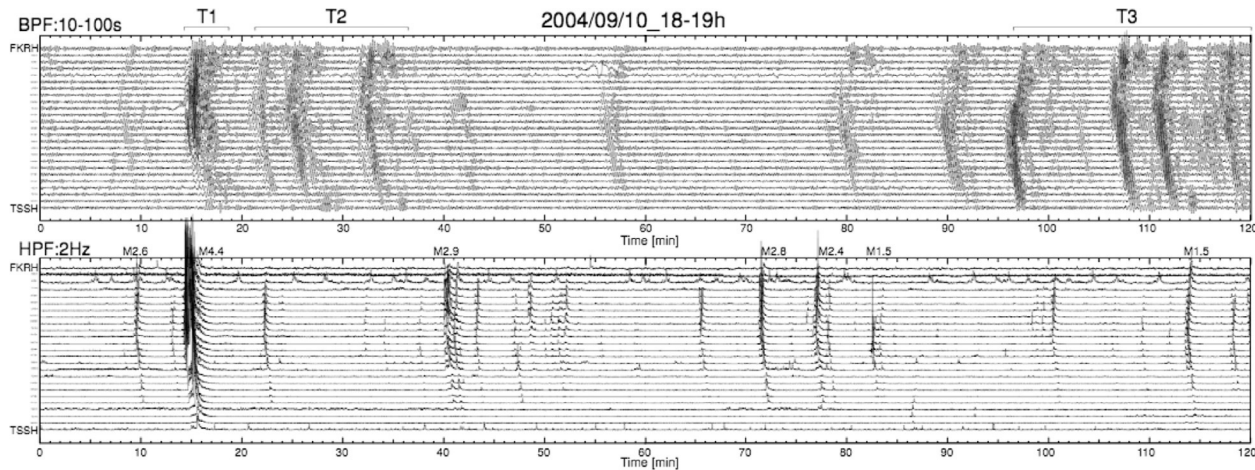


Figure 28 Times series showing very low-frequency earthquakes discovered in the accretionary prism of the Nankai Trough. Two hours of data are shown. Upper panel shows band-passed (10–100 s) ground motion. Lower panel shows rms ground motion for a high-pass filter with corner at 2 Hz. Labels at the top of the lower panel show magnitudes of earthquakes in the JMA catalog. Events in the upper panel at ~25, ~32, ~55, and ~90 min have no corresponding signature at high frequencies and are identified as VLF earthquakes. Reproduced from Ito Y and Obara K (2005) Very low frequency earthquakes excited by the 2004 off Kii peninsula earthquakes: A dynamic deformation process in the large accretionary prism. *Earth Planets and Space* 57: 321–326.

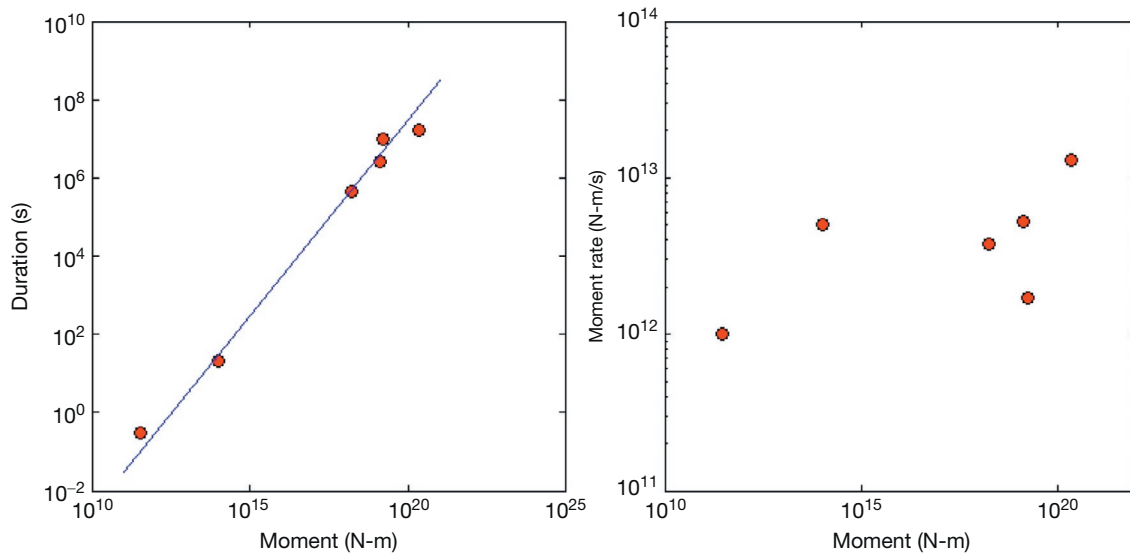


Figure 29 Left panel shows scaling of recently discovered anomalous earthquakes, including (from left to right) low-frequency earthquakes, very low-frequency earthquakes, and slow slip events (see Chapter 4.17). The duration scales linearly with seismic moment over 8 orders of magnitude in slow earthquake size. Panel on the right shows the variation of moment rate with changing moment for the same population. The moment rate is nearly constant over 8 orders of magnitude in seismic moment.

accompanying deep, nonvolcanic tremor (Figure 30). Deep, nonvolcanic tremor was discovered in Japan in the parts of the subduction zone where the Philippine Sea plate is subducting (Obara, 2002). It occurs at depths where dehydration reactions are thought to liberate water from the subducting plate (Seno and Yamasaki, 2003), and hence, it is natural to attribute the genesis of tremor to the movement of fluids at depth. Fluid generation of tremor is also thought to be operative in volcanic tremor that is observed in active magmatic systems (Chouet, 1988; Julian, 1994). Large silent earthquakes were discovered in Cascadia by

Dragert et al. (2001) and subsequently found by Miller et al. (2002) to be occurring periodically with a recurrence interval of 14 ± 1 months. The remarkable regularity of recurrence of these silent earthquakes stands in apparent stark contrast to the more variable recurrence of more typical large earthquakes.

A near-perfect correlation between tremor and silent earthquakes in Cascadia was discovered by Rogers and Dragert (2003) and is illustrated in Figure 31. A correlation between the two phenomena was subsequently documented in Japan as well (Obara et al., 2004), where silent earthquake recurrence is

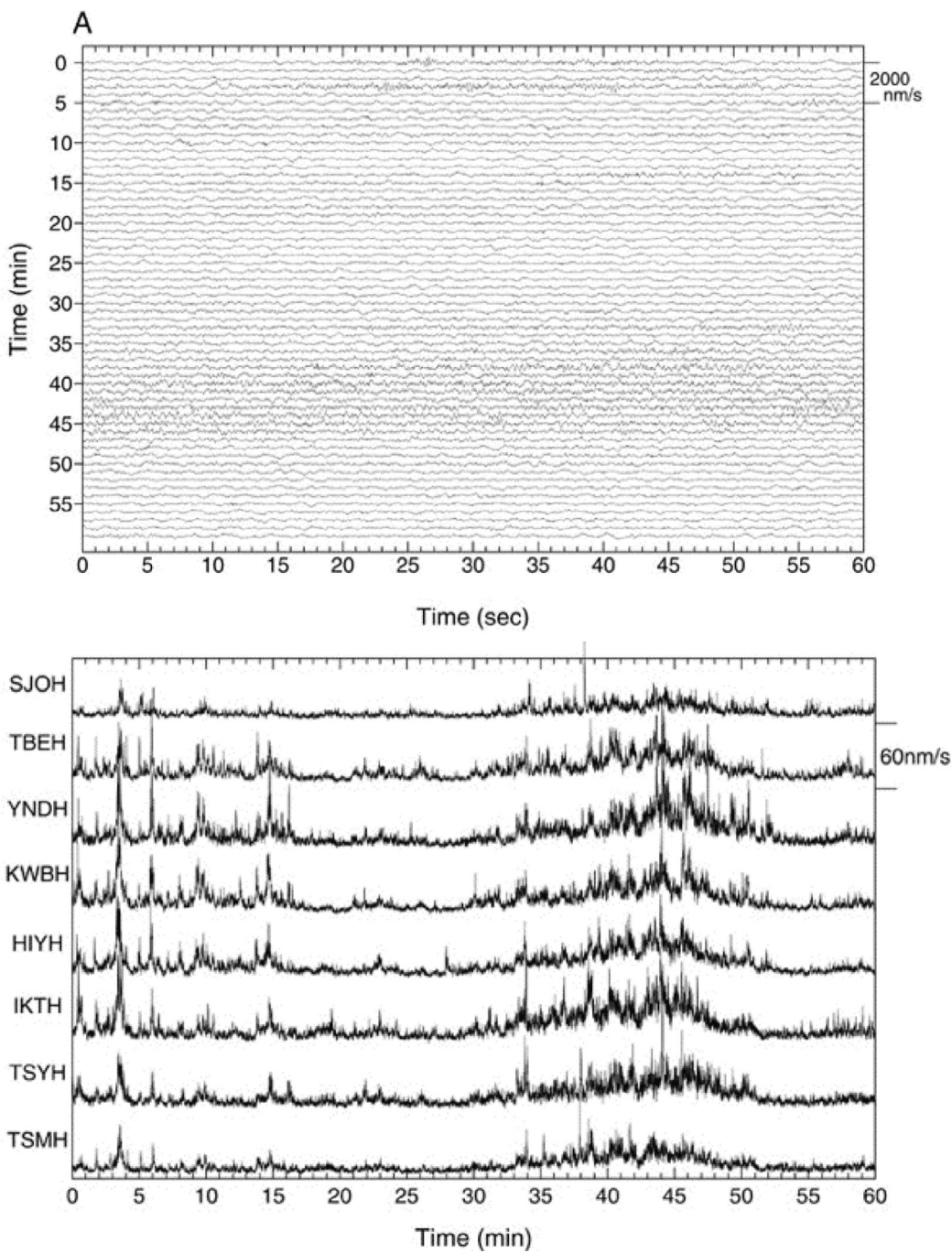


Figure 30 An example of signals from deep nonvolcanic tremor as observed by Obara (2002). The upper panel shows ground motion at a single station of the Hi-net borehole array of high-sensitivity/low-noise seismic network. The tremor is strongest from 40 to 47 min and is characterized by a chaotic signature with no clear, impulsive arrivals. Such signals could be attributable to a range of sources, but their similarity at widely spaced stations and the high phase velocity between them indicates that the signals have a common source, originating deep within the Earth.

less regular, but on the order of several months in eastern Shikoku. The two phenomena are so closely intertwined that they are commonly referred to with an acronym ETS, for episodic tremor and slip. Longer-term aseismic transients, lasting years, have been documented in several areas of Japan including the Bungo Channel (Hirose and Obara, 2005) and the Tokai region (Ozawa et al., 2005). In each of these cases,

the aseismic transients appear to arise due to aseismic slip on the plate interface just below the locked seismogenic zone. Given this location, they are certain to accelerate the loading of the source region of large megathrust earthquakes and hence should be capable of triggering such events.

The location of the tremor source at depths at which metamorphic dehydration reactions are expected and the fact that

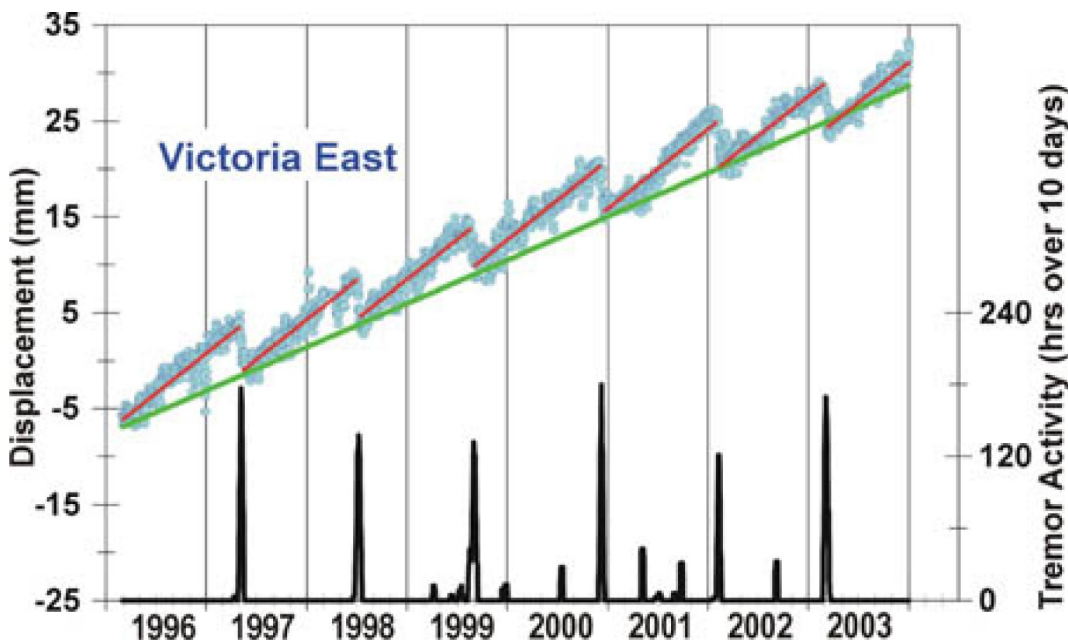


Figure 31 Comparison of slip and tremor activity for Victoria, British Columbia, Canada (http://seismescanada.rncan.gc.ca/pprs/research/ETS_e.php). Small blue circles show position of a GPS site near Victoria with respect to the interior of North America. Green line shows long-term eastward motion of the site. Red sawtooth line shows motion and includes reversals in motion approximately every 14 months. These and displacements observed at other GPS stations have been modeled as aseismic slip on the plate interface at depth. The bottom black graph shows the number of hours of tremor activity observed on southern Vancouver Island. The correlation between episodic tremor and aseismic slip is remarkable and has led to the two phenomena being referred to as episodic tremor and slip (ETS).

tremor is observed for Philippine Sea plate subduction, but not Pacific plate subduction, in Japan both point to a key role for fluids in the process (Julian, 2002). Fluids either may couple directly into ground motion as they are thought to do in the case of volcanic tremor or may act to trigger both phenomena. The discovery by Shelly et al. (2006) that low-frequency earthquakes that occur during tremor episodes represent slip on the plate interface indicates that at least part of the tremor signal arises from shear slip. Subsequent work (Ide et al., 2007a; Royer and Bostock, 2013; Shelly et al., 2007; Wech and Creager, 2007) supports the notion that the entire tremor signal is generated as shear slip on faults and that tremor is part of a family of slow earthquakes (Ide et al., 2007b). For more details on aseismic transients, see Chapter 4.17.

4.01.5 Physics of the Earthquake Source

In this introductory chapter, we have focused on the phenomenology of the earthquake source as it is studied using seismology. For the most part, we have not focused on the physical mechanisms underlying earthquake behavior. There is much about these physical mechanisms that we have yet to understand. In this section, we attempt to tie together the physics behind the observations.

4.01.5.1 Friction

Most earthquakes occur on preexisting faults. The friction acting across these faults provides the resistance to keep them from slipping in between earthquakes. Laboratory

measurements of friction indicate that for most rocks at seismogenic depth, the coefficient of friction should be ~ 0.6 (Byerlee, 1978). For earthquakes to propagate unstably, however, friction has to drop from a static level to some lower sliding level, as in the slip-weakening model (see next section). Even slip-weakening behavior, however, does not allow for faults to recover their frictional strength once slip has occurred, so realistic faults require a more complex frictional behavior.

More complex frictional behavior is, in fact, observed in laboratory experiments, and these second-order frictional effects may control much of fault behavior in the Earth. Static friction is not constant, but depends on the history of slip on the interface, with friction increasing as the logarithm of time of stationary contact in laboratory experiments (Dieterich, 1972). A related property is that dynamic sliding friction depends logarithmically on the slip rate. The sign of this dependence determines whether the dependence is weakening or strengthening with increasing slip rate (Scholz et al., 1972). A third property is that when the slip rate on a sliding surface changes suddenly from one steady rate to another, the coefficient of friction evolves to a new steady-state value after a critical amount of slip, D_c , has occurred. D_c is thought to represent the slip required to renew the true contact area between two rough surfaces (Dieterich, 1978). These three properties – the time dependence of static friction, the rate dependence of dynamic friction, and the evolution of sliding friction with slip – have been unified in a theory of rate- and state-dependent friction laws that describe the evolution of friction (Dieterich, 1979a,b; Ruina, 1983).

An important implication of these laws for earthquakes is that the effect of velocity arises from the combination of two

effects – the direct velocity effect and the evolution of friction with slip – that have opposite signs. Whether slip can occur unstably or must occur stably depends critically on their relative size. Rocks with steady-state velocity strengthening will always slip stably, while rocks with steady-state velocity weakening can slip unstably. The transition from steady-state velocity-weakening to steady-state velocity-strengthening behavior is thought to control the lower (Tse and Rice, 1986) and upper (Marone and Scholz, 1988) depth extent of the seismogenic zone. More on this topic can be found on [Chapters 4.06](#) and [4.04](#).

4.01.5.2 Energy Budget

In the time between large earthquakes, seismogenic faults remain frictionally locked. As plate motion continues, the crust around a fault will gradually distort and store energy in the form of gravitational energy and elastic strain energy. When the fault starts to slip, this gradually accumulated potential energy is suddenly converted to different forms. Some of it is used to overcome the initial resistance to shear failure. This component of the energy is referred to as the fracture energy. As slip continues during the earthquake at some lower frictional level, energy is converted to heat due to the work done against the resisting frictional force. Another term in the earthquake energy budget is the component that is radiated in the form of seismic waves. This is the seismic energy referred to in [Sections 4.01.2.1](#) and [4.01.3.4](#). Seismic energy is gradually dissipated and converted to heat elsewhere due to anelastic wave propagation effects. The energy balance can be expressed using a simple equality (Kostrov and Das, 1988) involving the radiated seismic energy, E_s ; the change in potential energy, ΔE_p ; the energy expended extending the crack, ΔE_y ; and the energy expended overcoming friction, ΔE_f :

$$E_s + \Delta E_p + \Delta E_y + \Delta E_f = 0$$

Of the terms in this equation, we have discussed the radiated seismic energy, a quantity that can be measured using seismic waves. The seismic energy can (with considerable uncertainty) be determined from seismological observations, and it is natural to ask what constraints the seismic energy places on the other terms in the energy balance.

A further observational constraint comes from measurements of the slip. Together with the friction, the slip determines how much energy is dissipated as heat on the fault. This is not as simple as it sounds, however, as it is unrealistic to assume that sliding friction is constant. Rate- and state-variable friction laws indicate otherwise, and there are other mechanisms, discussed in the subsequent section, that are expected to introduce much larger dynamic variations in fault strength.

The fracture energy has been estimated for a number of earthquakes. The total fracture energy is proportional to the faulted area, so if these measurements represent fracture energy on a planar fault, they would only be of consequence for very small earthquakes. Seismological observations of the shear fracture energy are quite large, on the order of 10^6 J m^{-2} . This is orders of magnitude larger than what is measured in the laboratory (Wong, 1982). One interpretation of this discrepancy is that the dissipation of energy being measured includes energy lost due to various forms of yielding near the rupture

front (Andrews, 2005). It has been suggested that finely pulverized rock observed in the near field of the San Andreas Fault and the tremendous surface area created in that process might be large enough to account for seismologically inferred fracture energies.

In the slip-weakening model (Ida, 1972), the resistance of the fault to motion is slip-controlled and decreases from some maximum when slip first begins, to a lower sliding frictional level once the slip-weakening distance is attained. Thereafter, slip can continue at the sliding frictional level of resistance. Seismologists have attempted to place constraints on the slip-weakening displacement. They have found that it is quite large in major earthquakes, reaching a value of $\sim 0.5\text{--}1 \text{ m}$ for the Kobe earthquake (Ide and Takeo, 1997). Here again, the inferred values are orders of magnitude larger than would be inferred by extrapolating measurements from the laboratory. At least some of this discrepancy may result from a lack of adequate resolution of the slip velocity function (Guatteri and Spudich, 2000).

Other informations on the energy balance may come from magnitude dependence of the radiated seismic energy. If the true fracture energy is only an important component of the energy budget for very small earthquakes, then one would expect to see more seismic energy radiated per unit fault slip for larger earthquakes. Seismic moment is more easily calculated than fault slip, so seismologists typically consider changes in the ratio of seismic energy to seismic moment, that is, E_s/M_0 . A possible source of a change in E_s/M_0 comes from the possibility that the resistance to fault motion may drop dramatically with increasing fault slip (Kanamori and Heaton, 2000) as discussed in the next section. Another interpretation is offered by Abercrombie and Rice (2005), who replaced the slip-weakening distance with a slip-weakening function for which the resistance to fault slip continues to decrease with increasing fault slip. As with more dramatic weakening mechanisms, E_s/M_0 is predicted to increase as an earthquake grows larger.

So what do the data indicate? There is a lot of scatter in the measurements, but representative values for large earthquakes are on the order of 5×10^{-5} . Some observations of the magnitude dependence of seismic energy suggest that the ratio of seismic energy to seismic moment increases as a function of earthquake size. That is, earthquakes become more efficient at radiating seismic waves as they grow larger. Measurements from a number of studies of earthquakes over a wide range of earthquake size indicate that E_s/M_0 is approximately a factor of 10 larger for $M_w 7$ earthquakes than it is for $M_w 2$ earthquakes (Kanamori and Heaton, 2000). Ide and Beroza (2001) found that many published E_s/M_0 measurements could be biased to low values for small earthquakes because of biases introduced by inadequate corrections for path effects or the limited instrumental bandwidth ([Figure 32](#)). Thus, whether or not the observed scaling of E_s/M_0 with earthquake size is a true property of earthquakes remains an open question.

4.01.5.3 Microscopic Processes

There are many processes that occur at the microscopic scale that may have no direct seismological signature, yet still have a profound effect on and may ultimately control macroscopic

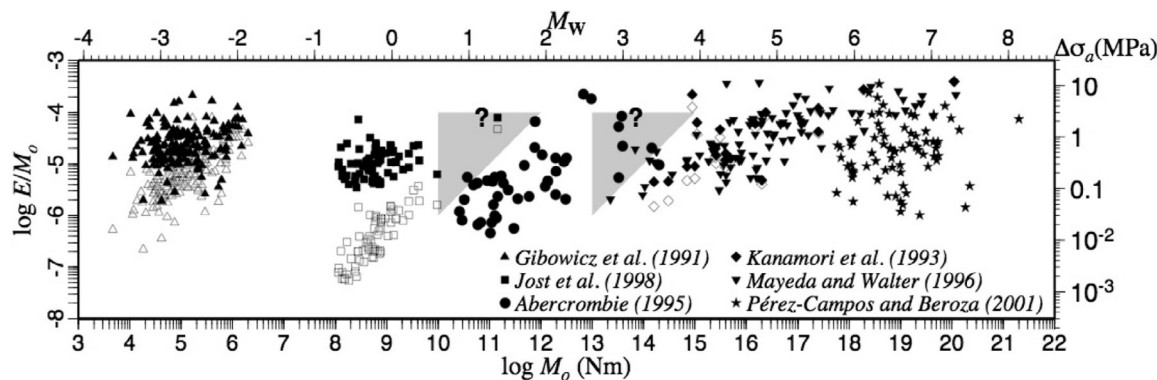


Figure 32 Plot of E_s/M_0 versus M_0 from several studies. Open symbols show original measurements, while filled symbols show values once seismic energy possibly missing due to limited bandwidth is restored. Gray triangles show areas where earthquakes are excluded from two studies due to limited bandwidth. Reproduced from Ide S and Beroza GC (2001) Does apparent stress vary with earthquake size? *Geophysical Research Letters* 28: 3349–3352

earthquake behavior. In this section, we briefly review several such phenomena.

4.01.5.3.1 Hydrologic processes

An important unknown in earthquake science is the importance of pore fluids on the faulting process. Fluids support normal stress, but do not support shear stress. Thus, one way in which pore fluids can effect faulting is by changing the effective normal stress. Briefly, the criterion for slip under the Coulomb failure criterion (e.g., Harris, 1998) states that fault slip will occur when the shear stress, τ , acting across the fault exceeds the sum of the cohesion, C , and the effective normal stress multiplied by the coefficient of friction, μ :

$$\tau > \mu(\sigma - P) + C$$

where the term in the parentheses is referred to as the effective normal stress and is the difference between the fault-normal stress, σ , and the pore pressure, P . The cohesion is usually assumed to be negligible. By this criterion, one way in which earthquakes can be triggered is by an increase in the pore pressure, P .

This effect has been cited by Hubert and Rubey (1959) as a possible explanation for the movement of large, nearly horizontal thrust faults due to the large frictional resistance expected from the considerable overburden. Fluids have been shown capable of artificially triggering earthquakes in controlled experiments (Healy et al., 1968; Raleigh et al., 1976); thus, it is reasonable to expect that they might play a similar role for tectonic earthquakes. Both the lack of a heat flow anomaly (Brune et al., 1969) and the nearly fault-normal stress orientation of some major fault zones (Zoback et al., 1987) could be understood if the effective normal stress is low, due to high pore fluid pressure, such that the fault slips at low shear stress. There are independent evidences that fluids and faults interact (Sibson, 1981) and that high pore pressures occur in fault zones (Figure 33), at least at shallow depths (Unsworth et al., 1997). Dehydration embrittlement, in which phase changes that expel water decrease the effective normal stress in subducting lithosphere, is cited as a possible enabling mechanism for intermediate-depth earthquakes (Kirby et al., 1996a,b).

Another way in which fluids can influence faulting is through poroelastic effects. In a poroelastic medium, pore pressure will decrease where the mean normal stress decreases and increase where the mean normal stress increases. The immediate change in pore pressure, ΔP , for what is known as undrained conditions can be related to the change in the mean normal stress, $\Delta\sigma_{kk}$, by the equation

$$\Delta P = B\Delta\sigma_{kk}$$

where Skempton's coefficient, B , a function of elastic moduli for drained and undrained conditions, is equal to one for fluid-saturated soils and ranges between 0.5 and 0.9 for a range of rock types (Rice and Cleary, 1976). With time, this undrained state evolves to the drained state as fluids flow and reequilibrate in response to pore pressure gradients.

Pore fluids can trigger earthquakes by inducing shear stress through a process referred to by Booker (1974) as consolidation. Consolidation in this usage refers to the process in which, in places where the mean normal stress and pore pressure increase, normal stress and pore pressure then gradually decrease as pore fluids migrate away from areas of high pore pressure. Where the mean normal stress and the pore pressure decrease, the mean normal stress will decrease further as pore fluids migrate into areas of lower pore pressure. The net effect is to couple normal and shear stress through pore fluid migration. Booker proposed this as a candidate mechanism for the gradual decay described in Omori's law of aftershock decay.

Yet another way in which fluids can influence earthquakes and faulting is through chemical effects and stress corrosion (Scholz, 1968). It is also worth noting that other fluids, notably magma and carbon dioxide (Miller et al., 2004), can have similar effects. For more details on the involvement of fluids in faulting, see Chapter 4.12.

4.01.5.3.2 Melting and flash heating

Rapid shear slip during earthquake faulting will lead to shear heating. If this heating is large enough, it can lead to very large changes in temperature and, possibly, to melting on the fault (Jeffreys, 1942; McKenzie and Brune, 1972). There are several variables that control whether or not melting occurs and, if it does, how extensive it is. The heat generated per unit area of the

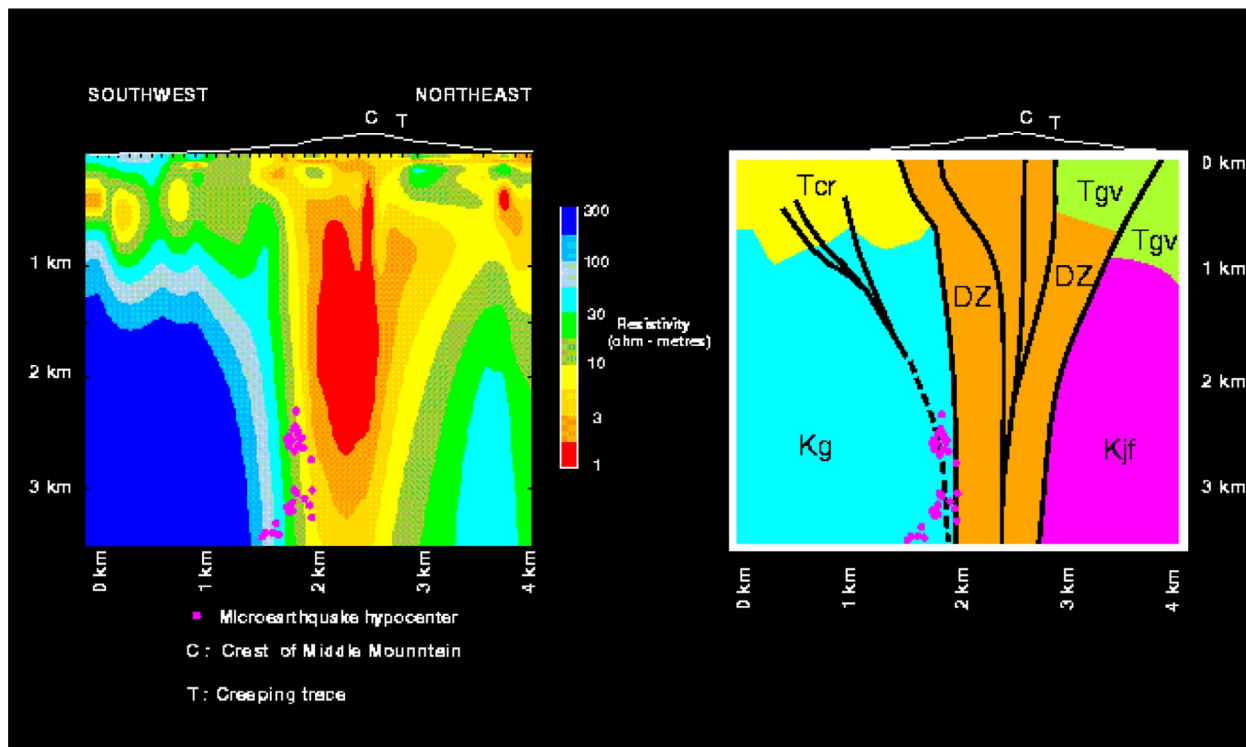


Figure 33 A cross section of imaged resistivity across the San Andreas Fault at Parkfield California (Unsworth et al., 1917). Resistivity (in Ωm) is shown on the left panel, with a corresponding geologic interpretation on the right panel. The areas of low resistivity (orange red) are interpreted as a fluid-saturated damaged zone (DZ) centered on the fault.

fault will be the product of the slip and the frictional resistance, so the slip and sliding friction will in part determine the conditions for possible melt generation. Melt may begin to form microscopically in the immediate vicinity of frictional contact, leading to initial loss of strength in a process known as 'flash heating' (Rice, 2006).

In addition, any real fault zone will be a shear zone of finite thickness. The thicker the shear zone, the more distributed heat production will be, and all other things being equal, the more slip required to initiate melting. The thermal conductivity will control how quickly heat diffuses away from the fault. Thermal conductivity of rocks is low enough that this will not likely be an important effect, unless either the slip rate is very low or pore fluids are present. The effect of melt on friction is not straightforward. Laboratory experiments suggest that the initial effect might be to increase fault strength due to viscous effects, but this effect might be diminished at high stress. In any case, further slip will lead to more heating and a reduction in viscosity and hence strength (Fialko and Khazan, 2005). A detailed treatment of temperature effects during faulting can be found in Chapter 4.03.

4.01.5.3.3 Thermal pressurization

The same frictional heating discussed in the previous section, in the presence of pore fluids, can lead to thermal pressurization of those fluids well before the onset of melting. Thermal pressurization can have a strong effect on faulting by reducing the effective normal stress. The absence of geologic evidence for melting near fault zones led Sibson (1973) to propose thermal

pressurization as a mechanism for reducing dynamic fault strength. For undrained conditions, a temperature change of ΔT leads to a pressure change, ΔP of, $\Delta P = \Lambda \Delta T$, where Λ is the thermal expansion coefficient of water. Representative values of Λ for upper crustal conditions are 0.78–0.93 MPa/ $^{\circ}\text{C}$ (Rempel and Rice, 2006). Thus, thermal pressurization is potentially a very large and efficient agent of fault weakening. Thermal pressurization was explored as a potential explanation for the lack of a heat flow anomaly on the San Andreas Fault by Lachenbruch and Sass (1980). For it to operate, fluids must be present and fault-zone permeability has to be low enough that the excess pressure does not diffuse into the host rock. Measurements of the permeability of fault zones and their surroundings are very low (Wiberley and Shimamoto, 2003); however, any dilatancy effects during rapid slip could rapidly increase that permeability and act to short circuit this weakening mechanism. More on this mechanism can be found in Chapter 4.03.

4.01.5.3.4 Silica gel formation

Another candidate weakening mechanism is the formation of silica gels (Goldsby and Tullis, 2002). In this scenario, sliding in the presence of water leads to the formation of a gel that facilitates sliding at low friction. Evidence for this comes primarily from the laboratory where sliding at fault slip speeds appropriate to earthquakes can lead to dramatic reductions in friction and for which flow textures are preserved as amorphous solids after sliding ceases (Di Toro et al., 2004). There is evidence for silica gels having formed on faults within the

Earth as well (Kirkpatrick et al., 2013). The laboratory data suggest that this mechanism, if important for large earthquakes, would only seem likely to operate in rocks of high silica content.

4.01.5.4 Fault-Zone Structure

Detailed geologic observations place important constraints on the physical processes that operate during faulting in the Earth. The geometric complexity of faults has a first-order effect on the faulting process. Geologic observations also provide constraints on the nature of the deforming or damaged zone in the direction normal to the fault. These observations are crucial for understanding the mechanics of faulting and bear directly on some of the most important problems in earthquake physics.

Seismological constraints on fault-zone structure are of much lower resolution, but they have the advantage of measuring properties of faults that are actively deforming and not exhumed. Earlier in this chapter, we outlined some of the recent progress on the fine structure of faults as revealed by precise earthquake locations (Figures 11 and 12). Precise earthquake locations bear directly on questions such as how wide the fault zone is at seismogenic depths and whether or not fault trace complexities observed at the surface reflect complexities in fault geometry at depth.

Another important constraint on the structure of fault zones comes from fault-zone guided waves (FZGWs). Because faults move geologic units past one another, they tend to be planes that separate materials with different properties. Moreover, the mechanical, chemical, and/or hydrologic alteration of materials within deforming fault zones leads to them being a locus of low seismic velocities. Variations in material properties either within or across fault zones lead to strong effects on seismic wave propagation. Waves that are trapped within the low-velocity material within several hundred meters of active fault zones are known as FZGWs. These are analogous to Love waves in vertically layered media in that they usually consist of critically reflected S-waves within the low-velocity material. FZGWs have been observed in the subduction zone in Japan (Fukao et al., 1983), continental normal faults (Leary et al., 1987), and

continental strike-slip environments (e.g., Li et al., 1990). Waves that refract horizontally due to a large contrast in velocity across a fault zone are known as fault-zone head waves. These have also been observed in diverse environments, including both subduction zones (Fukao et al., 1983) and continental strike-slip faults (e.g., McNally and McEvilly, 1977).

Fault-zone waves are very sensitive to the details of fault-zone structure and have the potential to place important constraints on the structure of active fault zones. If the geometric regularity of the waveguide is disrupted, then such waves may not propagate or may be strongly altered. For this reason, they can be used to explore fault segmentation. An outstanding question regarding FZGW is just how deep the waveguide extends. Some investigators find that it spans the entire depth of the seismogenic zone (Li et al., 2000), while others argue that it may only extend through the upper few kilometers (Ben-Zion et al., 2003). The recent observation of FZGW in the SAFOD borehole through the San Andreas Fault suggests that the fault-zone waveguide extends to seismogenic depths (Figure 34).

Other important questions regarding the fault-zone waveguide are to what extent it is a permanent feature and how much it is a transient that follows a large earthquake. Following the Landers earthquake, there is a clear and strong postseismic healing, or recovery of low velocities, indicating that at least some of the low-velocity zone is transient (Li et al., 1998).

The relationship between low-velocity fault zones and the mechanical behavior of faults in earthquakes is important for earthquake faulting. Observations of surface deformation obtained by satellite radar interferometry (Fialko et al., 2002) following the 2001 Hector Mine, California, earthquake indicate that nearby fault zones are characterized by relatively compliant zones that are on the order a kilometer wide. The effect of relatively low-strength materials is an important question that is just now being addressed.

4.01.5.5 Borehole Observations, Fault-Zone Drilling, and Seismicity in Mines

Another approach to the study of earthquakes and faulting is to make observations below the Earth's surface. This can take the

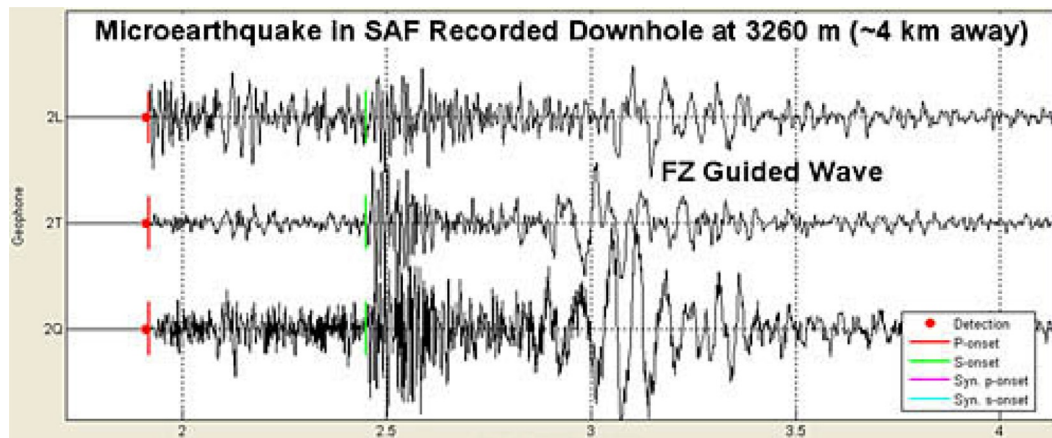


Figure 34 Fault-zone guided waves observed at 2.7 km depth in the SAFOD borehole from a magnitude 1.3 earthquake. The presence of these waves at this depth is diagnostic of a 200 m wide low-velocity zone associated with the San Andreas Fault. Reproduced from <http://www.earthscope.org/news/announcements/2006/FaultZone2006/seismogram-big.jpg>.

form of recording earthquakes with seismometers deployed in boreholes, direct drilling into active faults, or studying seismicity in deep mines. This approach has a number of distinct advantages.

Borehole seismic observations allow earthquake scientists to make observations below the highly attenuating and strongly scattering layers of the Earth's surface. Borehole measurements have had an important impact on seismology as they allow a relatively unobscured view of seismic waves as they are radiated from the earthquake source (see the section on stress within the Earth in the succeeding text). The Hi-net seismic network in Japan capitalizes on this idea as it uses sensitive borehole instruments to monitor the entire Japanese archipelago. It led directly to the discovery of deep, non-volcanic tremor ([Obara, 2002](#)). The idea of making measurements in the very near field of a fault at depth is a key element of the ongoing SAFOD project.

Deep drilling allows direct sampling of active faults *in situ*, which is a tremendous advantage. It also allows scientists to make stress measurements at depth near active faults. However, fault-zone drilling is a logistically challenging and expensive undertaking. These disadvantages of fault-zone drilling have prevented its wider application. The expense of drilling rises rapidly with increasing depth and hence only relatively shallow depths are typically targeted. Fault-zone drilling also allows only discrete sampling of a few select points on a fault surface. Despite these drawbacks, fault-zone drilling has played, and will continue to play, an important role in earthquake science.

Notable deep drilling projects directly related to earthquakes include the SAFOD project, which has drilled through the actively deforming San Andreas Fault zone near Parkfield, California. Among the goals of the project are to drill through the source of a repeating earthquake sequence and to compare it with nearby fault zone materials that exhibit creep rather than earthquakes. Another important fault-zone drilling experiment is the Taiwan Chelungpu fault drilling project. This project has drilled into the shallow part of the rupture of the M_w 7.6 1999 Chi-Chi, Taiwan, earthquake in order to study fault-zone properties in the immediate aftermath of a large earthquake. Other fault-zone drilling projects of note include the Gulf of Corinth Rift Laboratory, which seeks to understand a continental back-arc rifting environment, and the Nankai Trough Seismogenic Zone Experiment, which has the ambitious goal of drilling the accretionary prism of the Nankai Trough in Japan. These and other fault-zone drilling projects will provide important constraints on the fluids, fluid pressure, chemistry, permeability, deformation mechanisms, and stress as they relate to earthquake behavior.

If fault-zone drilling is carried out soon after an earthquake, it is possible to place constraints on the heat produced during faulting, and hence the amount of work done against friction, by measuring a temperature anomaly ([Brodsky et al., 2010](#)). This has been carried out for three earthquakes: the Chi-Chi, Taiwan, earthquake ([Kano et al., 2006; Tanaka et al., 2006](#)); the 2008 Wenchuan, China, earthquake ([Xue et al., 2013](#)); and the 2011 Tohoku-Oki, Japan, earthquake (Fulton et al., personal communication). In each case, the temperature anomaly is small, suggesting that slip occurred at very low levels of frictional resistance. A detailed discussion of fault-zone drilling projects can be found in [Chapter 4.07](#).

Another environment that is used to study earthquakes *in situ* is in deep mines. The act of mining removes load-bearing material and induces earthquakes. These earthquakes are extremely dangerous to miners, and hence, there is a great deal of interest in understanding and predicting them. They also have the potential to tell us much about how ordinary tectonic earthquakes work. Seismicity in mines offers some advantages over studying seismicity remotely. The location of mining operations is known and the likely areas of seismicity can be inferred from them. Another advantage is that seismic instruments can be deployed in three-dimensional arrays, which is not possible with strictly surface observations. Seismicity in mines is also at a scale that bridges the laboratory and usual seismological scale of observation. These are the principal motivation behind the multidisciplinary Natural Earthquake Laboratory in South African Mines (NELSAM) project, which is studying earthquakes in the western deep-level South African gold mine.

4.01.5.6 Earthquakes as a Complex System

Earthquakes do not happen in isolation, but interact strongly with each other. The same goes for faults, which might more properly be described as fault systems. A full numerical treatment of fault systems would require realistic geology, fault geometries, rheology, a full range of earthquake sizes, and multiple earthquakes. Although progress is being made on modeling earthquakes in ways that include each of these characteristics, combining them into a single comprehensive model is far beyond current capabilities. There is, however, an approach to studying earthquakes that seeks simplifications to the effect of these properties or characteristics while at the same time attempting to extract the important system-level behavior that affects earthquakes. Studies of this sort treat the behavior of large earthquake populations statistically, with the goal of understanding the macroscopic behavior based on an understanding of the system at a microscopic level. An example of this sort of treatment, which seeks to explain the b -value of seismicity distributions as a manifestation of self-organized criticality, is the study of [Bak and Tang \(1989\)](#). A review of this approach to understanding earthquake phenomena can be found in [Chapter 4.24](#).

4.01.6 State of Stress, Nucleation, and Triggering

4.01.6.1 State of Stress

The orientation of stress within the Earth can be determined by diverse methods such as earthquake focal mechanisms, borehole breakouts, and the orientation of volcanic dikes. As shown in [Figure 35](#), systematic compilations of stress orientations indicate that it is coherent over large scale length and generally consistent with what is expected from ongoing plate tectonic motion ([Zoback et al., 1989](#)). The magnitude of these stresses at seismogenic depth, as well as the orientation of stress in the vicinity of major fault zones, is much less clear and the subject of ongoing research.

The lack of a detectable heat flow anomaly centered on the San Andreas Fault ([Brune et al., 1969](#)), which is expected under the assumption that fault friction at depth is similar to that

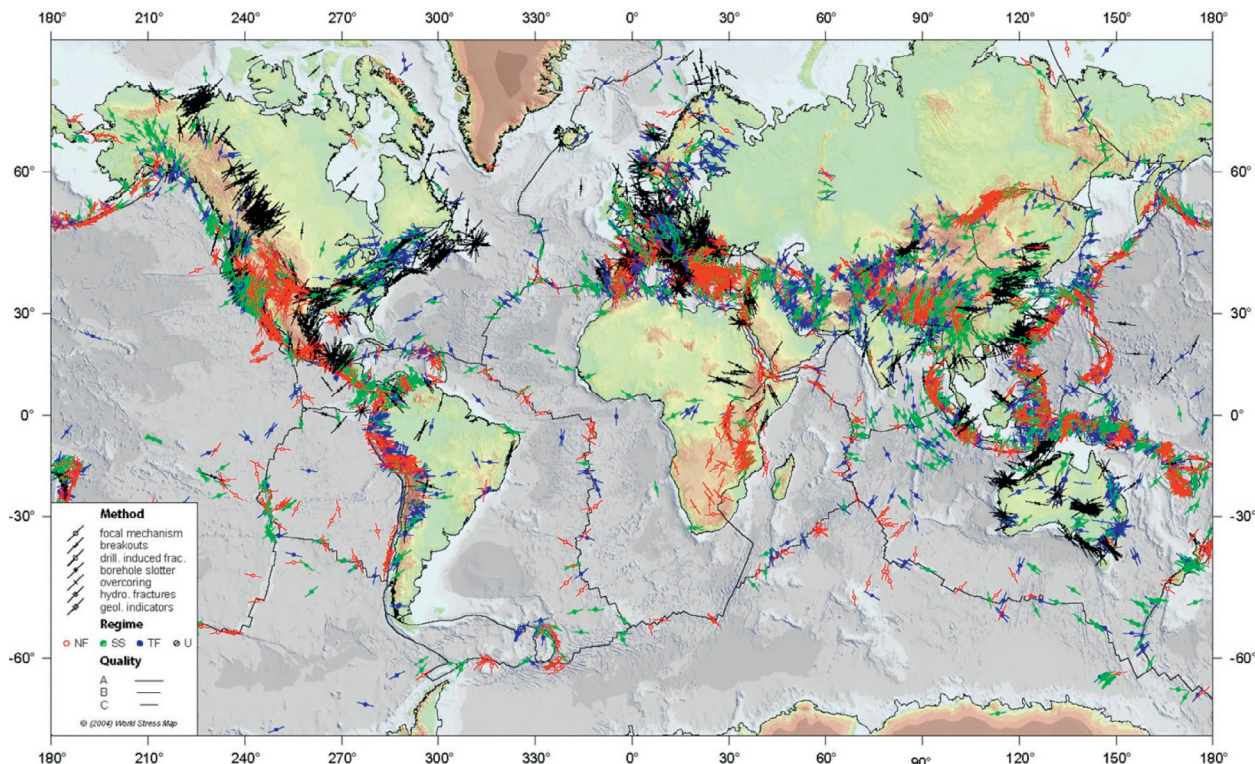


Figure 35 2005 version of the world stress map. Stress directions are determined by a range of techniques listed in the legend. Reproduced from Reinecker J, Heidbach O, Tingay M, Sperner B, and Müller B (2005) The release 2005 of the World Stress Map (available online at www.world-stress-map.org).

observed in the laboratory, indicates that friction is low, at least during slip in large earthquakes. The observation that stress along the San Andreas tends to be oriented such that the maximum compressive stress is close to fault normal (Zoback et al., 1987) is consistent with the notion that fault slip occurs at low levels of shear stress. This conclusion has been disputed by Scholz (2000) who argued that stress rotates near the San Andreas Fault to angles that are consistent with expectations from ordinary levels of friction. Further, borehole stress measurements suggest that stress increases with depth in accord with expectations from the laboratory. Scholz (2000) cited a much broader heat flow anomaly – ~80 km wide – centered on the San Andreas Fault (Lachenbruch and Sass, 1980) as the signature of heat generated during repeated large earthquakes. Larger permeabilities than have been measured in heat flow experiments would be required for convective heat transport to operate using crustal fluids, but if permeability is scale-dependent, then it could reach such an extent. Recent work on geologic signatures of transient heating (d'Alessio et al., 2003) and on transient heating in the immediate aftermath of large earthquakes (Kano et al., 2006) should help to resolve this important and long-standing controversy.

Earthquake focal mechanisms provide constraints on the local orientation of the stress field. Earthquakes can also provide information on changes in stress. During an earthquake, shear stress on the fault changes – for the most part dropping on parts of the fault that slipped and increasing on parts of the fault that did not. If the area of slip can be determined, then a characteristic dimension of faulting can be inferred from it. The

ratio of the average slip to the characteristic dimension can be thought of as a strain drop and interpreted through various simple models of source geometry as a drop in stress. This ‘stress drop’ represents how much the stress decreased from its initial level before the earthquake to the final level after the earthquake – at least on the parts of the fault that slipped. Thus, stress drop provides indirect, model-dependent, but nonetheless useful, constraints on the absolute level of stress. It is usually assumed that friction at depth is sufficiently large that shear stress does not drop below zero and act in the opposite direction following an earthquake, a condition that is termed ‘dynamic overshoot.’ Under this assumption, stress drops provide lower bounds on the level of shear stress acting on faults at seismogenic depths.

Stress drops (see Section 4.01.3.4) are determined seismically from a combination of the seismic moment and some measure of characteristic dimension. For shallow large earthquakes, the characteristic dimension can be estimated from various sources such as geodetic data, geologic data (e.g., surface break), tsunami source, slip inversion, aftershock area, and macroseismic data (e.g., intensity distribution). For small earthquakes, the source dimension cannot be directly determined and is usually taken as the radius of a circular crack. The radius is determined by measuring the corner frequency – the frequency of radiated waves at which the finiteness of the source of the earthquake first becomes apparent – with the assumption that the rupture speed is approximately equal to the shear-wave speed. Data from earthquakes, large and small, show that stress drops follow a scaling relation of the form $M_0 \sim r^3$. Since the faulted

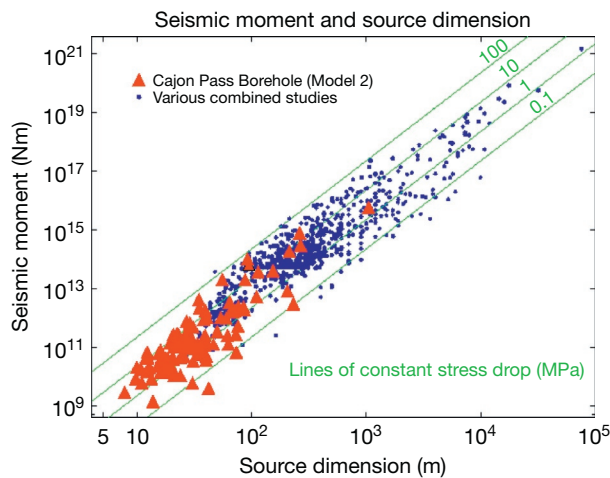


Figure 36 Abercrombie (1995) found from corner frequency measurements taken from a borehole seismometer that the relationship between source dimension and seismic moment for small earthquakes was the same as that for large earthquakes. Diagonal lines showing constant stress drop ($M_0 \sim r^3$) explain the trend in the data.

area, a , follows $a \sim r^2$, this leads to the average slip Δu , scaling as $\Delta u \sim r$, or in other words, the ratio of slip over length is constant (Figure 36).

Assuming that stress drop reflects the ambient stress, it is reasonable to expect that as depth increases, and the stress due to overburden changes with it, earthquake stress drops would increase as well. Such a correlation has proven difficult to find. In part, this may be due to the strong dependence of stress drop estimates on the corner frequency, which means that a small error in corner frequency will lead to a large error in the stress drop. By stacking over thousands of earthquakes, Shearer et al. (2006) had discerned just such a correlation (Figure 37). The depth dependence is much weaker, however, than would be expected if stress drops scaled with the overburden, and most of the dependence is in the upper third of the ~ 15 km depth extent of the seismogenic zone.

Another approach to determining stress drops is to use repeating earthquakes – earthquakes that repeatedly rupture a particular part of a fault – together with the assumption that these areas slip only seismically and keep up with long-term steady slip. For a given seismic moment, one can determine the average slip such that the slip matches the long-term rate. Stress drops determined by this approach (Nadeau and Johnson, 1998) are strongly scale-dependent. Stress drops for earthquakes of magnitude ~ 6 are comparable to those based on corner frequency measurements, but they find that stress drops measured using slip-rate matching of repeating earthquakes increase rapidly with decreasing earthquake size such that for the smallest earthquakes, they are one to two orders of magnitude higher.

4.01.6.2 Earthquake Nucleation and Short-Term Earthquake Prediction

Earthquake prediction can fairly be called the holy grail of seismology. While it may be that aspects of earthquakes are inherently unpredictable, the ability to predict behavior is the

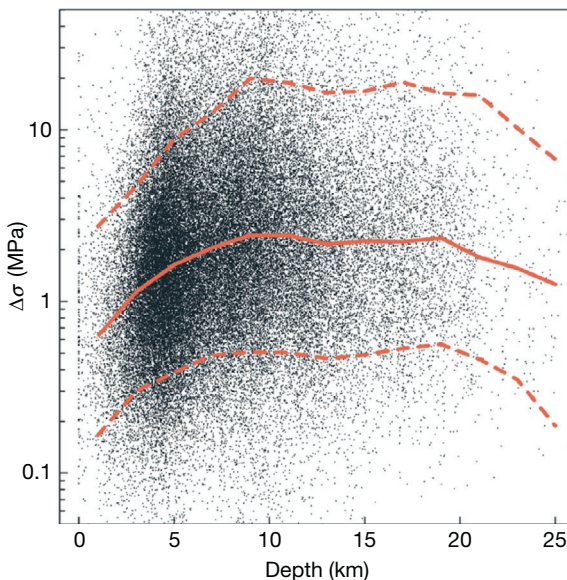


Figure 37 Shearer et al. (2006) were able to discern a depth dependence to stress drop for earthquakes in Southern California. Black dots show individual event stress drops. Solid line shows median values with depth and 10th and 90th percentiles shown as dashed lines.

sine qua non of science. Thus, over the long term at least, we can make predictions about earthquakes based on what we really do understand. For example, it is safe to ‘predict’ that over the next century, most earthquakes will occur on plate boundaries. This is not what most people have in mind when the phrase ‘earthquake prediction’ is used. Rather, it is understood to mean prediction of the location, size, and time of a specific earthquake to within a matter of days to months. Needless to say, this sort of prediction has not been realized, and there are many who maintain that the nature of the earthquake instability makes prediction on such short timescales intrinsically impossible.

The challenge of short-term earthquake prediction can be illustrated by comparing earthquakes with lightning – a phenomenon that shares some important similarities. Both earthquakes and lightning involve the catastrophic conversion of slowly accumulated potential energy to suddenly released kinetic energy. In the case of lightning, it is a slowly accumulated electrical charge that suddenly flows as electrical current in a lightning bolt and radiates sound waves as thunder. For earthquakes, it is gradually accumulated elastic strain energy stored in the Earth’s crust that suddenly accelerates the material on both sides of the fault and radiates energy in the form of seismic waves. The timescale of charge accumulation in a thunderhead can be measured in tens of seconds (order 10^1 s), whereas the timescale of strain accumulation in the Earth’s crust can be measured in centuries (order 10^{10} s). Based on the timescale of energy accumulation, predicting the size, location, and time of an earthquake to within a day (order 10^5 s) is equivalent to predicting the amperage, location, and time of a lightning bolt to within a tenth of a millisecond (order 10^{-4} s). At face value, this sounds wildly unrealistic, but with lightning, such a prediction is straightforward because lightning is preceded by a *nucleation* process.

The Earth's lower atmosphere is normally a very effective insulator. In order for a lightning bolt to propagate between a cloud and the ground, it must first create a conductive path for the lightning strike to follow. It does this through the formation of a stepped leader – the piecewise ionization of air that creates a path from cloud to ground. As the air is ionized, it transforms from an insulator to a conductor and forms a channel for the flow of current. Once a channel connects the cloud to the ground, the circuit is completed, charge can flow, and the discharge of the main lightning strike occurs, typically traveling from ground to cloud. For a lightning strike, the formation of the stepped leader is the nucleation phase. The stepped leader immediately precedes the lightning bolt and occurs over the entire length of the subsequent main event. The prediction of the time and location of a lightning bolt would be trivial once the stepped leader is observed. The key question for earthquake prediction is whether or not earthquakes have a similar nucleation process.

Laboratory ([Dieterich, 1979a,b](#)) and theoretical ([Andrews, 1976](#)) models of earthquake initiation both indicate that aseismic nucleation must occur before slip can propagate unstably across a fault, so it seems highly likely that nucleation of some sort must occur before earthquakes. Assuming it does, the question becomes, how extensive is the earthquake nucleation process? If it occurs over a very limited part of the fault, and thereafter earthquake rupture propagates as a self-sustaining process, then earthquake prediction will be very difficult – perhaps impossible. In this scenario, termed the Cascade model by [Ellsworth and Beroza \(1995\)](#), nucleation of small and large earthquakes might be identical. So for earthquake prediction to become a reality, not only would we need to observe the nucleation process, but also we would have to know that the fault is ready to host a self-sustaining, sometimes termed 'spontaneous,' rupture. This is a great deal more knowledge than we have about faults at present, and such information is likely to be hard to come by. If, on the other hand, the nucleation process scales with the size of the eventual earthquake, for instance, if the size of the nucleation zone were proportional to the size of the eventual earthquake, then earthquake prediction would be a good deal more likely, though still extremely challenging. Another source of significant uncertainty is multiple-fault interaction. The M_w 7.9 Denali, Alaska, earthquake of 2002, for example, began as a reverse faulting event on the Susitna Glacier fault, which led to a large strike-slip fault earthquake on the Denali Fault.

4.01.6.3 Earthquake Forecasting

The prospects for estimating earthquake likelihood over timescales of decades and longer, sometimes known as earthquake forecasting, are considerably brighter. We know that the great majority of earthquakes occur either on plate boundaries or on previously identified fault systems, so for the most part, we know where most earthquakes will occur. We also know quite accurately how rapidly plates are moving, so we have fault slip boundary conditions that must be met over a fault, or a system of faults that comprise a plate boundary, over time. This knowledge, together with information such as the time of the last major earthquake, or assumptions of the size distribution of large earthquakes, is enough to start estimating earthquake

likelihood. While earthquake forecasts are made routinely now as a part of seismic hazard assessment, the long timescales over which they apply make it difficult to test them rigorously. Moreover, to the extent that they have been tested, some studies have found them wanting.

The seismic gap hypothesis as formulated by [Fedotov \(1965\)](#), [Mogi \(1968\)](#), [McCann et al. \(1979\)](#), and [Kelleher et al. \(1973\)](#) holds that earthquakes are more likely to occur in areas prone to large earthquakes, but that have not recently had large earthquakes. [Kagan and Jackson \(1991\)](#) found that, as formulated, the seismic gap model has failed to predict where major earthquakes are more likely to occur. They interpreted this to mean that earthquakes are clustered in time, adding that because the theory of plate tectonics only provides long-term constraints on slip rates, it does not imply the regularity of earthquake recurrence.

Another possible interpretation of the failure of the seismic gap hypothesis is that it needs to be refined to take into account complicating factors, such as the possibility that earthquakes are not characteristic or that slip in earthquakes is strongly heterogeneous. As an example, consider the case of the 1981 Playa Azul and subsequent 1985 Michoacan, Mexico, earthquakes ([Singh et al., 1988](#); [Figure 38](#)). The two earthquakes occurred just 4 years apart and their spatial centroids are essentially the same, yet they clearly had very different, and most probably complementary, slip distributions. It should be possible to test a weaker form of the seismic gap hypothesis, such as whether or not earthquakes occur in areas that have not slipped recently, once geologic fault slip rates are taken into account. The Playa Azul and Michoacan earthquakes would pass this test while failing the original seismic gap hypothesis. It is interesting to note that the other seismic gap shown in [Figure 38](#), in the state of Guerrero, has not been the source of a large earthquake in the interval since [Singh et al. \(1988\)](#) published their paper. The Guerrero gap, however, has been the site of a $M_w \sim 7.5$ large silent earthquake ([Kostoglodov et al., 2003](#)), an observation that complicates the interpretation of this seismic gap. With the advent of GPS, earthquake forecasting has become significantly more quantitative.

A good example of forecasting is for the 2010 $M_w = 8.8$ Maule, Chile, earthquake. The earthquake occurred on the Chilean megathrust where another large earthquake had occurred in 1835 ($M \approx 8-8.5$). Charles Darwin experienced this earthquake and wrote a firsthand account of it in his 1845 book. Since that time, no major earthquake had occurred on this segment, called the Charles Darwin gap. The average repeat time of Chilean megathrust earthquakes is estimated to be 100–200 years. Thus, in the 1990s, the Charles Darwin gap had been expected to host another large earthquake in the near future. These are the boundary and the initial conditions to be used for forecasting the seismic activity in this gap. Having realized these conditions, several investigators began taking GPS measurements in this general area in 1996. Based on the displacement field determined by the 10-year GPS survey, [Ruegg et al. \(2009\)](#) concluded that if the plate coupling has been 100% since 1835, their results indicated ~ 10 m of slip deficit along this gap (slip deficit is the amount of slip that would occur if the accumulated strain were released in an earthquake) and forecasted that a M_w 8.5 earthquake would occur if the gap ruptured soon. Then, on 27 February 2010, a

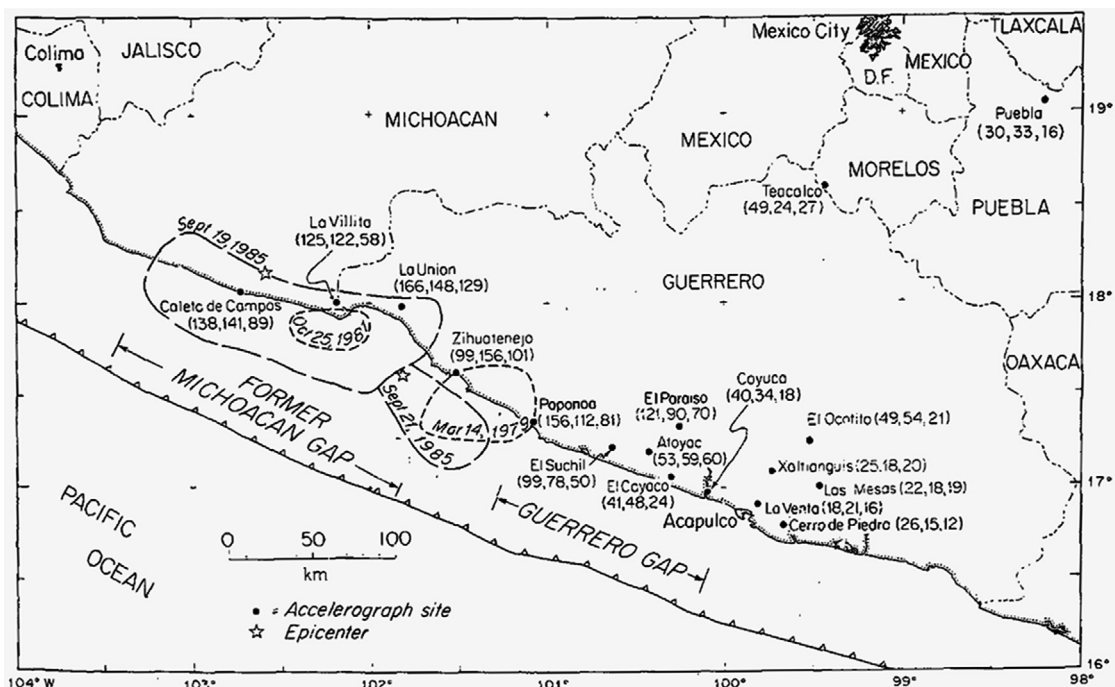


Figure 38 Map showing aftershock zones of the September 19 and 21 Michoacan, Mexico, earthquakes. Note that the rupture of the two earthquakes abuts, but that the 1985 rupture is much larger than, and entirely envelopes, the rupture zone of the 25 October 1981 Playa Azul earthquake. If such behavior is common, then it will greatly complicate attempts to apply the seismic gap hypothesis. Reproduced from Singh SK, Mena E, and Castro R (1988) Some aspects of source characteristics of the 19 September 1985 Michoacan earthquake and ground motion amplification in and near Mexico City from strong motion data. *Bulletin of Seismological Society of America* 78: 451–477.

$M_w=8.8$ earthquake did occur in the expected area with the expected mechanism (e.g., Delouis et al., 2010; Lay et al., 2010; Lorito et al., 2011; Vigny et al., 2011). The magnitude was slightly larger than what had been forecast, but some uncertainty is inevitable considering the complexities of the subduction zone structure and the stochastic elements associated with fracture phenomena like an earthquake.

In contrast to the case of the 2010 Chile earthquake, the case of the 2011 $M_w=9.0$ Tohoku-Oki earthquake illustrates the difficulty in forecasting of very complex natural processes like earthquakes even if extensive GPS data are available. For the subduction zone off the Tohoku coast, many GPS studies had previously been conducted in which onshore GPS data were extensively modeled (e.g., Hashimoto et al., 2009; Ito et al., 2000; Loveless and Meade, 2010; Mazzotti et al., 2000; Nishimura et al., 2004; Suwa et al., 2006). All results indicated evidence for large strain accumulation offshore. However, because of the limited spatial coverage (i.e., only onshore) of strain measurements, the location of strain accumulation could not be determined very well, especially in the east–west direction. Furthermore, because of the presence of many $M \sim 7.5$ earthquakes in the last several hundred years of historical record off Miyagi Prefecture, and the absence of direct evidence for, or possibly irregular occurrence of, extremely large earthquakes, together with the spatially heterogeneous mechanical or frictional properties of the plate boundary, the seismic potential of this region had been poorly understood, and the devastating $M_w=9.0$ earthquake occurred as a big surprise to most seismologists. Thus, this example clearly demonstrates the difficulty in making accurate scientific forecasts of great

earthquakes even with extensive GPS data. Nevertheless, as we improve our knowledge by ocean-bottom measurements and by studying many earthquakes in other tectonic environments, we will be able to reduce these uncertainties.

4.01.6.4 Static Stress Triggering

Over the past few decades, it has become increasingly obvious that our ability to forecast earthquakes is strongly dependent on our understanding of how earthquakes interact with one another. This is a critical question for earthquake hazard assessment that will inevitably depend on essential aspects of earthquake physics. How does the occurrence of one earthquake influence the occurrence of another? The seismic gap hypothesis is a limiting case of this in which the effect of an earthquake on a subsequent earthquake at the same place on the plate boundary is considered. Beyond this, the most obvious such interaction is an aftershock sequence in which many smaller earthquakes occur in the aftermath of a larger ‘main-shock.’ Large earthquakes are sometimes implicated in the triggering of other large earthquakes too, with the most famous example being the twentieth-century sequence of large earthquakes that eventually ruptured most of the North Anatolian Fault in Turkey (Toksoz et al., 1979).

Earthquake interaction is thought to occur through stress triggering, that is, failure in a future earthquake is either encouraged or discouraged by the static stress change induced by an earthquake that precedes it. Invoking the same criterion as in the subsection on faulting and pore fluids, fault slip will occur when the shear stress, τ , acting across the fault exceeds

the sum of the cohesion, C , and the effective normal stress multiplied by the coefficient of friction, μ :

$$\tau > \mu(\sigma - P) + C$$

where the term in the parentheses is referred to as the effective normal stress and is the difference between the fault-normal stress, σ , and the pore pressure, P . The cohesion is usually assumed to be negligible. By this criterion, earthquakes can be triggered by either an increase in shear stress, τ ; a decrease in normal stress, σ ; an increase in the pore pressure, P ; or some combination of the three. There is now a substantial body of literature that explores static stress triggering (Stein, 1999) and its implications for earthquake physics, for earthquake interaction, and for time-dependent seismic hazard assessment. Figure 39 shows perhaps the clearest example of static stress triggering: the progression of earthquakes across the North Anatolian Fault in Turkey during the twentieth century (Stein et al., 1997). As outlined in Section 4.01.5.1, friction on faults is thought to be dependent on slip rate and the past slip history of a fault. Changes in long-term earthquake probabilities due to stress steps induced by nearby earthquakes under rate- and state-variable friction laws have been explored by Parsons et al. (2000).

Perhaps, less obvious than the triggering of earthquakes by static stress changes is the notion of a stress shadow, in which earthquakes are inhibited because the stress necessary to drive them is relieved by a nearby large earthquake. The most famous and convincing example of this may be the almost complete lack of significant earthquakes in Northern California following the 1906 San Francisco earthquake (Ellsworth et al., 1981). Over the 100 years since the 1906 earthquake, there have been several earthquakes near the ends of the 1906 earthquake rupture – most notably the 1989 Loma Prieta earthquake, but nowhere near the level of seismicity that occurred in the 50 years leading up to the 1906 earthquake (Working Group on California Earthquake Probabilities, 2002). Stress shadows are important because they provide an opportunity to distinguish between static triggering and dynamic triggering (next section). The presence of stress shadows is strong supporting evidence for the importance of static stress changes in triggering earthquake activity (Toda et al., 2012). The topic of static stress change triggering of earthquakes is covered in detail in Chapter 4.10.

4.01.6.5 Dynamic Triggering

The examples cited earlier are of earthquakes either encouraging or inhibiting other earthquakes as a consequence of the static stress change that they induce. Another mode of earthquake interaction is through dynamic stress changes, that is, the transient stresses that are transmitted in the form of seismic waves. These were first clearly recognized in the aftermath of the 1992 Landers, California, earthquake in which ‘aftershocks’ were triggered at extreme distances of more than 1000 km from the mainshock (Hill et al., 1993). At these distances, static stress changes induced by the earthquake are much smaller than the periodic stress changes induced by solid Earth tides and are thus unlikely to act effectively as a trigger. Dynamic stress changes, on the other hand, are still quite substantial at great distances. This is attributable to the fact that static stress

changes decay approximately as distance cubed once a distance comparable to the source extent is exceeded. In contrast, dynamic stresses associated with surface waves decay much more slowly.

Since the Landers earthquake, dynamic triggering at great distance has been documented in the 1999 Izmit earthquake, the 2002 Denali earthquake, the 2004 Sumatra earthquake, and other events. In the case of Sumatra, microearthquakes were triggered at Mt. Wrangell, Alaska, at a distance of nearly 11 000 km from the rupture zone. In this instance, the triggered earthquakes were observed to occur during the maximum vertical displacement of the large and extremely long-period Rayleigh waves (Figure 40) generated by that event (West et al., 2005).

4.01.6.6 Temporal Distribution of Earthquakes

Large earthquakes are typically followed by numerous aftershocks. The rate of aftershocks R , as a function of time, t , following a large earthquake typically decays in time following a relation known as Omori’s law, which in its modified form (Utsu, 1961), can be written

$$R(t) \sim (t + c)^{-p}$$

where c is a constant and the exponent, p , is usually observed to be ~ 1 . Aftershocks are usually thought to occur in response to the stress change imposed by the mainshock they follow (Scholz, 1990). The mechanism behind the temporal decay of Omori’s law has been attributed to many physical effects. Elastic effects act immediately and do not explain the gradual decay. Among the mechanisms that have been proposed to explain the temporal decay of aftershock rate are pore fluid flow (Nur and Booker, 1972), viscoelastic relaxation (Freed and Lin, 2001), stress corrosion (Scholz, 1968), and earthquake nucleation under rate- and state-variable friction (Dieterich, 1994).

Since dynamic stresses can trigger earthquakes at large distance, it stands to reason that they can trigger earthquakes at short distances as well. This might explain the diverse aftershocks of the 1989 Loma Prieta earthquake and the observation that they were not favored by the mainshock-induced stress change (Beroza and Zoback, 1993). Felzer and Brodsky (2006) showed that the distance decay of aftershocks was consistent with dynamic triggering, even for small, local earthquakes.

Whether by static triggering, dynamic triggering, or other processes such as poroelastic effects, it is clear that earthquakes interact with each other. That is, the occurrence of one earthquake affects the probability of other earthquakes. This is true not only for large earthquakes but also for small earthquakes. Models that attempt to document and quantify the consequences of these interactions have come to be known by the acronym ‘ETAS,’ which stands for epidemic-type aftershock sequences (Ogata, 1988). These and other seismicity models are covered in more detail in Chapter 4.24.

4.01.7 Associated Problems

4.01.7.1 Strong Motion Prediction

From a societal perspective, the prediction of strong ground motion is arguably one of the most important issues that

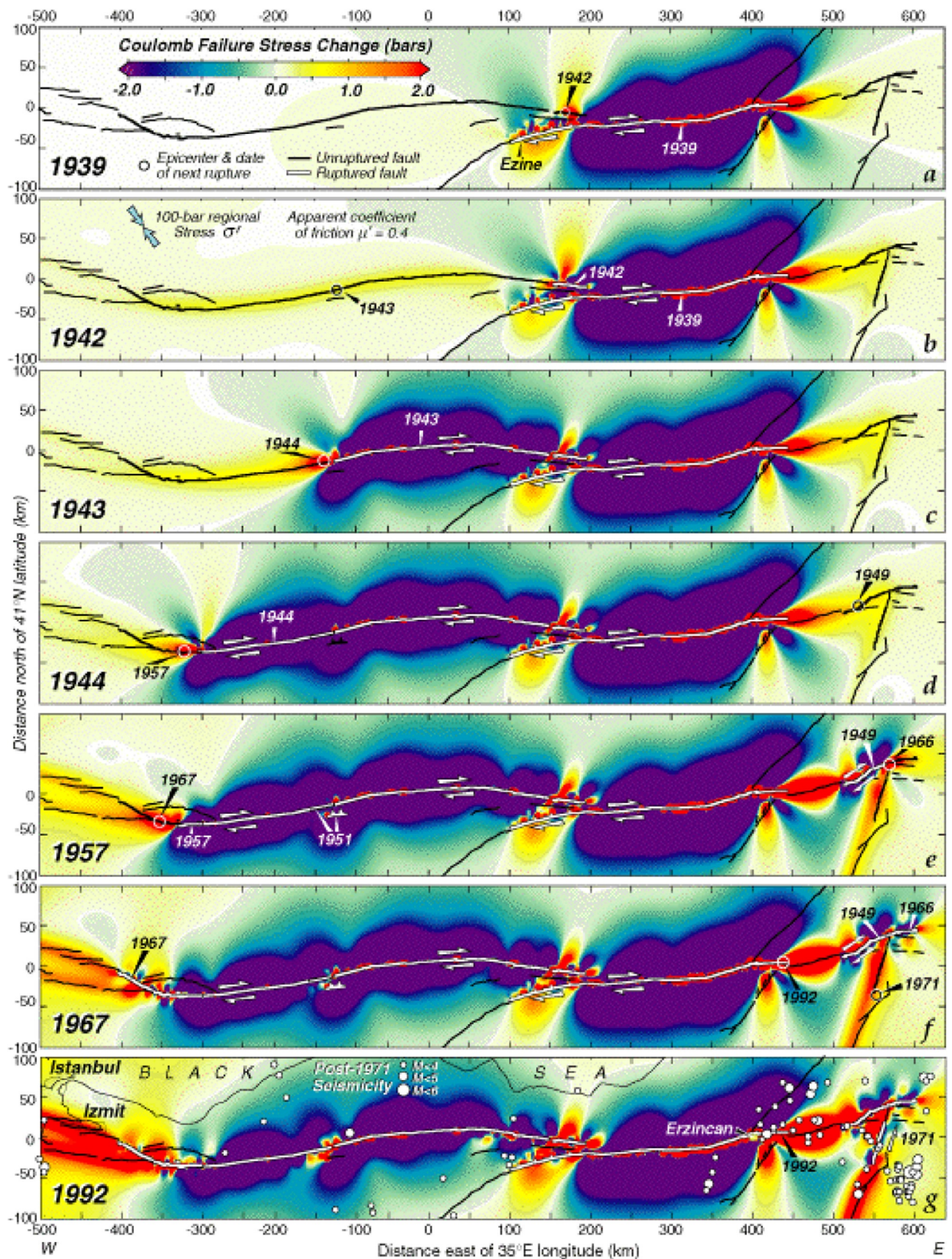


Figure 4 17 Oct 96 Stein et al.

Figure 39 Cumulative Coulomb stress changes caused by large earthquakes on the North Anatolian Fault in Turkey since 1939. In each panel, the epicenter of the next earthquake to rupture is circled. All but the 1943 epicenter lie in regions where the stress rose significantly, typically by 2–5 bar, owing to a combination of previous earthquakes and deep fault slip. Relocated earthquakes (Engdahl et al., 1998) are shown in the last panel, with the 1992 aftershock sequence removed. Calculations are made assuming a Poisson, elastic half-space. Slip is assumed uniform from 0 to 12.5 km depth. Fault is projected such that regional stress maintains a nearly fixed angle relative to the fault. Reproduced from <http://quake.usgs.gov/research/deformation/modeling/papers/anatolia.html>.

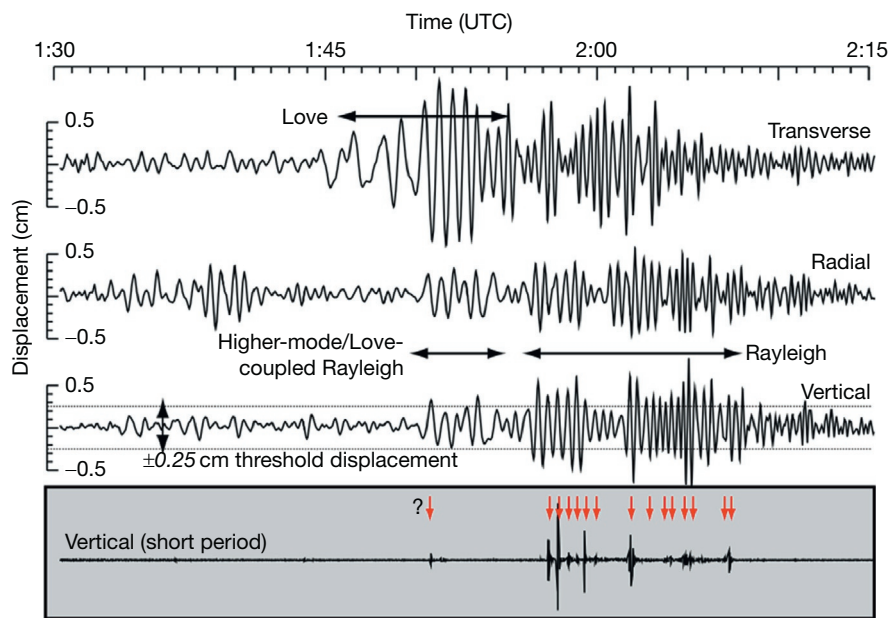


Figure 40 Three-component displacement records for the Sumatra earthquake as recorded at PAX. The bottom trace is from station WANC and has been filtered on 0.5–20 Hz to show timing of local events at Wrangell Volcano. The timing and spacing of the triggered events (highlighted with red arrows) with the Rayleigh wave phase and amplitude indicate Rayleigh motion is responsible for the triggering. Despite comparable amplitudes, there is no such correlation for the Love wave (screen grab from http://www.aeic.alaska.edu/input/west/wa_trigger/).

seismologists can address. Much of the risk that earthquakes pose, particularly to property, could not be mitigated by short-term prediction, which is an area of seismological research that is afforded a lot more attention by the general public. Even if short-term earthquake prediction should someday prove possible and reliable, it would not be possible, for example, to retrofit large engineered structures on a timescale of days to weeks.

The wave propagation properties of the Earth's crust are strongly heterogeneous on all scales. As a result, the seismic wave field becomes strongly distorted as it propagates through the crust. Compounding this wave field complexity is the possible complexity of the earthquake source itself, which can be substantial for the large damaging earthquakes that are of concern in strong ground motion prediction. Understanding and predicting this variability in strong ground motion pose a major challenge to engineering seismologists and civil engineers who have to design structures based on anticipated ground motions.

So how is strong ground motion predicted? Work in this area bridges the disciplines of seismology and earthquake engineering and thus is termed 'engineering seismology.' Engineering seismology seeks to predict the intensity of ground shaking likely to occur in future earthquakes. The standard procedure for predicting strong ground motion proceeds as follows.

The first step is to decide what intensity measure is to be used, which is an engineering decision based on what information is needed for structural design. Commonly used intensity measures include PGA, peak ground velocity, spectral acceleration (Sa), spectral velocity (Sv), and spectral displacement (Sd). Then, a dataset of strong motion recordings is assembled. A great deal of care is taken in the process to ensure

that the ground motion parameter of interest is not somehow obscured by particular characteristics of the recording site. Moreover, reliable information such as the distance to the fault plane and the geologic characteristics of the recording site are required in order to take full advantage of the data.

Once these data are assembled, and the intensity measure is determined for them, we posit a parametric relationship between relevant aspects of the earthquake of interest and the strong ground motion intensity measure. These relationships are usually called 'attenuation relations' despite the fact that they are dominated by effects other than anelastic attenuation. Examples of the factors that are used to develop these relationships include magnitude, closest distance to fault rupture, earthquake mechanism, and the nature of the soils at the site of interest. Next, a regression between these factors and the intensities observed in earthquakes is carried out in order to determine the coefficients of the attenuation relation.

The current scarcity of strong motion data at short distances from large earthquakes means that there are inadequate data to represent the hazard from the most dangerous events. Ground motion computer simulation provides a way to fill this gap in the data. Another argument in favor of ground motion simulation stems from the need of civil engineers for a more complete description of ground motion (i.e., seismograms) instead of a scalar intensity measurement, such as the spectral acceleration.

Simulation of near-fault ground motion that is accurate enough to be used to take the place of attenuation relations is an emerging technology that is not quite ready for application. A major source of uncertainty for these efforts remains an accurate characterization of the earthquake source and, in particular, the relationship between source parameters implied by rupture dynamics (Guatteri et al., 2004). Pseudodynamic

models are useful for incorporating the effects of rupture physics in attempts to simulate strong ground motion (Graves et al., 2011). Also crucial to strong ground motion prediction is the ability to model path effects, that is, the effect of wave propagation through the complex geologic structure of the Earth's crust. This includes not only elastic wave propagation but also loss of wave energy due to anelasticity and changes to the wave field due to nonlinear site effects. The approach of using small earthquakes as empirical Green's functions (eGfs) is a very promising avenue of research for the prediction of high-frequency strong ground motion (Joyner and Boore, 1986). The advantage of the eGf approach is that it includes the true complexity of wave propagation effects. In practice, its application is limited by the availability of suitable eGf events and the possibility that nonlinearities present during the strong ground motion of the mainshock will not affect the relatively weak motions of the eGf event.

4.01.7.2 Tsunamis

A tsunami is a long-period wave train that propagates as a shallow water wave in the open ocean. By 'shallow,' we mean that the wavelength is much longer than the depth of the ocean, such that particle trajectories in the wave are nearly horizontal. This criterion is easily satisfied by earthquake-generated tsunamis, which can have wavelengths 100 s of kilometers long – an order of magnitude greater than the depth of even the deepest ocean trenches. Because they are shallow water waves, tsunamis propagate at high speed across the open ocean – at speeds that approach the speed of travel by commercial jets.

Earthquakes represent one of the primary triggers of tsunamis, but tsunamis can be generated in many ways. The permanent deformation of the sea floor due to an earthquake is the source of some of the largest, most destructive tsunamis, but other important potential tsunami sources include submarine landslides, volcanic eruptions, and bolide impacts. For some earthquakes, such as the 1946 earthquake in the Aleutian Islands, tsunami modeling suggests that landslides triggered by earthquakes may have been the principal tsunami source (Fryer et al., 2004), though Lopez and Okal (2006) modeled the tsunami generation using a very large, but slow earthquake rupture. Clearly both triggered landslides and deformation of the sea floor due to earthquake rupture must be considered capable of tsunami generation regardless of whether one particular tsunami arose from one source or the other. For a detailed treatment of tsunamis as they relate to earthquakes, see Chapter 4.19.

4.01.7.3 Test Ban Treaty Verification

Since a nuclear bomb was first tested underground in 1957, seismology has played a key role in nuclear monitoring and Test Ban Treaty verification. Much of the impetus and funding to establish the WWSSN in the early 1960s and its successor the Global Seismic Network nearly three decades later came not from the need to monitor earthquakes, but from the need to monitor nuclear testing. The proliferation of nuclear weapons to additional countries, and the reduction in the target monitoring threshold from 150 kt of TNT to 10 kt, required a truly global seismological network that spans all the continents and

records data over a broad range of frequencies. The multilateral nature of the Comprehensive Test Ban Treaty also meant that the data had to be openly available to all interested parties. This combination has served the purposes of Test Ban Treaty verification research, but it has also been a bonanza to earthquake seismology in general. It is also fair to say that earthquake monitoring has been an important source of sustenance for these same networks.

There are a number of issues that arise in Test Ban Treaty verification research. First, and perhaps foremost, is the need to detect and locate small magnitude events that represent possible low-yield nuclear tests. The second task is to discriminate explosions from earthquakes (and, in addition, nuclear tests from other explosions). Figure 35 shows a comparison of a seismogram from an earthquake with one from an explosion. The relatively efficient generation of P-waves relative to S-waves is one means for discriminating explosions from earthquakes. A third task is to assess the feasibility of various evasion scenarios in which a clandestine test could be sufficiently decoupled from the Earth or somehow disguised such that it would go unreported. As the size threshold decreases, all of these tasks become more difficult due to reduced signal-to-noise ratio, a larger number of small earthquakes, and an increasing population of ordinary chemical explosions in the same size range. Yet another task is to estimate the explosive yield of a test. This was a critical issue for the Threshold Test Ban Treaty in the 1970s and 1980, but it continues to be important. Through precise relative amplitude measurements, the yield of the 2013 test in North Korea has been found to be 12 kt of TNT energy equivalent (Zhang and Wen, 2013). This follows the 2006 test, which is widely regarded as a fizzle, and it is much higher than the 2009 North Korea test, which was only slightly larger than 2 kt (Zhao et al., 2012) (Figure 41).

4.01.7.4 Solid Earth–Atmospheric Coupling

Seismic waves are generated not only by earthquakes but also by other sources. Volcanoes, for example, are obviously prodigious sources of earthquakes and other seismic sources such as harmonic tremor. Large landslides on volcanoes are another source. All of these represent processes within the solid Earth. Vigorous volcanic eruptions disturb the atmosphere sufficiently that the acoustic and gravitational waves in the atmosphere couple to the solid Earth and excite seismic waves (Kanamori and Mori, 1992; Widmer and Zürn, 1992). The 15 February 2013 Chelyabinsk meteorite was the largest since the 1908 Tunguska event. The airburst caused damage and injuries. It also generated Rayleigh waves detectable at distances of up to 4000 km that were equivalent in amplitude to those from an M_S 3.7 earthquake (Tauzin et al., 2013).

The impedance of the atmosphere is much smaller than that of the solid Earth. As a result, a displacement of the Earth's surface will translate more or less directly into a displacement of the atmosphere. This effect is so small that it is usually neglected, but there are circumstances in which it is important and has a detectable effect. The density of the atmosphere decreases exponentially with increasing altitude. As a result, a perturbation that is modest at the Earth's surface grows dramatically as it propagates upward through the atmosphere. For

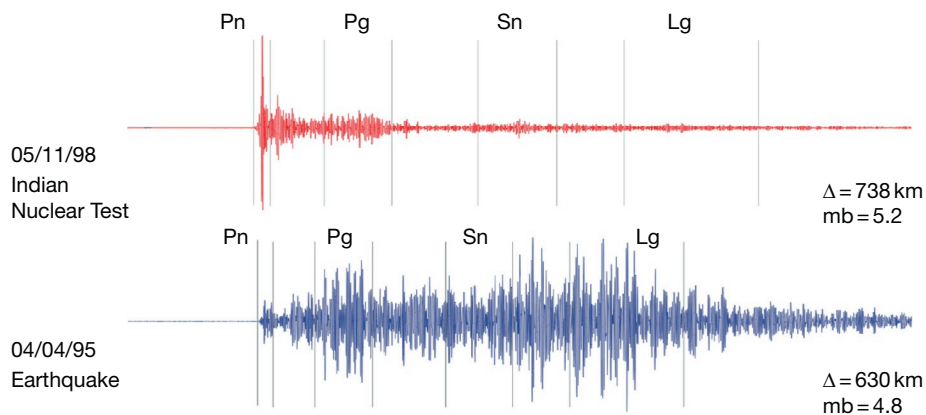


Figure 41 Seismograms recorded on the same instrument at Nilore, Pakistan. Upper seismogram shows ground motion due to an Indian nuclear test. Lower seismogram shows seismogram due to an earthquake at a similar distance. The phases Pn, Pg, Sn, and Lg are shown with vertical lines. Note that the S-wave arrivals from the earthquake are systematically much larger than for the explosion. Clues such as these help to discriminate underground nuclear tests from earthquakes. Reproduced from Walter WR, Rodgers AJ, Mayeda K, Myers SC, Pasanos M, and Denny M (1998) Preliminary regional seismic analysis of nuclear explosions and earthquakes in Southwest Asia. In: *Proceedings of the 20th Annual Seismic Research Symposium on Monitoring a Comprehensive Test Ban Treaty*. Department of Defense and Department of Energy Report, pp. 442–452.

a major earthquake, this leads to a large and easily detectable change in the ionosphere. Because the ionosphere has a strong effect on electromagnetic waves propagating through it, changes in the ionosphere caused by earthquakes can be detected using, for example, transmissions from GPS satellites (Calais and Minster, 1995). The displacements caused by a large tsunami have also generated detectable ionospheric perturbations (Artru et al., 2005).

The continuous excitation of the very long-period free oscillations (Suda et al., 1998) also appears to result from coupling between the Earth and its atmosphere and/or oceans. The basic observation is that the Earth's very low-frequency fundamental spheroidal modes of oscillations are excited even during periods where there are no earthquakes to account for them. The excitation has an annual signature that strongly suggests it is not driven by processes within the solid Earth. Early explanations for this excitation focused on atmospheric disturbances as the cause (Kobayashi and Nishida, 1998), but more recent analysis suggests excitation by oceanic infragravity waves (Figure 42) is more likely (Rhee and Romanowicz, 2004). For more details on this subject, see Chapter 4.16.

4.01.8 Earthquake Risk Mitigation

Efficient mitigation of the risk posed by earthquakes requires as a foundation a quantitative measurement of the hazard that earthquakes pose. Once this is understood, informed policy decisions on building codes and their enforcement and on priorities for retrofitting susceptible structures can be made. Much of the work in earthquake hazard analysis casts strong ground motion prediction as a probabilistic statement in a process called probabilistic seismic hazard analysis (PSHA).

PSHA was developed to integrate multiple factors that control the likelihood and strength of shaking to be expected, each of which can be treated as a stochastic process. PSHA asks, for example, what is the ground motion that has a 2% probability of being exceeded over a 50-year time interval? To determine

this number, and to map it spatially, requires combining information on earthquake likelihood for all relevant earthquake sources (i.e., active nearby faults) with strong motion attenuation laws that include site effects. The output of PSHA is a map of ground motion intensities at a specified exceedance probability that can be used in building codes to develop design criteria for buildings and by policymakers to develop priorities for earthquake risk reduction. Figure 43 shows an example calculation for the entire planet.

Given the importance of PSHA to earthquake risk characterization and mitigation, it is important that it be tested to the extent possible. This is challenging because the timescales involved are long, and the probabilities are low. Under the ergodic assumption, it is possible to supplement the short time record of recorded ground motions, by considering a large spatial area. Tests of this kind consider PSHA predictions against observed ground motion (Stirling and Petersen, 2006) or extend it into the preinstrumental era using historical catalogs and ground motion prediction equations (Ward, 1995).

Another important area in seismic risk reduction is earthquake early warning. Earthquake early warning systems rely on the fact that although seismic waves travel at high speed, information that an earthquake has occurred can be transmitted at the speed of light, such that an alert that a significant earthquake is under way can be issued before damaging seismic waves arrive. Earthquake early warning systems are operational in Japan, Mexico, and Taiwan and are in the planning stages in Romania, Turkey, and the United States. The amount of warning that such systems can provide for large earthquakes under favorable circumstances can be several 10 s of seconds. For more details on seismic hazard and real-time warning systems, see Chapter 4.23.

4.01.9 Conclusions

In this chapter, we have taken a synoptic view of earthquake seismology and several closely related fields of study. In the

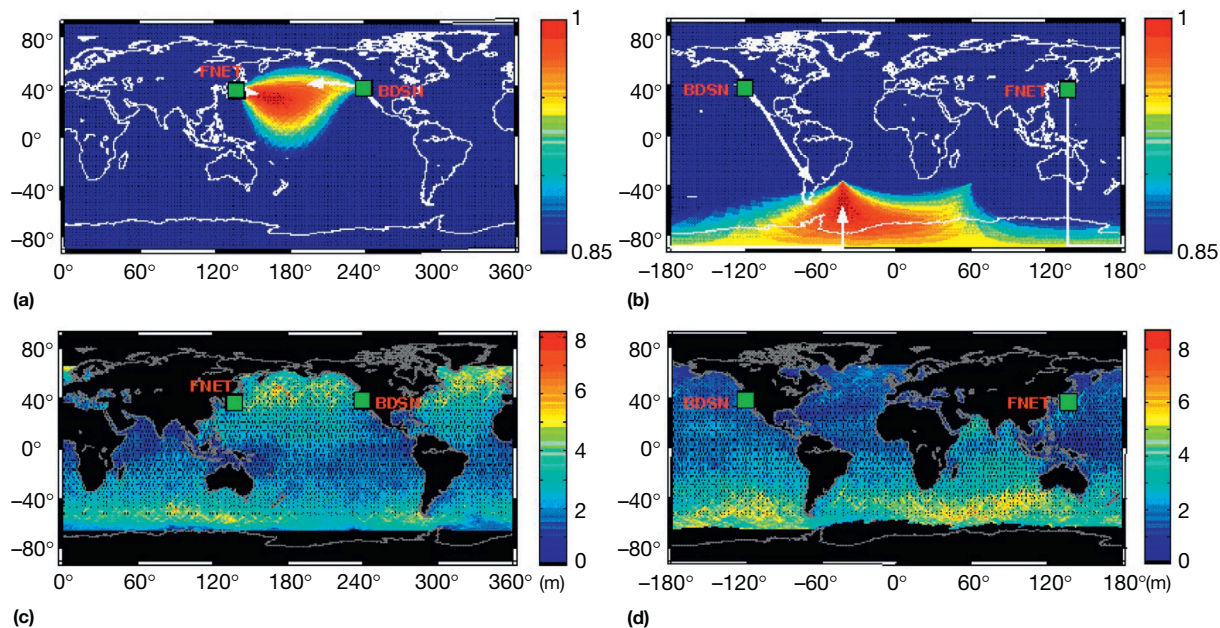


Figure 42 Localization of the source of background excitation of the Earth's free oscillations (Rhee and Romanowicz, 2004) using arrays in Japan and the United States. Arrows in upper panels point from the arrays to the source of excitation (red area) for two different time periods. The excitation on the left is for the northern Pacific and on the right for the southern Atlantic. Sources are more active in boreal and austral winter seasons. Lower panels show monthlong significant wave heights for those seasons from TOPEX/Poseidon measurements.

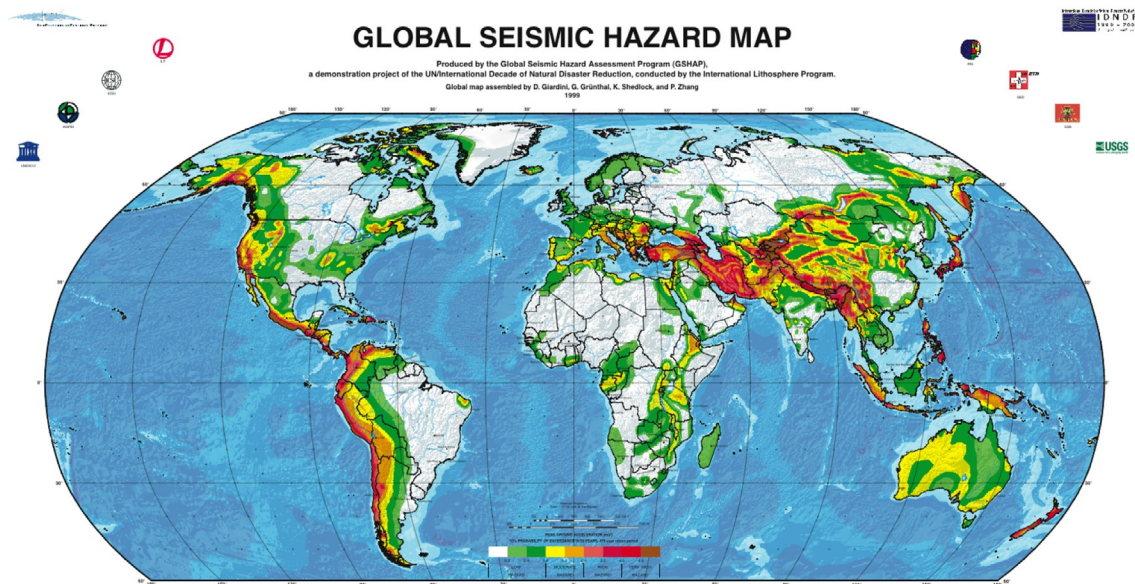


Figure 43 Global seismic hazard map. Areas of red are of highest seismic hazard, while clear areas are of lowest seismic hazard. Seismic hazard is dominated by plate boundary seismicity, except in continental collisions zones – most notably the Alpine belt. Reproduced from the home page of the global seismic hazards assessment program, <http://www.seismo.ethz.ch/GSHAP/>.

chapters that follow, many of the same topics are covered, but in much greater detail. The field of earthquake seismology is rapidly evolving. This evolution is driven by several factors. Perhaps, the most important single factor is rapid progress in the quality, density, and wide availability of seismic data. Seismic data centers, which house many terabytes of seismic

data and have easy availability via the Internet, have resulted in access for interested seismologists to literally millions of seismograms. These large data volumes enable fundamentally new ways of looking at earthquakes. They also mean that visual analysis of seismograms, except on a proof-of-concept basis, is rapidly becoming a thing of the past. The computational

capabilities of computers have kept pace with the rapid rise in data availability. As data collection and computational resources continue a rapid upward trajectory, imaginative seismologists are presented with an unprecedented opportunity to pose, and to answer, new questions about the earthquake process.

As a result, we can look forward to rapid progress in the field of earthquake and volcano seismology. This progress will be punctuated by large, devastating earthquakes. As in the past, important aspects of these earthquakes will not be expected, which testifies to the fact that earthquake science remains a young and exciting field of research. The havoc future earthquakes will wreak and will also serve to remind seismologists, and those who depend on their research, of the profound societal relevance of earthquake science.

References

- Aagaard BT and Heaton TH (2004) Near-source ground motions from simulations of sustained intersonic and supersonic fault ruptures. *Bulletin of the Seismological Society of America* 94: 2064–2078.
- Abercrombie RE (1995) Earthquake source scaling relationships from –1 to 5 ML, using seismograms recorded at 2.5 km depth. *Journal of Geophysical Research* 100: 24015–24036.
- Abercrombie RE, McGarr A, Kanamori H, and Di Toro G (eds.) (2006) *Earthquakes: Radiated Energy and the Physics of Faulting*, In: AGU Geophysical Monograph Series 170: p. 327.
- Abercrombie RE and Rice JR (2005) Can observations of earthquake scaling constrain slip weakening? *Geophysical Journal International* 162: 406–424. <http://dx.doi.org/10.1111/j.1365-246X.2005.02579.x>.
- Aki K (1966) Generation and propagation of G waves from the Niigata earthquake of June 16, 1964: Part 2. Estimation of earthquake moment, released energy and stress drop from the G wave spectra. *Bulletin of the Earthquake Research Institute, University of Tokyo* 44: 73–88.
- Andrews DJ (1976) Rupture velocity of plane strain shear cracks. *Journal of Geophysical Research* 81: 5679–5687.
- Andrews DJ (2005) Rupture dynamics with energy loss outside the slip zone. *Journal of Geophysical Research* 110. <http://dx.doi.org/10.1029/2004JB003191>.
- Andrews DJ and Ben-Zion Y (1997) Wrinkle-like slip pulse on a fault between different materials. *Journal of Geophysical Research* 102: 553–571.
- Argus DF and Gordon RG (2001) Present tectonic motion across the Coast Ranges and San Andreas fault system in central California. *Geological Society of America Bulletin* 113: 1580–1592.
- Artru J, Ducic V, Kanamori H, Lognonne P, and Murakami M (2005) Ionospheric gravity waves induced by tsunamis. *Geophysical Journal International* 160: 840–848. <http://dx.doi.org/10.1111/j.1365-246X.2005.02552.x>.
- Arvidsson R (1996) Fennoscandian earthquakes: Whole crustal rupturing related to postglacial rebound. *Science* 274: 744–746.
- Astiz L, Lay T, and Kanamori H (1988) Large intermediate-depth earthquakes and the subduction process. *Physics of the Earth and Planetary Interiors* 53: 80–166. [http://dx.doi.org/10.1016/0031-9201\(88\)90138-0](http://dx.doi.org/10.1016/0031-9201(88)90138-0).
- Backus G and Mulcahy M (1976) Moment tensors and other phenomenological descriptions of seismic sources II. Discontinuous displacements. *Geophysical Journal of the Royal Astronomical Society* 47: 301–329.
- Bak P and Tang C (1989) Earthquakes as a self-organized critical phenomenon. *Journal of Geophysical Research* 94: 15635–15637.
- Bakun WH and Wentworth CM (1997) Estimating earthquake location and magnitude from intensity data. *Bulletin of Seismological Society of America* 87: 1502–1521.
- Barazangi M and Dorman J (1969) World seismicity maps compiled from ESSA, Coast and Geodetic Survey, epicenter data, 1961–1967. *Bulletin of Seismological Society of America* 59: 369–380.
- Beck ME (1983) On the mechanism of tectonic transport in zones of oblique subduction. *Tectonophysics* 93: 1–11.
- Ben-Zion Y, Peng Z, Okaya D, et al. (2003) A shallow fault-zone structure illuminated by trapped waves in the Karadere-Duzce branch of the North Anatolian Fault, Turkey. *Geophysical Journal International* 152: 699–717.
- Beroza GC and Zoback MD (1993) Mechanism diversity of the Loma Prieta aftershocks and the mechanics of mainshock-aftershock interaction. *Science* 259: 210–213.
- Bilham R (1995) Global fatalities in the past 2000 years: Prognosis for the next 30. In: Rundle J, Klein F, and Turcotte D (eds.) *Reduction and Predictability of Natural Disasters. Santa Fe Institute Studies in the Sciences of Complexity*, 25, pp. 19–31. Boston, MA: Addison-Wesley.
- Boatwright J and Bundock H (2005) Modified Mercalli intensity maps for the 1906 San Francisco earthquake plotted in shake-map format. US Geological Survey Open-File Report 2005-1135.
- Bolt BA (1993) *Abridged Modified Mercalli Intensity Scale, Earthquakes*: W.H. Freeman and Co, Appendix C, 331 pp.
- Booker JR (1974) Time dependent strain following faulting of porous medium. *Journal of Geophysical Research* 79: 2037–2044.
- Bouchon M, Bouin MP, Karabulut H, Toksoz MN, and Dietrich M (2001) How fast does rupture propagate during an earthquake? New insights from the 1999 Turkey earthquakes. *Geophysical Research Letters* 28: 2723–2726.
- Bouchon M and Vallée M (2003) Observation of long supershear rupture during the magnitude 8.1 Kunlunshan earthquake. *Science* 301: 824–826.
- Brodsky EE, Mori J, and Fulton PM (2010) Drilling into faults quickly after earthquakes. *Eos, Transactions American Geophysical Union* 91: 237–238.
- Brune JN (1968) Seismic moment, seismicity, and rate of slip along major fault zones. *Journal of Geophysical Research* 73: 777–784.
- Brune JN, Heney TL, and Roy RF (1969) Heat flow, stress and rate of slip along San Andreas fault, California. *Journal of Geophysical Research* 74: 3821–3827.
- Byerlee JD (1978) Friction of rocks. *Pure and Applied Geophysics* 116: 615–626.
- Calais E and Minster JB (1995) GPS detection of ionospheric perturbations following the January 17, 1994, Northridge earthquake. *Geophysical Research Letters* 22: 1045–1048.
- Campbell DL (1978) Investigation of the stress-concentration mechanism for intraplate earthquakes. *Geophysical Research Letters* 5: 477–479.
- Chapple WM and Forsyth DW (1979) Earthquakes and bending of plates at trenches. *Journal of Geophysical Research* 84: 6729–6749.
- Chouet B (1988) Resonance of a fluid-driven crack: Radiation properties and implications for the source of long-period events and harmonic tremor. *Journal of Geophysical Research* 93: 4375–4400.
- Chouet B (1996) Long-period volcano seismicity: Its source and use in eruption forecasting. *Nature* 380: 309–316.
- Chung W-Y and Kanamori H (1976) Source process and tectonic implications of the Spanish deep-focus earthquake of March 29, 1954. *Physics of the Earth and Planetary Interiors* 13: 85–96.
- D'Alessio MA, Blythe AE, and Burgmann R (2003) No frictional heat along the San Gabriel fault, California: Evidence from fission-track thermochronology. *Geology* 31: 541–544. <http://dx.doi.org/10.1130/0091-7613>.
- Delouis B, Nocquet J-M, and Vallée M (2010) Slip distribution of the February 27, 2010 Mw = 8.8 Maule earthquake, central Chile, from static and high-rate GPS, InSAR, and broadband teleseismic data. *Geophysical Research Letters* 37(17), L17305.
- Di Toro G, Golbsby DL, and Tullis TE (2004) Friction falls toward zero in quartz rock as slip velocity approaches seismic rates. *Nature* 427: 436–439.
- Dieterich JH (1972) Time-dependent friction in rocks. *Journal of Geophysical Research* 77: 3690–3697.
- Dieterich JH (1978) Time-dependent friction and the mechanics of stick-slip. *Pure and Applied Geophysics* 116: 790–806.
- Dieterich JH (1979a) Modeling of rock friction, 1. Experimental results and constitutive equations. *Journal of Geophysical Research* 84: 2161–2168.
- Dieterich JH (1979b) Modeling of rock friction, 2. Simulation of preseismic slip. *Journal of Geophysical Research* 84: 2169–2175.
- Dieterich JH (1994) A constitutive law for rate of earthquake production and its application to earthquake clustering. *Journal of Geophysical Research* 99: 2601–2618.
- Dragert H, Wang K, and James TS (2001) A silent slip event on the deeper Cascadia subduction interface. *Science* 292: 1525–1528.
- Dunham EM and Archuleta RJ (2004) Evidence for a supershear transient during the 2002 Denali fault earthquake. *Bulletin of the Seismological Society of America* 94: S256–S268.
- Dunham EM, Belanger D, Cong L, and Kozdon JE (2011) Earthquake ruptures with strongly rate-weakening friction and off-fault plasticity, 2: Nonplanar faults. *Bulletin of the Seismological Society of America* 101(5): 2308–2322. <http://dx.doi.org/10.1785/0120100076>.
- Dziewonski AM, Chou T-A, and Woodhouse JH (1981) Determination of earthquake source parameters from waveform data for studies of global and regional seismicity. *Journal of Geophysical Research* 86: 2825–2852.
- Ellsworth WL and Beroza GC (1995) Seismic evidence for an earthquake nucleation phase. *Science* 268: 851–855.
- Ellsworth WL, Lindh AG, Prescott WH, and Herd DG (1981) The 1906 San Francisco earthquake and the seismic cycle. In: Simpson DW and Richards PG (eds.)

- Earthquake Prediction: An International Review. Maurice Ewing Series*, vol. 4, pp. 126–140. Washington, DC: AGU.
- Engdahl ER, van der Hilst R, and Buland R (1998) Global teleseismic earthquake relocation with improved travel times and procedures for depth determination. *Bulletin of Seismological Society of America* 88: 722–743.
- Fedotov SA (1965) Regularities of the distribution of strong earthquakes in Kamchatka, the Kurile Islands, and northeast Japan. *Trudy Inst Fiz. Zemli Acad. Nauk. SSSR* 36: 66.
- Felzer KR and Brodsky EE (2006) Decay of aftershock activity with distance indicates triggering by dynamic stress. *Nature* 441: 735–738.
- Fialko Y and Khazan Y (2005) Fusion by earthquake fault friction: Stick or slip? *Journal of Geophysical Research* 110: B12407. <http://dx.doi.org/10.1029/2005JB003869>.
- Fialko Y, Sandwell D, Agnew D, Simons M, Shearer P, and Minster B (2002) Deformation on nearby faults induced by the 1999 Hector Mine earthquake. *Science* 297: 1858–1862.
- Fitch TJ (1972) Plate convergence, transcurrent faults, and internal deformation adjacent to southeast Asia and the western Pacific. *Journal of Geophysical Research* 77: 4432–4460.
- Frankel A, Fletcher JB, and Vernon FL (1986) Rupture characteristics and tomographic source imaging of $M_L \sim 3$ earthquakes near Anza, Southern California. *Journal of Geophysical Research* 91(12): 633–650.
- Freed AM and Lin J (2001) Delayed triggering of the 1999 Hector Mine earthquake by viscoelastic stress transfer. *Nature* 411: 180–183.
- Freund LB (1990) *Dynamic Fracture Mechanics*. Cambridge, UK: Cambridge University Press, 563 pp.
- Frohlich C (1989) The nature of deep focus earthquakes. *Annual Review of Earth and Planetary Sciences* 17: 227–254.
- Fryer GJ, Watts P, and Pratson LF (2004) Source of the great tsunami of 1 April 1946: A landslide in the upper Aleutian forearc. *Marine Geology* 203: 201–218.
- Fukao Y, Hori S, and Uwaka M (1983) A seismological constraint on the depth of the basalt–eclogite transition in a subducting oceanic crust. *Nature* 303: 413–415.
- Goldsby DL and Tullis TE (2002) Low frictional strength of quartz rocks at subseismic slip rates. *Geophysical Research Letters* 29: 1844. <http://dx.doi.org/10.1029/2002GL015240>.
- Gordon RG (1998) The plate tectonic approximation: Plate nonrigidity, diffuse plate boundaries, and global plate reconstructions. *Annual Review of Earth and Planetary Sciences* 26: 615–642.
- Graves R, Jordan TH, and Callaghan S (2011) Cybershake: A physics-based seismic hazard model for Southern California. *Pure and Applied Geophysics* 168: 367–381.
- Guatteri M, Mai PM, and Beroza GC (2004) A pseudo-dynamic approximation to dynamic rupture models for strong ground motion prediction. *Bulletin of the Seismological Society of America* 94(6): 2051–2063. <http://dx.doi.org/10.1785/0120040037>.
- Guatteri M and Spudich P (2000) What can strong-motion data tell us about slip-weakening fault-friction laws. *Bulletin of Seismological Society of America* 90: 98–116. <http://dx.doi.org/10.1785/0119990053>.
- Gutenberg B (1955) Magnitude determination for larger Kern County shocks, 1952; Effects of station azimuths and calculation methods. *California Division of Mines and Geology Bulletin* 171: 171–175.
- Gutenberg B and Richter CF (1936) Magnitude and energy of earthquakes. *Science* 83: 183–185.
- Gutenberg B and Richter CF (1954) *Seismicity of the Earth and Associated Phenomenon*, 2nd edn. Princeton: Princeton University Press.
- Gutenberg B and Richter CF (1942) Earthquake magnitude, intensity, energy, and acceleration. *Bulletin of the Seismological Society of America* 32: 163–191.
- Gutenberg B and Richter CF (1956) Magnitude and energy of earthquakes. *Annali di Geofisica* 9: 1–15.
- Hagerty MT, Schwartz SY, Garces MA, and Protti M (2000) Analysis of seismic and acoustic observations at Arenal volcano, Costa Rica, 1995–1997. *Journal of Volcanology and Geothermal Research* 101: 27–65.
- Hanks TC and Kanamori H (1979) A moment magnitude scale. *Journal of Geophysical Research* 84: 2348–2350.
- Harris R (1998) Introduction to special section: Stress triggers, stress shadows, and implications for seismic hazard. *Journal of Geophysical Research* 103: 24347–24358. <http://dx.doi.org/10.1029/98JB01576>.
- Hashimoto C, Noda A, Sagiya T, and Matsu'ura M (2009) Interplate seismogenic zones along the Kuril–Japan trench inferred from GPS data inversion. *Nature Geoscience* 2(2): 141–144.
- Healy JH, Rubey WW, Griggs DT, and Raleigh CB (1968) The Denver earthquakes. *Science* 161: 1301–1310.
- Heaton TH (1990) Evidence for and implications of self-healing pulses of slip in earthquake rupture. *Physics of the Earth and Planetary Interiors* 64: 1–20.
- Hill DP, Reasenberg PA, Michael A, et al. (1993) Seismicity in the western United States remotely triggered by the M 7.4 Landers, California, earthquake of June 28, 1992. *Science* 260: 1617–1623.
- Hirose H and Obara K (2005) Repeating short- and long-term slow slip events with deep tremor activity around the Bungo channel region, southwest Japan. *Earth, Planets and Space* 57: 961–972.
- Hough SE and Page M (2011) Toward a consistent model for strain accrual and release for the New Madrid Seismic Zone, central United States. *Journal of Geophysical Research* 116: B03311. <http://dx.doi.org/10.1029/2010JB007783>.
- Hubbert MK and Rubey WW (1959) Role of fluid pressure in mechanics of overthrust faulting 1. Mechanics of fluid-filled porous solids and its application to overthrust faulting. *Geological Society of America Bulletin* 70: 115–166.
- Huixian L, Housner GW, Lili X, and Duxin H (2002) The great Tangshan earthquake of 1976. Technical Report: CaltechEERL:EEERL.2002.001. California Institute of Technology.
- Ida Y (1972) Cohesive force across the tip of a longitudinal-shear crack and Griffith's specific fracture energy. *Journal of Geophysical Research* 77: 3796–3805.
- Ide S and Beroza GC (2001) Does apparent stress vary with earthquake size? *Geophysical Research Letters* 28: 3349–3352.
- Ide S, Beroza GC, and McGuire JJ (2005) Imaging earthquake source complexity. In: *Seismic Earth: Array Analysis of Broadband Seismograms. Geophysical Monograph Series*, 157. Washington, DC: AGU. <http://dx.doi.org/10.1029/157GM08>.
- Ide S, Beroza GC, Shelly DR, and Uchide T (2007) A scaling law for slow earthquakes. *Nature* 447: 76–79. <http://dx.doi.org/10.1038/nature05780>.
- Ide S, Shelly DR, and Beroza GC (2007) The mechanism of deep low frequency earthquakes: Further evidence that deep non-volcanic tremor is generated by shear slip on the plate interface. *Geophysical Research Letters* 34: L03308. <http://dx.doi.org/10.1029/2006GL028890>.
- Ide S and Takeo M (1997) Determination of constitutive relations of fault slip based on seismic wave analysis. *Journal of Geophysical Research* 102: 27379–27392. <http://dx.doi.org/10.1029/97JB02675>.
- Ishii M, Shearer PM, Houston H, and Vidale J (2005) Extent, duration and speed of the 2004 Sumatra–Andaman earthquake imaged by the Hi-Net array. *Nature* 435: 933–936.
- Ito Y and Obara K (2005) Very low frequency earthquakes excited by the 2004 off Kii peninsula earthquakes: A dynamic deformation process in the large accretionary prism. *Earth, Planets and Space* 57: 321–326.
- Ito Y and Obara K (2006) Dynamic deformation of the accretionary prism excites very low frequency earthquakes. *Geophysical Research Letters* 33. <http://dx.doi.org/10.1029/2005GL025270>.
- Ito T, Yoshioka S, and Miyazaki Si (2000) Interplate coupling in northeast Japan deduced from inversion analysis of GPS data. *Earth and Planetary Science Letters* 176(1): 117–130. [http://dx.doi.org/10.1016/S0012-821X\(99\)00316-7](http://dx.doi.org/10.1016/S0012-821X(99)00316-7).
- Jeffreys H (1942) On the mechanics of faulting. *Geological Magazine* 79: 291–295.
- Johnston AC and Kanter LR (1990) Earthquakes in stable continental crust. *Scientific American* 262(3): 68–75.
- Joyner WB and Boore DM (1986) On simulating large earthquakes by Green's function addition of smaller earthquakes. In: *Earthquake Source Mechanics*, pp. 269–274. Washington, DC: American Geophysical Union.
- Julian BR (1994) Volcanic tremor: Nonlinear excitation by fluid flow. *Journal of Geophysical Research* 99(11): 859–878.
- Julian BR (2002) Seismological detection of slab metamorphism. *Science* 296: 1625–1627.
- Julian BR, Miller AD, and Foulger GR (1998) Non-double-couple earthquakes. 1. Theory. *Reviews of Geophysics* 36: 525–549.
- Kagan YY and Jackson DD (1991) Seismic gap hypothesis: Ten years after. *Journal of Geophysical Research* 96: 21419–21431.
- Kanamori H (1972) Mechanism of tsunami earthquakes. *Physics of the Earth and Planetary Interiors* 6: 346–359.
- Kanamori H (1977) The energy release in great earthquakes. *Journal of Geophysical Research* 82: 2981–2987.
- Kanamori H and Given JW (1982) Analysis of long-period seismic waves excited by the May 18, 1980, eruption of Mount St. Helens: A terrestrial monopole. *Journal of Geophysical Research* 87: 5422–5432.
- Kanamori H and Heaton TH (2000) Microscopic and macroscopic physics of earthquakes. *Geophysics and the Complexity of Earthquakes. Geophysical Monograph*, 120, pp. 147–163. American Geophysical Union.
- Kanamori H and Mori J (1992) Harmonic excitation of mantle Rayleigh waves by the 1991 eruption of Mount Pinatubo, Philippines. *Geophysical Research Letters* 19: 721–724.
- Kane MF (1977) Correlation of major eastern earthquake centers with mafic/ultramafic basement masses. US Geological Survey Professional Paper, 1028-O.
- Kano Y, Mori J, Fujio R, et al. (2006) Heat signature on the Chelungpu fault associated with the 1999 Chi-Chi, Taiwan earthquake. *Geophysical Research Letters* 33. <http://dx.doi.org/10.1029/2006GL026733>.

- Kelleher JA, Sykes LR, and Oliver J (1973) Possible criteria for predicting earthquake locations and their applications to major plate boundaries of the Pacific and Caribbean. *Journal of Geophysical Research* 78: 2547–2585.
- Kirby S, Engdahl ER, and Denlinger R (1996) Intermediate-depth intraslab earthquakes and arc volcanism as physical expressions of crustal and uppermost mantle metamorphism in subducting slabs. In: Bebout GE, et al. (ed.) *Subduction: Top to bottom*. *Geophysical Monograph*, 96, pp. 195–214. Washington, DC: American Geophysical Union. <http://dx.doi.org/10.1029/2001JB000522>, 2043.
- Kirby SH, Stein S, Okal EA, and Rubie DC (1996) Metastable mantle phase transformations and deep earthquakes in subducting oceanic lithosphere. *Reviews of Geophysics* 34: 261–306.
- Kirkpatrick JD, Rowe CD, White JC, and Brodsky EE (2013) Silica gel formation during fault slip: Evidence from the rock record. *Geology* 41: 1015–1018. <http://dx.doi.org/10.1130/G34483.1>.
- Kobayashi N and Nishida K (1998) Continuous excitation of planetary free oscillations by atmospheric disturbances. *Nature* 395: 357–360. <http://dx.doi.org/10.1038/26427>.
- Kostoglodov V, Singh SK, Santiago JA, Larson KM, Lowry AR, and Bilham R (2003) A large silent earthquake in the Guerrero seismic gap, Mexico. *Geophysical Research Letters* 30. <http://dx.doi.org/10.1029/2003GL017219>.
- Kostrov BV and Das S (1988) Principles of earthquake source mechanics. In: *Cambridge Monographs on Mechanics and Applied Mathematics*, p. 286. Cambridge: Cambridge University Press.
- Kozdon JE and Dunham EM (2013) Rupture to the trench: Dynamic rupture simulations of the 11 March 2011 Tohoku earthquake. *Bulletin of Seismological Society of America* 103: 1275–1289. <http://dx.doi.org/10.1785/0120120136>.
- Kozdon JE, Dunham EM, and Nordstrom J (2013) Simulation of dynamic earthquake ruptures in complex geometries using high-order finite difference methods. *Journal of Scientific Computing* 55(1): 92–124. <http://dx.doi.org/10.1007/s10915-012-9624-5>.
- Lachenbruch A and Sass J (1980) Heat flow and energetics of the San Andreas fault zone. *Journal of Geophysical Research* 85: 6185–6222.
- Lapusta N, Rice JR, Ben-Zion Y, and Zheng G (2000) Elastodynamic analysis for long deformation history with spontaneous rupture episodes on faults with rate- and state-dependent friction. *Journal of Geophysical Research* 105: 23765–23789.
- Lay T, Kanamori H, and Ammon CJ (2012) Depth-varying properties of subduction zone megathrust faults. *Journal of Geophysical Research* 117. B04311. <http://dx.doi.org/10.1029/2011JB009133>.
- Lay T, et al. (2010) Teleseismic inversion for rupture process of the 27 February 2010 Chile (Mw 8.8) earthquake. *Geophysical Research Letters* 37(13), L13301.
- Leary P, Li YG, and Aki K (1987) Observations and modeling of fault-zone fracture anisotropy I. P., SV, SH travel times. *Geophysical Journal of the Royal Astronomical Society* 91: 461–484.
- Li YG, Leary P, Aki K, and Malin P (1990) Seismic trapped modes in the Oroville and San Andreas fault zones. *Science* 249: 763–766.
- Li YG, Vidale JE, Aki K, and Xu F (2000) Depth-dependent structure of the Landers fault zone from trapped waves generated by aftershocks. *Journal of Geophysical Research* 105: 6237–6254.
- Li YG, Vidale JE, Aki K, Xu F, and Burdette T (1998) Evidence of shallow fault zone strengthening after the 1992 M 7.5 Landers, California, earthquake. *Science* 279: 217–219.
- Linde AT, Gladwin MT, Johnston MJS, and Gwyther RL (1996) A slow earthquake sequence on the San Andreas fault. *Nature* 383: 65–69.
- Lorito S, et al. (2011) Limited overlap between the seismic gap and coseismic slip of the great 2010 Chile earthquake. *Nature Geoscience* 4(3): 173–177.
- Loveless JP and Meade BJ (2010) Geodetic imaging of plate motions, slip rates, and partitioning of deformation in Japan. *Journal of Geophysical Research-Solid Earth* 115(B2), B02410.
- Ma S and Andrews DJ (2010) Inelastic off-fault response and three-dimensional dynamics of earthquake rupture on a strike-slip fault. *Journal of Geophysical Research* 115. <http://dx.doi.org/10.1029/2009JB006382>.
- Ma S and Beroza GC (2008) Rupture dynamics on a bi-material interface for dipping faults. *Bulletin of Seismological Society of America* 98: 1642–1658. <http://dx.doi.org/10.1785/0120070201>.
- Mai PM and Beroza GC (2002) A spatial random-field model to characterize complexity in earthquake slip. *Journal of Geophysical Research* 107(B11): 2308. <http://dx.doi.org/10.1029/2001JB000588>.
- Mallet R and Mallet JW (1858) The earthquake catalogue of the British Association, with the discussion, curves, and maps, etc. Transaction of the British Association for the advancement of Science, London.
- Marone C and Scholz CH (1988) The depth of seismic faulting and the upper transition from stable to unstable slip regimes. *Geophysical Research Letters* 15: 621–624.
- Marza VI (2004) On the death toll of the 1999 Izmit (Turkey) major earthquake. *ESC General Assembly Papers*. Potsdam: European Seismological Commission.
- Mazzotti S, Le Pichon X, Henry P, and Miyazaki S-I (2000) Full interseismic locking of the Nankai and Japan-west Kurile subduction zones: An analysis of uniform elastic strain accumulation in Japan constrained by permanent GPS. *Journal of Geophysical Research-Solid Earth* 105(B6): 13159–13177.
- McCaffrey R (1992) Oblique plate convergence, slip vectors, and forearc deformation. *Journal of Geophysical Research* 97: 8905–8915.
- McCann WR, Nishenko SR, Sykes LR, and Krause J (1979) Seismic gaps and plate tectonics: Seismic potential for major plate boundaries. *Pure and Applied Geophysics* 117: 1082–1147.
- McGuire JJ, Zhao L, and Jordan TH (2002) Predominance of unilateral rupture for a global catalog of large earthquakes. *Bulletin of Seismological Society of America* 92: 3309–3317.
- McKenzie D and Brune JN (1972) Melting on fault planes during large earthquakes. *Geophysical Journal of the Royal Astronomical Society* 29: 65–78.
- McNally KC and McEvily TV (1977) Velocity contrast across the San Andreas Fault in central California: Small scale variations from P-wave nodal plane distortion. *Bulletin of the Seismological Society of America* 67: 1565–1576.
- McNutt SR (2005) Volcanic seismology. *Annual Review of Earth and Planetary Sciences* 32: 461–491. <http://dx.doi.org/10.1146/annurev.earth.33.092203.122459>.
- Meng L, Ampuero J-P, Stock J, Duputel Z, Luo Y, and Tsai VC (2012) Earthquake in a maze: Compressional rupture branching during the 2012 Mw 8.6 Sumatra earthquake. *Science* 337(6095): 724–726. <http://dx.doi.org/10.1126/science.1224030>.
- Michael AJ (1990) Energy constraints on kinematic models of oblique faulting: Loma Prieta versus Parkfield-Coalinga. *Geophysical Research Letters* 17: 1453–1456.
- Michael AJ (2011) Random variability explains apparent global clustering of large earthquakes. *Geophysical Research Letters* 38. L21301. <http://dx.doi.org/10.1029/2011GL049443>.
- Miller SA, Collettini C, Chiaraluce L, Cocco M, Barchi M, and Kaus BJ (2004) Aftershocks driven by a high-pressure CO₂ source at depth. *Nature* 427: 724–727.
- Miller MM, Melbourne T, Johnson DJ, and Sumner WQ (2002) Periodic slow earthquakes from the Cascadia subduction zone. *Science* 295: 2423.
- Mitsui Y, Kato N, Fukuhata Y, and Hirahara K (2012) Megaquake cycle at the Tohoku subduction zone with thermal fluid pressurization near the surface. *Earth and Planetary Science Letters* 325: 21–26. <http://dx.doi.org/10.1016/j.epsl.2012.01.026>.
- Mogi K (1968) Some features of recent seismic activity in and near Japan, 1. *Bulletin of the Earthquake Research Institute Tokyo University* 46: 1225–1236.
- Molnar P, Freedman D, and Shih JSF (1979) Lengths of intermediate and deep seismic zones and temperatures in downgoing slabs of lithosphere. *Geophysical Journal International* 56: 41–54.
- Montelli R, Nolet G, Dahmen FA, Masters G, Engdahl ER, and Hung S-H (2004) Finite-frequency tomography reveals a variety of plumes in the mantle. *Science* 303: 338–343. <http://dx.doi.org/10.1126/science.1092485>.
- Nadeau RM and Johnson LR (1998) Seismological studies at Parkfield VI: Moment release rates and estimates of source parameters for small repeating earthquakes. *Bulletin of Seismological Society of America* 88: 790–814.
- Nason RD and Tocher D (1970) Measurement of movement on the San Andreas fault. In: Mansinha L, Smylie DE, and Beck AE (eds.) *Earthquake Displacement Fields and the Rotation of the Earth*, pp. 246–254. Dordrecht, Netherlands: Reidel.
- National Research Council of the National Academies (2003) Living on an Active Earth, perspectives on earthquake science. Committee on the Science of Earthquakes Board on Earth Sciences and Resources Division on Earth and Life Studies. Washington, D.C.: The National Academies Press.
- Nishimura T, et al. (2004) Temporal change of interplate coupling in northeastern Japan during 1995–2002 estimated from continuous GPS observations. *Geophysical Journal International* 157(2): 901–916.
- Nur A and Booker JR (1972) Aftershocks caused by pore fluid flow? *Science* 175: 885–887.
- Obara K (2002) Nonvolcanic deep tremor associated with subduction in southwest Japan. *Science* 296: 1679–1681.
- Obara K, Hirose H, Yamamoto F, and Kasahara K (2004) *Geophysical Research Letters* 31. L23602. <http://dx.doi.org/10.1029/2004GL020848>.
- Ogata Y (1988) Statistical-models for earthquake occurrences and residual analysis for point-processes. *Journal of the American Statistical Association* 83: 9–27.
- Okal EA (1992) Use of the mantle magnitude M_m for the reassessment of the moment of historical earthquakes I: Shallow events. *Pure and Applied Geophysics* 139: 17–57.
- Okal E and Stewart LM (1982) Slow earthquakes along oceanic fracture zones: Evidence for asthenospheric flow away from hotspots? *Earth and Planetary Science Letters* 57: 75–87.

- Osawa S, Murakami M, Kaidzu M, and Hatanaka Y (2005) Transient crustal deformation in Tokai region, central Japan, until May 2004. *Earth, Planets and Space* 57: 909–915.
- Parsons T, Toda S, Stein RS, Barka A, and Dieterich JH (2000) Heightened odds of large earthquakes near Istanbul: An interaction-based probability calculation. *Science* 288: 661–665.
- Perrin G, Rice JR, and Zheng G (1995) Self-healing slip pulse on a frictional surface. *Journal of the Mechanics and Physics of Solids* 43: 1461–1495.
- Peyrat S, Olsen KB, and Madariaga R (2001) Dynamic modeling of the 1992 Landers earthquake. *Journal of Geophysical Research* 106(26): 467–482.
- Poupinet G and Ellsworth WL (1984) Monitoring velocity variations in the crust using earthquake doublets: An application to the Calaveras fault, California. *Journal of Geophysical Research* 89: 5719–5732.
- Quin H (1990) Dynamic stress drop and rupture dynamics of the October 15, 1979 Imperial Valley, California earthquake. *Tectonophysics* 175: 93–117.
- Raleigh CB, Healy JH, and Bredehoeft JD (1976) An experiment in earthquake control at Rangely, Colorado. *Science* 191: 1230–1237.
- Reinecker J, Heidbach O, Tingay M, Sperner B, and Müller B (2005) The release 2005 of the World Stress Map (available online at www.world-stress-map.org).
- Rempel AW and Rice JR (2006) Thermal pressurization and onset of melting in fault zones. *Journal of Geophysical Research* 111. <http://dx.doi.org/10.1029/2006JB004314>.
- Rhie J and Romanowicz B (2004) Excitation of Earth's continuous free oscillations by atmosphere-ocean-seafloor coupling. *Nature* 431: 552–556. <http://dx.doi.org/10.1038/nature02942>.
- Rice JR (1980) The mechanics of earthquake rupture. In: Dziewonski AM and Boschi E (eds.) *Physics of the Earth's Interior*, pp. 555–649. Amsterdam: North-Holland.
- Rice JR (2006) Heating and weakening of faults during earthquake slip. *Journal of Geophysical Research* 111. <http://dx.doi.org/10.1029/2005JB004006>.
- Rice JR and Cleary MP (1976) Some basic stress diffusion solutions for fluid-saturated elastic porous media with compressible constituents. *Reviews of Geophysics and Space Physics* 14: 227–241.
- Richter CF (1935) An instrumental earthquake magnitude scale. *Bulletin of Seismological Society of America* 25: 1–32.
- Richter CF (1958) *Elementary Seismology*. San Francisco, CA: W. H. Freeman and Co, 758 pp.
- Risk Management Solutions Inc (1995) *What if the 1923 Earthquake Strikes Again? A Five Prefecture Tokyo Region Scenario*. Menlo Park, CA: Risk Management Solutions Inc., 97 pp.
- Rogers G and Dragert H (2003) Episodic tremor and slip on the Cascadia subduction zone: The chatter of silent slip. *Science* 300: 1942–1943.
- Rosakis AJ, Samudrala O, and Coker D (1999) Cracks faster than the shear wave speed. *Science* 284: 1337–1340.
- Royer AA and Bostock MG (2013) A comparative study of low frequency earthquake temblors in northern Cascadia. *Earth and Planetary Science Letters* 42: 247–256. <http://dx.doi.org/10.1016/j.epsl.2013.08.040>.
- Royer J-Y and Gordon RG (1997) The motion between the Capricorn and Australian Plates. *Science* 277: 1268–1274.
- Rubin AM, Gillard D, and Got J-L (1999) Streaks of microearthquakes along creeping faults. *Nature* 400: 635–641.
- Ruegg JC, et al. (2009) Interseismic strain accumulation measured by GPS in the seismic gap between constitución and concepción in Chile. *Physics of the Earth and Planetary Interiors* 175(1–2): 78–85.
- Ruina A (1983) Slip instability and state variable friction laws. *Journal of Geophysical Research* 88(10): 359–370.
- Savage JC (1983) A dislocation model of strain accumulation and release at a subduction zone. *Journal of Geophysical Research* 88: 4984–4996.
- Sbar ML and Sykes LR (1973) Contemporary compressive stress and seismicity in eastern North America: An example of intra-plate tectonics. *Geological Society of America Bulletin* 84: 1861–1882.
- Schaaff DP, Bokelmann GHR, Beroza GC, Waldhauser F, and Ellsworth WL (2002) High resolution image of Calaveras Fault seismicity. *Journal of Geophysical Research* 107(B9): 2186. <http://dx.doi.org/10.1029/2001JB000633>.
- Schaaff DP, Bokelmann GHR, Ellsworth WL, Zanzerka E, Waldhauser F, and Beroza GC (2004) Optimizing correlation techniques for improved earthquake location. *Bulletin of Seismological Society of America* 94: 705–721.
- Scholz CH (1968) Microfractures, aftershocks, and seismicity. *Bulletin of Seismological Society of America* 58: 1117–1130.
- Scholz CH (1989) Mechanics of faulting. *Annual Review of Earth and Planetary Sciences* 17: 309–334.
- Scholz CH (1990) *The Mechanics of Earthquakes and Faulting*. New York: Cambridge University Press.
- Scholz CH (2000) Evidence for a strong San Andreas Fault. *Geology* 28: 163–166. <http://dx.doi.org/10.1130/0091-7613>.
- Scholz CH, Molnar P, and Johnson T (1972) Frictional sliding of granite and earthquake mechanism implications. *Journal of Geophysical Research* 77: 6392–6406.
- Seno T and Yamasaki T (2003) Low-frequency tremors, intraslab and interplate earthquakes in Southwest Japan—From a viewpoint of slab dehydration. *Geophysical Research Letters* 30. <http://dx.doi.org/10.1029/2003GL018349>.
- Shearer PM, Prieto GA, and Haakansson E (2006) Comprehensive analysis of earthquake source spectra in southern California. *Journal of Geophysical Research* 111: B06303. <http://dx.doi.org/10.1029/2005JB003979>.
- Shearer PM and Stark PB (2012) The global risk of big earthquakes has not recently increased. *Proceedings of the National Academy of Sciences* 109: 717–721. <http://dx.doi.org/10.1073/pnas.1118525109>.
- Shelly DR, Beroza GC, and Ide S (2007) Non-volcanic tremor and low frequency earthquake swarms. *Nature* 446. <http://dx.doi.org/10.1038/nature05666>.
- Shelly DR, Beroza GC, Ide S, and Nakamura S (2006) Low-frequency earthquakes in Shikoku, Japan, and their relationship to episodic tremor and slip. *Nature* 442: 188–191.
- Shibasaki B, Matsuzawa T, Tsutsumi A, Ujiie K, Hasegawa A, and Ito Y (2011) 3D modeling of the cycle of a great Tohoku-Oki earthquake, considering frictional behavior at low to high slip velocities. *Geophysical Research Letters* 38: L21305. <http://dx.doi.org/10.1029/2011GL049308>.
- Sibson RH (1973) Interaction between temperature and pore-fluid pressure during earthquake faulting—A mechanism for partial or total stress relief. *Nature* 243: 66–68.
- Sibson RH (1981) In: Simpson DW and Richards PG (eds.) *Earthquake Prediction: An International Review. Maurice Ewing Series*, 4: pp. 593–603. Washington, DC: AGU Press.
- Singh SK, Mena E, and Castro R (1988) Some aspects of source characteristics of the 19 September 1985 Michoacan earthquake and ground motion amplification in and near Mexico City from strong motion data. *Bulletin of Seismological Society of America* 78: 451–477.
- Singh SK and Ordaz M (1994) Seismic energy release in Mexican subduction zone earthquakes. *Bulletin of Seismological Society of America* 84: 1533–1550.
- Somerville PG, Smith NF, Graves RW, and Abrahamson NA (1997) Modification of empirical strong ground motion attenuation relations to include the amplitude and duration effects of rupture directivity. *Seismological Research Letters* 68: 199–222.
- Stein RS (1999) The role of stress transfer in earthquake occurrence. *Nature* 402: 605–609. <http://dx.doi.org/10.1038/45144>.
- Stein RS, Barka AA, and Dieterich JH (1997) Progressive failure on the North Anatolian fault since 1939 by earthquake stress triggering. *Geophysical Journal International* 128: 594–604.
- Stirling MW and Petersen M (2006) Comparison of the historical record of earthquake hazard with seismic-hazard models for New Zealand and the continental United States. *Bulletin of Seismological Society of America* 96: 1978–1994.
- Stirling M, Wesnousky SG, and Shimizaki K (1996) Fault trace complexity, cumulative slip, and the shape of the magnitude-frequency distribution for strike-slip faults—A global survey. *Geophysical Journal International* 124: 833–868.
- Suda N, Nawa K, and Fukao Y (1998) Earth's background free oscillations. *Science* 279: 2089–2091. <http://dx.doi.org/10.1126/science.279.5359.2089>.
- Suwa Y, Miura S, Hasegawa A, Sato T, and Tachibana K (2006) Interplate coupling beneath NE Japan inferred from three-dimensional displacement field. *Journal of Geophysical Research-Solid Earth* 111(B4), B04402.
- Sykes LR (1967) Mechanism of earthquakes and nature of faulting on the mid-oceanic ridges. *Journal of Geophysical Research* 72: 2131–2153.
- Tanaka H, Chen W-M, and Wang C-Y (2006) Frictional heat from faulting of the 1999 Chi-Chi, Taiwan, earthquake. *Geophysical Research Letters* 33: L16316. <http://dx.doi.org/10.1029/2006GL026673>.
- Tauzin B, Debayle E, Quatrin C, and Coltice N (2013) Seismoacoustic coupling induced by the breakup of the 15 February 2013 Chelyabinsk meteor. *Geophysical Research Letters* 40: 3522–3526. <http://dx.doi.org/10.1002/grl.506832013>.
- Titus SJ, DeMets C, and Tikoff B (2006) Thirty-five-year creep rates for the creeping section of the San Andreas Fault and the effects of the 2004 Parkfield earthquake; constraints from alignment arrays, continuous global positioning system, and creepmeters. *Bulletin of Seismological Society of America* 96: S250–S268. <http://dx.doi.org/10.1785/0120050811>.
- Toda S, Stein RS, Beroza GC, and Marsan D (2012) Aftershocks halted by static stress shadows. *Nature Geoscience* 5: 410–413. <http://dx.doi.org/10.1038/ngeo1465>.
- Toksöz MN, Shakal AF, and Michael AJ (1979) Space-time migration of earthquakes along the North Anatolian fault zone and seismic gaps. *Pure and Applied Geophysics* 117: 1258–1270.
- Toppozada TR (1975) Earthquake magnitude as a function of intensity data in California and western Nevada. *Bulletin of Seismological Society of America* 65: 1223–1238.

- Toppozada TR, Real CR, and Park DL (1981) Preparation of isoseismal maps and summaries of reported effects for pre-1900 California earthquakes. California. Division of Mines and Geology Open File Pert. 81-11 SAC, 182 pp.
- Tse ST and Rice JR (1986) Crustal earthquake instability in relation to the depth variation of frictional slip properties. *Journal of Geophysical Research* 91: 9452–9472.
- Unsworth MJ, Malin PE, Egbert GD, and Booker JR (1997) Internal Structure of the San Andreas fault at Parkfield, California. *Geology* 25: 359–362.
- Utsu T (1961) A statistical study on the occurrence of aftershocks. *Geophysical Magazine* 30: 521–605.
- Vanek J, Zapotek A, Karnik V, et al. (1962) Standardization of magnitude scales. *Izvestiya Akademii Nauk SSSR Seriya Geofizicheskaya* 2: 153–158.
- Vigny C, et al. (2011) The 2010 Mw 8.8 Maule megathrust earthquake of central Chile, monitored by GPS. *Science* 332(6036): 1417–1421.
- Wald DJ and Heaton TH (1994) Spatial and temporal distribution of slip for the 1992 Landers, California earthquake. *Bulletin of the Seismological Society of America* 84: 668–691.
- Wald DJ, Quitoriano V, Heaton T, and Kanamori H (1999) Relationships between peak ground acceleration, peak ground velocity, and modified Mercalli intensity in California. *Earthquake Spectra* 15: 557–564.
- Waldbauer F and Ellsworth WL (2000) A double-difference earthquake location algorithm: Method and application to the northern Hayward Fault, California. *Bulletin of Seismological Society of America* 90: 1353–1368.
- Waldbauer F, Ellsworth WL, Schaff DP, and Cole A (2004) Streaks, multiplets, and holes: High-resolution spatio-temporal behavior of Parkfield seismicity. *Geophysical Research Letters* 31, L18608.
- Walter WR, Rodgers AJ, Mayeda K, Myers SC, Pasaynos M, and Denny M (1998) Preliminary regional seismic analysis of nuclear explosions and earthquakes in Southwest Asia. In: Proceedings of the 20th Annual Seismic Research Symposium on Monitoring a Comprehensive Test Ban Treaty, pp. 442–452. Department of Defense and Department of Energy Report.
- Ward SN (1995) Area-based tests of long-term seismic hazard predictions. *Bulletin of Seismological Society of America* 85: 1285–1298.
- Wech AG and Creager KC (2007) Cascadia tremor polarization evidence for plate interface slip. *Geophysical Research Letters* 34: L22306. <http://dx.doi.org/10.1029/2007GL031167>.
- Wesnousky SG (1994) The Gutenberg–Richter or characteristic earthquake distribution, which is it? *Bulletin of Seismological Society of America* 84: 1940–1959.
- Wesson RL (1988) Dynamics of fault creep. *Journal of Geophysical Research* 93: 8929–8951.
- West M, Sanchez JJ, and McNutt SR (2005) Periodically triggered seismicity at Mount Wrangell, Alaska, after the Sumatra earthquake. *Science* 308: 1144–1146. <http://dx.doi.org/10.1126/science.1112462>.
- Wibberley CAJ and Shimamoto T (2003) Internal structure and permeability of major strike-slip fault zones: The median tectonic line in mie prefecture, Southwest Japan. *Journal of Structural Geology* 25: 59–78.
- Widmer R and Zürn W (1992) Bichromatic excitation of long-period Rayleigh and air waves by the Mount Pinatubo and El Chichón volcanic eruptions. *Geophysical Research Letters* 19: 765–768.
- Wong T-F (1982) Shear fracture energy of Westerly granite from postfailure behavior. *Journal of Geophysical Research* 87: 990–1000.
- Working Group on California Earthquake Probabilities (2002) Earthquake probabilities in the San Francisco Bay region: 2002–2031. USGS Open File Report 03-214.
- Wu J, Wallace T, and Beck S (1995) A very broadband study of the 1994 deep Bolivia earthquake sequence. *Geophysical Research Letters* 22: 2237–2240.
- Xue L, Li H-B, and Brodsky EE (2013) Continuous permeability measurements record healing inside the Wenchuan earthquake fault zone. *Science* 340: 1555–1559. <http://dx.doi.org/10.1126/science.1237237>.
- Yong C, Tsoi K-L, Feibi C, Henhuan GZ, Qijia Z, and Zhangli C (1988) *The Great Tangshan Earthquake of 1976: An Anatomy of Disaster*. Oxford: Pergamon Press, 153 pp.
- Yu G, Wesnousky SG, and Ekstrom G (1993) Slip partitioning along major convergent plate boundaries. *Pure and Applied Geophysics* 140: 183–210.
- Zhang M and Wen L (2013) High-precision location and yield of North Korea's 2013 nuclear test. *Geophysical Research Letters* 40: 2941–2946. <http://dx.doi.org/10.1002/2012GL050607>.
- Zhao L-F, Xie X-B, Wang W-M, and Yao Z-X (2012) Yield estimation of the 25 May, 2009 North Korean nuclear explosion. *Bulletin of Seismological Society of America* 102: 467–478. <http://dx.doi.org/10.1785/0120110163>.
- Zoback ML, Zoback MD, Adams J, et al. (1989) Global patterns of tectonic stress. *Nature* 341: 291–298. <http://dx.doi.org/10.1038/341291a0>.
- Zoback MD, Zoback ML, and Mount V (1987) New evidence on the state of stress on the San Andreas fault system. *Science* 238: 1105–1111.